LEVEL

AD

TECHNICAL REPORT ARBRL-TR-02355

A PARAMETRIC STUDY OF THE MUZZLE

BLAST FROM A 20mm CANNON

Edward M. Schmidt
Edmund J. Gion
Kevin S. Fansler

DTIC
ELECT
OCT 1 5 1981
A

August 1981

US ARMY ARMAMENT RESEARCH AND DEVELOPMENT COMMAND
BALLISTIC RESEARCH LABORATORY
ABERDEEN PROVING GROUND, MARYLAND

Approved for public release; distribution unlimited.

81 10 14

REPORT DOCUMENTATION PAGE		READ INSTRUCTIONS BEFORE COMPLETING FORM
1. REPORT NUMBER TECHNICAL REPORT ARBRL-TR-02355	2. GOVT ACCESSION NO. AD-A105531	3. RECIPIENT'S CATALOG NUMBER
4. TITLE (and Subtitle) A Parametric Study of the Muzzle Blast from a 20mm Cannon.		5. TYPE OF REPORT & PERIOD COVERED Final rept. 6. PERFORMING ORG. REPORT NUMBER
7. AUTHOR(s) Edward M. Schmidt, Edmund J. Gion, Kevin S. Fansler		8. CONTRACT OR GRANT NUMBER(s)
9. PERFORMING ORGANIZATION NAME AND ADDRESS U.S. Army Ballistic Research Laboratory (ATTN: DRDAR-BLL) Aberdeen Proving Ground, Maryland 21005		10. PROGRAM ELEMENT, PROJECT, TASK AREA & WORK UNIT NUMBERS RDT&E 1L161102AH43
11. CONTROLLING OFFICE NAME AND ADDRESS U.S. Army Armament Research & Development Command U.S. Army Ballistic Research Laboratory (ATTN: DRDAR-BL) Aberdeen Proving Ground, MD 21005		12. REPORT DATE AUGUST 1981 13. NUMBER OF PAGES 93
14. MONITORING AGENCY NAME & ADDRESS(if different from Controlling Office)		15. SECURITY CLASS. (of this report) Unclassified 15a. DECLASSIFICATION/DOWNGRADING SCHEDULE

16. DISTRIBUTION STATEMENT (of this Report)

Approved for public release; distribution unlimited.

17. DISTRIBUTION STATEMENT (of the abstract entered in Block 20, if different from Report)

18. SUPPLEMENTARY NOTES

19. KEY WORDS (Continue on reverse side if necessary and identify by block number)

Muzzle Blast
Muzzle Brake
3-D Unsteady Flow
Compensators

20. ABSTRACT (Continue on reverse side if necessary and identify by block number) (ner)

The muzzle flow properties of a 20mm cannon are measured for a range of launch velocities from 260 m/s through 1000 m/s. Sequential spark shadowgraphs are taken of the developing muzzle blast. Pressure surveys are made of the blast field over a range from 10 to 40 calibers from the muzzle. An idealized muzzle device is inserted in the flow and surface pressure distributions taken for a variety of geometries relative to the gun tube. Experimental results are compared with available theoretical and numerical models.

TABLE OF CONTENTS

LIST OF ILLUSTRATIONS

5

LIST OF ILLUSTRATIONS

6

I. INTRODUCTION

Currently, the Army is restricted in the operation of two major howitzer systems due to excessive levels of blast in the crew area. The installation of medium caliber cannon on aircraft has produced concern as to the fatigue life of surfaces loaded by the blast pulse. Proving grounds are forced to curtail operation when adverse atmospheric conditions are present which permit blast focusing on populated areas. To treat the problem of predicting and eventually reducing muzzle blast, an understanding of the flow properties in the vicinity of the weapon muzzle and its influence on the formation and propagation of the blast wave must be developed.

A range of research has been performed to address different aspects of the problem[1-9]. The blast from aircraft cannon has been studied experimentally by Mabey and Capps[1]. They conducted wind tunnel

1. D. G. Mabey and D. S. Capps, "Blast from Moving Guns," AIAA Journal of Aircraft, Vol. 14, 1977, pp 687-692.

2. J. Erdos and P. Del Guidice, "Calculation of Muzzle Blast Flow Fields," AIAA J., Vol. 13, No. 8, August 1975, pp 1048-1056.

3. T. D. Taylor and T. C. Lin, "A Numerical Model for Muzzle Blast Flow Fields," AIAA Paper No. 80-0273, January 1980.

4. J. Yagla, "Analysis of Gun Blast Phenomena for Naval Architecture, Equipment, and Propellant Charge Design," 3d International Symposium on Ballistics, Karlsruhe, Germany, March 1977, ADPA, Washington, D.C.

5. C. S. Zoltani, "Numerical Simulation of the Muzzle Flow Field with a Moving Projectile," 1st International Symposium on Ballistics, Orlando, FL, November 1974, ADPA, Washington, D.C.

6. G. Moretti, "Muzzle Blast Flow and Related Problems," AIAA Paper 78-1190, July 1978.

7. G. Klingenberg, "Investigation of Combustion Phenomena Associated with the Flow of Hot Propellant Gases," Combustion and Flame, Vol. 29, 1977, pp. 289-309.

8. F. Smith, "A Theoretical Model of the Blast from Stationary and Moving Guns," 1st International Symposium on Ballistics, Orlando, FL, November 1974, ADPA, Washington, D.C.

9. M. Walther, "Gun Blast from Naval Guns," TR 2733, Naval Weapons Laboratory, Dahlgren, VA, August 1972. AD 902672L.

tests over a range of Mach numbers from low subsonic through supersonic. Firings of a 7.62mm rifle were made in the tunnel over a simulated aircraft surface. The data from this program agree well with the scaling laws developed by Smith[8].

Erdos and DelGuidice[2] have developed a spherically symmetric treatment of the muzzle flow which is valid along the axis of symmetry of the gun tube. They assume that the core flow of the propellant gas jet is determined by the predictions of a steady, method of characteristics computation. They use a finite difference scheme to calculate the propagation of the shock layer between the jet Mach disc and air blast wave. The model agrees well with available data.

Taylor and Lin[3], Yagla[4], and Zoltani[5] apply shock capturing, finite difference techniques to solve the axially symmetric problem. Moretti[6] is developing a shock fitting methodology which holds promise for the accurate definition of overpressure pulse far from the muzzle. These codes have been used to account for the projectile, axially symmetric muzzle devices, and, potentially, the precursor flow. A problem faced by codes is the lack of experimental data describing both the muzzle blast field and the details of the weapon emptying conditions.

Klingenberg[7] has conducted detailed experiments upon both small and medium caliber guns to measure in-bore and propellant exhaust gas-dynamics as it relates to muzzle flash. Walther[9] has compiled blast data on Naval weapons but does not present muzzle exit conditions. Schmidt and Shear[10] address the details of the flow development around a small caliber weapon, but give little information on the gun muzzle properties during tube emptying.

The present report describes the results of a series of experiments intended to define the gun tube emptying and muzzle blast flow properties of a selected gun system. Firings of a 20mm cannon were conducted to: first, determine the conditions at the muzzle during the exhaust cycle; second, measure the development of the near muzzle plume structure; third, obtain pressure data in the blast field outside of the propellant gas jet; and finally, investigate impingement of the muzzle flow upon baffle surfaces similar to those in silencers or recoil brakes. Data were collected over a range of launch conditions in order to identify important parameters which govern the strength of the muzzle blast overpressure field. The experimental results are compared with theory and used to develop a potentially useful scaling relation.

10. E. M. Schmidt and D. D. Shear, "Optical Measurements of Muzzle Blast," AIAA J., Vol. 13, No. 8, August 1975, pp. 1086-1091.

8

II. TEST APPARATUS

The weapon tested is a 20mm cannon having a barrel length of 1.52 m, a chamber volume of 4.17×10^{-5} m^3, and a twist of rifling of one turn in 25 calibres. The projectile is the M55A2 training round weighing 0.098 kg and having L/D = 3.75. The propellant is WC870 having the following properties:

$$T_{adiab.} = 2577^{\circ} K,$$

$$e = \text{specific energy}$$

$$= 9.55 \times 10^5 \text{ m}^2/\text{s}^2,$$

$$\gamma = 1.25,$$

$$R = 365.5 \text{ m}^2/\text{s}^{2 \circ} K.$$

The propellant loading was varied from 3.56 g to 38.9 g to produce a range in muzzle velocities from 260 m/s to 1000 m/s. This provided for a systematic variation in weapon exhaust properties and resultant muzzle blast over a set of launch velocities similar to that of field artillery.

The exhaust properties of the propellant gases were measured using two types of pressure transducer arrangements. The first, Figure 1, consisted of an array of six Kistler 603A piezoelectric transducers placed in an adaptor attached to the muzzle. The transducers were arranged along the boreline at intervals of 1.27 cm beginning 1.27 cm from the actual muzzle of the cannon. These measure the pressure history as the gun empties and are capable of determining the speed at which the expansion wave propagates upstream from the exit of the adaptor following shot ejection. From this wave speed, it is possible to determine the speed of sound in the propellant gases and through a proper equation of state, to compute the propellant gas temperature. The details of the measurement and data reduction procedure have been discussed previously[11]. The second type of muzzle adaptor (Figure 2) was simply intended to measure the pressure time history at the muzzle. The device consisted of a 1.27 cm extension of the muzzle in which a Kistler 603A transducer was mounted. In both cases, transducer output was recorded on Tektronix, Type 551, Dual-Beam Oscilloscopes.

The muzzle exhaust flow is observed using a sequential spark shadowgraph technique[10] which permits the definition of discontinuity trajectories in space and time. The properties of the blast wave, once

---

11. E. M. Schmidt, E. J. Gion, and D. D. Shear, "Acoustic Thermo-
     metric Measurements of Propellant Gas Temperatures in Guns,"
     AIAA J., Vol. 15, No. 2, February 1977, pp. 222-226.

it passed from the field of view of the optics, were measured using static or side-on pressure transducers[12]. These data were recorded in a cylindrical coordinate system (Figure 3) The time scale is defined as originating at zero when the base of the projectile crosses the face of the muzzle. Since the obturating band on the projectile is located 8 mm forward of the base, there is some leakage of propellant gases prior to the base clearance. The spark shadowgraph and pressure data are acquired simultaneously on each round fired; thus, it is possible to tie the two sets of data together by including the signal from spark firing on the output traces of the pressure transducers.

In another series of tests, a circular steel plate (Figure 4) was positioned in the muzzle flow. The plate has a diameter of 457 mm, a thickness of 31 mm, and a central hole of 24 mm to permit projectile passage. The plate is instrumented with Kistler 603A and 201B piezoelectric transducers. The flow field over the plate is observed using the sequential spark shadowgraph technique. No blast field data was taken during these tests. The plate was oriented both vertically to generate an axially symmetric geometry and at a $50°$ angle to the axis of the gun in order to generate a three dimensional geometry. When inclined, the central hole had to be enlarged to 35 mm for projectile passage. These tests were conducted at only one launch velocity.

III. GUN TUBE EMPTYING PROPERTIES

As mentioned in the introduction, previous surveys of weapon blast fields generally neglect the definition of gun tube emptying conditions. Since the exhausting propellant gases and their resultant expansion drive the blast wave, this information is crucial to the performance of rational analytical or numerical treatment of the flow. Through the use of the two types of pressure transducer arrangements described in the previous section, it was possible to measure the flow properties immediately behind the projectile just prior to shot ejection[11] and to measure the pressure decay following shot ejection. While it would be desirable to measure additional properties during emptying using

---

12. P. Westine and F. Hoese, "Blast Gauge for Measuring Shocks with Short Wavelengths," IR-02-2643-01, Southwest Research Institute, San Antonio, TX, May 1970. AD 907402L.

spectroscopic[6] or scattering[13,14] techniques, such data were either not available or not completely developed for the 20mm cannon in question. As an alternative, the full set of muzzle emptying properties are developed by assuming an isentropic emptying process. Since the inbore combustion process does not occur at constant pressure, temperature, or adiabatically, the assumption that the gases are evolved isentropically is not correct; however, the decay of temperature and velocity predicted should be qualitatively correct.

The exit conditions measured using acoustic thermometry[11] are presented in Figure 5. Again these properties are those in the propellant gases at the muzzle just before separation of the projectile. The muzzle flow testing was conducted at five distinct loadings, indicated by the data points in Figure 5a. The exit conditions are summarized in the table below.

Table I. Measured Gun Tube Exit Conditions and Computed Sonic Exit Conditions (Quantities in brackets are estimates based on trends in measured data). Measurements are the average of three separate firings for each velocity.

m_c (g)	V_p (m/s)	T_e (°K)	M_e	p_e/p_∞	u^* (m/s)	T^* (°K)	p^*/p_∞
3.6	280	1000	0.44	27	632	875	14
9.7	463	1000	0.69	63	653	933	45
17.8	615	1085	0.86	117	695	1052	101
25.9	775	1320	1.00	189	775	1320	189
38.9	1050	(1705)	(1.19)	287	-	-	-

13. W. D. Williams and H. M. Powell, "Laser-Raman Measurements in the Muzzle Blast Region of a 20-mm Cannon," AEDC-TR-79-72, Arnold Engineering Development Center, Tullahoma, TN, August 1980. AD A088729.

14. W. M. Farmer, et.al., "Laser Velocimetry Measurements of the Chronological Velocity at Selected Positions in the Muzzle Blast from 20mm Cannon," University of Tennessee Space Institute, Tullahoma, TN, September 1979.

From the measured temperature and launch velocity, the exit Mach number, M_e, of the propellant gases was calculated. For the first three launch velocities, the flow behind the projectile was subsonic; thus, a centered expansion wave propagates back up the gun tube following shot ejection, see Figure 6. The strength of this wave may be simply computed if it is assumed that the process is one-dimensional. While this assumption is not strictly correct in the region very close to the muzzle (Figure 7) due to the presence of the projectile base, the flow becomes more nearly one-dimensional as the projectile moves downrange allowing the sonic line to close across the muzzle face and as the waves from around the annulus (between the projectile base and muzzle) converge and intersect forming a nearly planar front. Using one-dimensional theory[15], the following relations may be determined:

$$u^*/a_e = \frac{2}{\gamma+1} + \frac{\gamma-1}{\gamma+1} \frac{u_e}{a_e}$$

$$p^*/p_e = \left[\frac{2}{\gamma+1} + \frac{\gamma-1}{\gamma+1} \frac{u_e}{a_e} \right]^{2 \gamma/(\gamma-1)}$$

where sonic conditions are indicated by an asterisk.

The importance of definition of the sonic exit conditions should be clear since it is this "internally expanded" flow which drives the external expansion of the muzzle gases and associated air blast. For this reason, these properties are included in Table I. For the last two launch velocities, 775 and 1050 m/s, the propellant gas was either just sonic or supersonic. Under the supersonic exit condition, no waves propagate back upstream until the continued in-bore expansion causes the muzzle flow conditions to decay to sonic values. In this case, any subsequent in-bore expansion wave is reflected back upstream as an expansion; and, in this manner, sonic exit flow is maintained. However, no centered expansion wave is formed at shot ejection in either of these last two cases.

Acoustic thermometry has an extremely limited range of utility in the present application[11], namely, just a single data point in time. The subsequent emptying of the gun tube was recorded solely through the use of a pressure transducer located as near to the muzzle as possible.

---

15. A. H. Shapiro, *The Dynamics and Thermodynamics of Compressible Fluid Flow*, Ronald Press, New York, 1953.

12

The proximity to the muzzle is important in attempting to accurately measure the pressure variation through the centered muzzle expansion. If the transducer is located a significant distance (greater than 0.5-1.0 calibres) from the exit plane, the continuing in-bore expansion interacting with the centered wave make interpretation of the data difficult. The pressure data is shown in Figure 8 for the five launch velocities of interest. In the traces for the two lowest launch velocities, the influence of the centered expansion is clearly shown, but as launch velocity increases, its presence disappears. It is interesting to compare the rates of pressure decay. For the low launch velocities, the muzzle pressure decreases rather slowly after the initial drop associated with passage of the muzzle expansion. On the other hand, the muzzle pressure decay for high velocity launches is quite rapid. As a result, all of the traces show similar levels of muzzle pressure by about eight milliseconds. No attempt was made to measure the actual time required for flow from the muzzle to cease, but these data seem to indicate that it could be quite similar for all of the conditions tested.

As noted, the remaining gasdynamic properties at the muzzle were not measured; therefore, they are computed under the assumption that the emptying process is isentropic. Since pressure is the measured quantity and the initial temperature is known, the equations take the following form:

$$T^* = T_i \; (\frac{p^*}{p_i})^{\frac{\gamma-1}{\gamma}}$$

$$T_s^{\;*} = \frac{\gamma+1}{2} \; T^*$$

$$u^* = \sqrt{\gamma R T^*}$$

where asterisks refer to sonic conditions which are assumed to exist at the muzzle throughout the emptying process. This applies to the highest launch velocity, 1050 m/s, where the short period of supersonic exhaust is neglected. For each of the launch conditions, the temperature and velocity of the propellant gas as it passes the muzzle exit is plotted (Figure 9).

Comparison of the decay of pressure (Figure 8) with the decays of temperature and velocity of the exhaust flow shows that even when the muzzle pressure drops to nearly atmospheric levels (at around 8 ms), the temperature and velocity of the propellant gases are still quite high. A high velocity in the gases could continue the exhaust cycle of the weapon in a manner which would generate sub-atmospheric pressures in the tube. Recovery would then occur through the propagation of a shock wave into the gun tube. This in turn would reflect

13

from the breech of the weapon and re-emerge from the muzzle. Such over-expansion and shock recovery is observed in both theory and experiment[16] of spherical charges or pressurized container rupture. In these cases, an inward facing shock forms in the expanding detonation products. The shock first propagates outward, but reverses direction as the gases over-expand. The shock travels to the origin of the spherical charge where it reflects. The process can repeat a number of times until damped out by viscous and thermal losses (Figure 10) In the case of the muzzle exhaust flow, the inward facing shock is the Mach disc which forms in the supersonic plume. As the exit pressure decays, the Mach disc moves in toward the muzzle. While the propagation of the wave into the gun tube and its subsequent reflection was not observable, the occurrence of flow reversals on the present muzzle pressure data*, and sequential ventings can be observed in high speed motion pictures of cannon firings.

Another interesting feature of the temperature and velocity variations (Figure 9) is the occurrence of an inflection point or "knee" in the curves. For example, the knee occurs at roughly 4 ms in the curve for V_p = 280 m/s. The knee is taken to represent the return of the centered nozzle expansion following propagation down the tube and reflection from the breech. Since the wave reflects as an expansion, its arrival at the muzzle results in increased rate of property value decay. With these data and approximations to define the venting of the gun tube following shot ejection, it is now possible to better examine the properties of the flow external to the weapon muzzle.

IV. BARE MUZZLE FLOW FIELD

The flow from the muzzle of a gun consists of two impulsive jets, see Figure 11. The first, or precursor flow, develops as the air in the gun tube is forced out ahead of the accelerating projectile. The second, or propellant gas flow, develops when these high pressure gases are released following projectile separation. The muzzle pressures associated with these two flows are vastly different. For example, at the lowest launch velocity tested, V_p = 280 m/s, the precursor muzzle

---

16. *Principles of Explosive Behavior, AMCP 706-180, Army Materiel Command, Washington, D. C., 1972.*

The lack of ability to measure the inward propagation of the recovery shock is partially due to the use of rather insensitive transducers required to measure and survive the peak muzzle pressure. To measure the low pressure phenomena near the end of the emptying cycle, more sensitive transducers would be required.

pressure is approximately 2.5 atmospheres (Figure 12) compared to a propellant gas muzzle pressure of 27 atmospheres. For the highest launch velocity tested, V_p = 1050 m/s, the precursor muzzle pressure is 15 atmospheres and the propellant gas muzzle pressure is 287 atmospheres. The order of magnitude change in pressure at the muzzle following shot ejection results in a rapid expansion of the propellant gases over the projectile and through the boundaries of the precursor jet. However, the presence of the precursor flow does effect the development of the propellant gas blast. Since the propellant gas expands into a heated, moving precursor flow, the initial conditions for the formation of the blast are not those of an expansion into a static ambient; rather, both spatial and temporal variations in the ambient are present. The precursor/propellant gas interactions can be observed through examination of the optical data.

A series of spark shadowgraphs were taken to demonstrate the variation in structure of the precursor flow and in the nature of the precursor/propellant gas interaction with launch velocity, Figures 13a - 13e. At the lower launch velocities, the precursor flow begins very early in the launch process. This is due to the high propagation velocity of the shock wave relative to the projectile velocity (note: the acoustic speed is 335 m/s compared to the launch velocity of 280 m/s). At the lowest launch velocity (Figure 13a) the precursor flow exhausts at low pressure and the shock structure of a slightly underexpanded jet is observed; however, downstream of the supersonic portion of the flow, an extensive, subsonic, turbulent jet is seen. At the time of shot ejection, the leading front of this turbulent jet is 14 calibres from the muzzle. When the propellant gases expand behind the projectile, a blast wave is formed in the undisturbed air external to the precursor jet; however, along the axis, no density discontinuity is observed. Apparently, the higher wave speed in the moving, heated turbulent jet combined with the blocking effect of the projectile either prevents the formation of the shock wave on axis or sufficiently weakens it that it can not be observed with the optics employed in the experiment.

As the launch velocity is increased, greater compression occurs in the precursor gases. This results in a shortening of the downrange propagation of the flow prior to shot ejection. The increased exit pressure of the precursor flow provides greater lateral speading of the jet and an enlarged supersonic core. The higher propellant gas pressures develop a stronger blast and the shock wave is clearly seen to develop along the axis; although a definite forward bulge is seen in Figures 13b and c. At the highest launch velocity tested, the interaction between the precursor and propellant gas flow changes from predominantly a long region of limited interaction along the axis of symmetry to a shorter region of extensive interaction throughout the flow. Literally, the whole front portion of the blast wave experiences significant distortion.

15

The trajectories of the Mach disc, propellant gas/air contact surface, and blast wave along the axis of symmetry have been measured from the spark shadowgraphs (Figures 14a-14e). In the lower velocity cases, the blast wave was located by measuring the radial distance of the spherical portion of the front from the muzzle. For the high velocity cases, Figures 14d and 14e, this was not practical and the blast wave position is the distance from the muzzle to the point on the front nearest the axis of symmetry. The position of the contact surface can not be accurately measured in the spark shadowgraphs due to obscuration of the axis by intervening layers of turbulent, opaque propellant gas in the higher velocity, lateral shear layers of the jet.

Also shown on these figures are the predictions of the one-dimensional analysis of Erdos and Del Guidice[2]. For the low velocity cases, the agreement between theory and experiment is good; however, for the higher velocities, the prediction is in error. The reason for this discrepancy is the failure of the model to account for interactions between the precursor and propellant gas flows. As noted above, these interactions produce forward bulges in the blast wave which were removed from the low velocity data during reduction, but of necessity remain in the high velocity results. The disagreement in the Mach disc trajectories reflects the lower pressure level behind the blast wave in the actual interacting case.

To further explore this behavior, the gun tube was sealed and a vacuum was drawn in the air ahead of the projectile prior to the weapon being fired. A cellophane diaphragm was placed across the muzzle and an "O" ring was placed around the projectile forward of the rotating band. This arrangement permitted the gun tube to be evacuated to 30 μm Hg prior to firing and effectively eliminated the precursor flow, Figure 15. Only a weak shock propagates from the small amount of precursor gas ejected prior to projectile exit. The propellant gases rapidly expand through this precursor and form a clearly undisturbed blast. The trajectories of the blast wave and contact surface were measured, Figure 16; however, the Mach disc could not be observed in the photographs due to opacity of the exhaust flow. The agreement between theory and the trajectories from the evacuated tube is greatly improved over that previously obtained.

The influence of the precursor-propellant gas interaction on the strength of the blast wave was examined through pressure probing. A stagnation pressure transducer was placed 60mm from the muzzle along a ray making a 40° angle to the axis of symmetry (Figure 15). Pressures were measured for the evacuated and ambient tube (Figure 17).

For the evacuated tube there is no measurable precursor blast. The propellant gas blast arrives and reflects from the probe generating a peak pressure of 94 atmospheres. The propellant gas jet then impinges on the probe and a quasi-steady decay of pressure ensues as

16

the gun tube empties. In the case of the ambient tube, the precursor blast is clearly seen. The peak pressure behind the propellant gas blast reaches a value of 57 atmospheres prior to arrival of the propellant gas jet. The comparison of the two peak (94 versus 57 atmospheres) clearly shows that the presence of the precursor flow provides a higher velocity, higher temperature medium within which the blast wave strength does not reach "undisturbed" or evacuated tube values. The theoretical prediction[2] for the reflected shock overpressure is 74.8 atmospheres. While higher than the measured value for the ambient tube, this pressure is lower than measured for the case with a pitot probe in front of the evacuated tube.

While it is not clear what effect the precursor/propellant gas interaction has upon far field blast, it will have a significant influence on near muzzle gasdynamics and in particular upon muzzle device flows. The peak loadings upon a muzzle brake are due to impingement and reflection of the propellant gas blast[17]; thus, a computation of this phenomena which treats only the propellant gas blast would overpredict pressure levels. While this does provide a built-in structural safety factor if design is based on such a code, the existence of the interacting flows should be noted if quantitative comparison between theory and experiment is attempted.

V. BLAST FIELD AND CORRELATION

The static pressure levels in the blast wave were measured for all test conditions. Figures 18a-18e present contours of peak overpressure, where

$$\overline{\Delta p} = (p - p_\infty)/p_\infty$$

As expected the pressure is greater at the same position in the field for the higher launch velocity cases than for the lower velocities.

The geometric similarity in the overpressure contours for the five launch velocities tested suggests that some scaling or correlation parameter should be capable of unifying these results. Smith[8] introduces a dimensional scaling parameter to account for variations in gun barrel length (which alters the exit velocity), altitude, gun platform velocity, and propellant. His correlation also accounts for azimuthal variation of overpressure; however, the relationship has been used only with a 7.62mm rifle pressure field. Westine[18] proposes a scaling

17. *E. M. Schmidt, E. J. Gion, and K. S. Fansler, "Measurement of and in the Muzzle Blast of 20mm Cannon," 4th International Symposium on Ballistics, Monterey, CA, ADPA, Washington, D.C., October 1978.*

18. *P. Westine, "The Blast Field About the Muzzle of Guns," Shock and Vibration Bulletin, Vol. 39, Part 6, March 1969, pp. 139-149.*

of the overpressure parameter at geometrically similar positions in the blast field.

Essentially, Westine defines a non-dimensional parameter,

$$\phi = \Delta p \; D^2 L/W$$

where

D, L = gun tube diameter, length

$$W = E - m_p V_p^2/2$$

= energy of propellant less the projectile kinetic energy at launch

His scaling law states that at identically scaled locations in the blast field (X/D, r/D) the value of the parameter, ϕ, will be equal to that of the standard weapon.

The strength of this correlation parameter may be examined by attempting to scale the measured overpressures along the 90° radial from the muzzle (Figure 19). These data have been collapsed using the parameter, ϕ, and are compared with Westine's standard (Figure 20). The full range of launch velocities is included in the spread of the symbol representing the present data. Westine's parameter succeeds in collapsing the relatively wide spread in the overpressure data shown in Figure 19 into a more systematic presentation; however, the curve representing the standard scaling law falls outside the spread.

An alternative form of scaling involves stretching the geometric coordinates in accordance with the strength of the source. In the case of a gun, the blast is driven by the expanding propellant gases which themselves have a definite structure. The development of the Mach disc is interesting to examine for use as a dimensional scaling parameter in that it reflects the initial unsteady nature of the flow and the subsequent quasi-steady decay of the supersonic jet structure as the gun tube empties. The stabilized location of the Mach disc can be determined from the spark shadowgraphs and compared with the empirical relationship for steady jets[19]:

$$X/D = 0.7 \; M_e \; (\gamma p_e/p_\infty)^{1/2}$$

where M_e is the exit Mach number of the flow behind the projectile and

---

19. C. H. Lewis and D. J. Carlson, "Normal Shock Locations in Underexpanded Gas and Gas-Particle Jets," AIAA J., Vol. 2, No. 4, April 1964, pp. 776-777.

18

p_e is the exit pressure. The value of M_e must always be greater than one. For subsonic exit Mach numbers, the one-dimensional expansion to sonic exit conditions must be computed. In which case,

$$X/D = 0.7 \ (\gamma p^*/p_\infty)^{1/2}$$

For the muzzle jet of the 20mm cannon used in the current tests, the Mach disc has been measured and is compared with the predictions of the above relationships using the tabulated exit properties:

TABLE II. Mach Disc Locations

V_p (m/s)	280	463	615	775	1050
$X/D_{comp.}$	3.0	5.2	7.9	10.8	15.8
$X/D_{meas.}$	2.6	5.6	8.0	10.8	

The comparison of the predicted Mach disc location (using the correlation and gun tube exit conditions from Table I) and measured values is good. For the highest velocity case, data was not taken at times long enough for the Mach disc to stabilize.

Using the stabilized positions of the Mach disc from the above table, the overpressure variations of the 20mm blast tests (Figure 19) were scaled (Figure 21). The resulting correlation of the data is seen to be reasonably good. However, the extent of the data in terms of pressure levels, positions in the blast field, and gun types does not permit generalization of conclusions regarding the universal applicability of this scaling parameter.

VI. PLATE SURFACE PRESSURE DATA

A. Vertical Plate*.

In this series of tests, the plate was aligned perpendicular to the axis of the gun (Figure 4) The launch velocity tested was 615 m/s. Data was taken of the surface pressure on the plate at several axial stations from 0.5 through 8.0 calibers from the muzzle. The first

---

*Some of these data have been reported previously[17]; however, repetition is made for the sake of completeness.

transducer is located 0.02 m (1 caliber) from the axis of symmetry
with the others set at 0.01 m intervals. The measured pressure traces
are all quite similar (Figure 22). Initially, there is a rapid increase
in pressure when the blast arrives at and is reflected from the plate.
The pressure level reached is the maximum in the emptying cycle. Expan-
sion of the blast causes the pressure to drop. The initial, highly
transient portion of the flow lasts for 50 - 100 μs, until the pro-
pellant gases arrive and are deflected by the surface. Once the pro-
pellant gas jet impinges upon the surface, the pressure levels stabilize
and decay at relatively slow rate dependent upon the variation of muzzle
exit conditions during gun tube emptying.

The quasi-steady nature of the flow field within the jet core can
be demonstrated by using muzzle exit properties, which change in time,
as reference parameters to non-dimensionalize data acquired on the plate
surface. The pressure variation on the plate surface as a function of
time is shown in Figure 23. The plate is located 1.5 calibers from the
muzzle and the gauge station is 1.5 calibers off the line of fire. The
data are for three different launch velocities and include only pressure
values following the peak blast loading; i.e., plume impingement pressure
is shown. The variation in pressure with time is significant, particu-
larly with the data for the high velocity launch. If the pressure on
the plate surface is normalized by the muzzle exit pressure as measured
at equivalent time (Figure 8) temporal variations in the resulting non-
dimensional pressure parameter, p/p_m, are nearly eliminated, Figure 24.

In addition, the data from the three different launch velocities are
collapsed to a single value, $p/p_m \doteq 0.068$. This result is not un-
expected since the flow within the core of a supersonic jet (within
the bounding shock waves, Figure 11) has been demonstrated[20] to be
independent of boundary conditions other than those at the nozzle exit
or origin of the plume. In addition, the only exit parameters needed
to uniquely define this core flow are the exit Mach number and ratio
of specific heats. The nozzle exit pressure ration, p_e/p_∞, enters into
consideration only in the determination of the geometric extent of this
core flow.

20. P. Owen and C. Thornhill, "The Flow in an Axially Symmetric
    Supersonic Jet from a Nearly Sonic Orifice into a Vacuum,"
    R 30/48, Royal Armament Research and Development Establishment,
    Kent, UK, 1948. AD 57 261.

The property distribution within the supersonic core of a jet typical of a muzzle exhaust plume have been computed by the method of characteristics[21]. The centerline variations of some important parameters are presented in Figure 25 with the centerline variation of Mach number being given below, Table III.

Table III. Centerline Variation of Mach Number for an Axially Symmetric Jet ($M_e = 1.0$, $\theta_e = 0°$, $\gamma = 1.25$, $p_e/p_\infty = 500$)

X/D	M	X/D	M	X/D	M	X/D	M
0	1.0	1.5	3.09	4.5	4.88	8.0	6.02
0.2	1.15	2.0	3.44	5.0	5.08	9.0	6.30
0.4	1.42	2.5	3.89	5.5	5.26	10.4	6.68
0.6	1.83	3.0	4.18	6.0	5.42	12.6	7.35
0.8	2.20	3.5	4.44	6.5	5.57	13.9	7.72
1.0	2.49	4.0	4.68	7.0	5.72	15.5	8.18

Based on the method of characteristics calculation, Newtonian impact theory was used to estimate the pressure on the plate surface, Figure 24. The theoretical value is somewhat low. This is in part due to the fact that at x/D = 1.5, the centerline Mach number is only 3.09, a value which is not truly hypersonic as required for application of Newtonian theory, i.e., $C_p = 2 \sin^2\theta$. However, similar disagreement has been observed in comparing simple predictions with measured impingement pressures of steady jets[22]. In this case, the failure to accurately model the standoff of the normal shock generated in the plume ahead of the surface was determined to be the origin of the discrepancy.

In the design of muzzle devices, two values of pressure are of particular interest, the maximum and steady state values (Figure 26). The maximum pressure sets the structural strength requirement of any muzzle device, while the steady state value provides the momentum exchange needed to reduce recoil. Both pressures show similar variation

21. A. R. Vick, et al, "Comparison of Experimental Free-Jet Boundaries with Theoretical Results Obtained with the Method of Characteristics," TN D-2327, NASA, June 1964.

22. C. D. Donaldson and R. S. Snedeker, "A Study of Free Jet Impingement," Journal of Fluid Mechanics, Vol. 45, Part 2, 1971, pp. 281-319.

across the plate. At a given axial station, there is a rapid decay of pressure in the direction of increased radius. In fact, at stations $X/D = 0.5$, 1.0, 1.5, and 2.0, the steady state pressure drops to sub-atmospheric values at extreme radial locations. Carling and Hunt[23] indicate that for supersonic jet impingement on flat surfaces without central holes, the flow expands from subsonic conditions behind the normal shock on the axis through a sonic line to supersonic velocities near the outer edges. This produces overexpansion to pressure below ambient and recovery occurs through a series of shock waves. In the present data, overexpansion was observed; however, sufficient instrumentation was not available to observe the details of the recovery process.

For practical application as a muzzle device, the outermost extent of the transducers, $r/D = 3.5$, is beyond the limit of size and weight. Yet, it is interesting to note the additional constraint imposed by the basic flow, i.e., increased baffle radius can produce decreased efficiency in recoil reduction due to overexpansion of the flow.

At $X/D = 6.0$ and 8.0, the maximum pressure profiles (Figure 26) do not show monotonic decay across the plate. Apparently, this behavior is caused by the bifurcation of the shock system (Figure 13c). Near the axis, the forward protuberance reflects from the surface, whereas at greater radii, the main blast reflects generating the secondary peak in pressure.

The pressure history at a given station may be estimated by using the analysis of Erdos and Del Guidice[2] in conjunction with the method of characteristics computation of the supersonic core[21]. For the launch conditions under consideration, the predictions of Erdos and Del Guidice, see Figure 14c, are in reasonable agreement with the measured discontinuity trajectories. For a given location of the plate, the relative geometry between its surface and the spherical shock may be determined. The peak pressure behind the shock is estimated using reflection coefficients from nuclear blast research[24]. The duration of the unsteady pulse can be determined as the period between arrival of the blast and arrival of the Mach disc. The steady state pressure may be estimated from the method of characteristics computation of the supersonic core of the jet, from the relative geometry, and from Newtonian theory. A simple linear

23. J. Carling and B. Hunt, "The Near Wall Jet of a Normally Impinging, Uniform, Axisymmetric, Supersonic Jet," JFM, Vol. 66, 1974, pp. 159-176.

24. S. Glasstone (ed), The Effects of Nuclear Weapons, AEC, Government Printing Office, Washington, D.C., 1976.

22

extrapolation between the peak and steady state values, while accounting
for the pulse width, produces the prediction of Figure 27. While the
agreement between the estimate and measurement is good for the steady
state value, the peak is too high in the predicted case. As has been
previously discussed, this overprediction is due to the fact that the
theory does not treat the effects of precursor-propellant gas inter-
actions. Another problem lies with difficulties in obtaining a con-
verged starting solution using the Erdos model. The code uses a
starting algorithm which requires approximately two calibres of blast
wave travel prior to convergence; thus, with actual brakes having
baffles located closer to the muzzle than this distance, the reflection
approach used here would fail.

The steady state pressure levels across the plate surface for two
different axial stations are compared with the Newtonian approximation
in Figure 28. The agreement is quite good. Similar results have been
reported by Eastman and Radtke[25] in examining steady jet impingement on
surfaces. An obvious difficulty in directly applying this simple
calculation procedure to an actual weapon muzzle device such as a recoil
brake is the failure to account for attachment cowls. The present data
were acquired for a free jet impinging upon a plane baffle. For an
actual cannon, the baffle surfaces must be connected to the weapon in
some manner. The resulting attachment devices act as nozzles to
influence the development of the exhaust plume. The alternation of
the flow must be accounted for in attempting to design a muzzle device
for strength or efficiency.

B. Inclined Plate.

In a second series of tests on the plate, its axis of symmetry was
inclined at an angle of $40°$ with respect to the gun tube axis. This
generates a three dimensional geometry in the flow over the plate
surface. These experiments were a simulation of the muzzle flow over
a compensator device. Tests were conducted at a launch velocity of
775 m/s.

The hole for the projectile passage required enlargement, thereby
eliminating the first gage station at r/D = 1.0. Additional stations
were installed at six radial locations from r/D = 4.0 to 6.5. The
axial location of the plate was varied from X/D = 1.25 to 5.0. The
surface was rotated about its axis of symmetry to provide full azimuthal
coverage, from $\Psi = 0°$ to $180°$ (Figure 3).

---

25. D. W. Eastman and L. P. Radtke, "Flow Field of an Exhaust Plume
     Impinging on a Simulated Lunar Surface," AIAA J., Vol. 1, No. 6,
     June 1963, pp 1430-1431.

The pressure-time histories on the plate surface are similar to
those obtained in the vertical plate tests. An initial peak is observed
corresponding to the arrival and reflection of the blast wave at the
plate surface. This is followed by a decay in pressure to the quasi-
steady plateau value corresponding to immersion of the plate in the
core of the exhaust plume. The maximum and the (quasi-) steady state
pressures are plotted in Figures 29 and 30 respectively. Each graph
contains a series of curves corresponding to a single axial station
but different azimuthal generators of the plate surface. The coordinate,
s, is the distance along the surface.

The distributions of maximum and steady state pressures are
similar. The highest pressure is recorded along the $\Psi = 180°$ ray since
the angle of incidence of the flow passes through $90°$ surface is in
closest proximity to the weapon muzzle along the ray. The rapid decay
in pressure along rays is due to decreasing incidence angle and in-
creasing expansion of the flow off the axis of symmetry of the jet.
These effects are illustrated by observing contours of streamline
inclination angle, θ, and Mach number obtained from a method of charac-
teristics computation of a steady jet flow (Figure 31).

The properties obtained from the method of characteristics solution
may be used in conjunction with Newtonian theory to estimate the steady
state pressure distributions on the plate surface. This procedure is
discussed in Appendix A and the results of a sample computation are
shown in Figure 32. To better illustrate the surface pressure distri-
butions, the data is plotted along rays from $\Psi = 0°$ to $90°$ with both
positive and negative values of s/D used to indicate the upper and
lower half planes of the flow field, respectively. The agreement
between Newtonian theory and measurement is reasonable. Trends in the
data are clearly delineated. In all cases tested, with the exception
of data for X/D = 5.0, the highest pressures on the surface occurred
at values of s/D less than 1.5; i.e., at positions where no transducers
were located. For X/D = 5.0, however, the peak moves onto the trans-
ducer array and can be observed in both sets of data (Figures 30 and
31) to occur near s/D = 3.0 in the lower half plane ($\Psi = 180°$). The
migration of the peak is associated with the variation in flow properties
with stand-off from the muzzle. At large distances, the flow becomes
increasing more spherically symmetric and, in the limiting case of a
plate having infinite extent with the flow expanding into a vacuum, the
peak would asymptote to the location of the surface normal connecting
the plate and the weapon muzzle.

The data for X/D = 5.0 also shows multiple peaks and plateaus in
the maximum pressure distributions (Figure 30d). These may be associated
with bifurcations in the incident shock or formation of a Mach stem as
the shock incidence angle varies across the plate surface.

24

VII. CONCLUSIONS

Experimental results are presented which define the muzzle exit conditions, free field muzzle blast, and muzzle flow over obstacles for a 20mm cannon. A range of weapon launch conditions are tested in order to establish the changes in the blast field properties associated with changes in exit conditions.

The experimental results show that the effect of precursor/propellant gas interaction should be included if an exact representation of the muzzle flow is desired. This is especially true at higher values of exit pressure and velocity.

Comparison with simple models of the flow field produces reasonable agreement between theory and experiment. The nature of the experimental data makes it ideal for comparison against more exact treatment, e.g., two dimensional, unsteady.

Figure 1. Photograph of Muzzle Adapter for Acoustic Thermometry Measurements

Figure 2. Photograph of Muzzle Adapter for Exit Pressure
Measurements
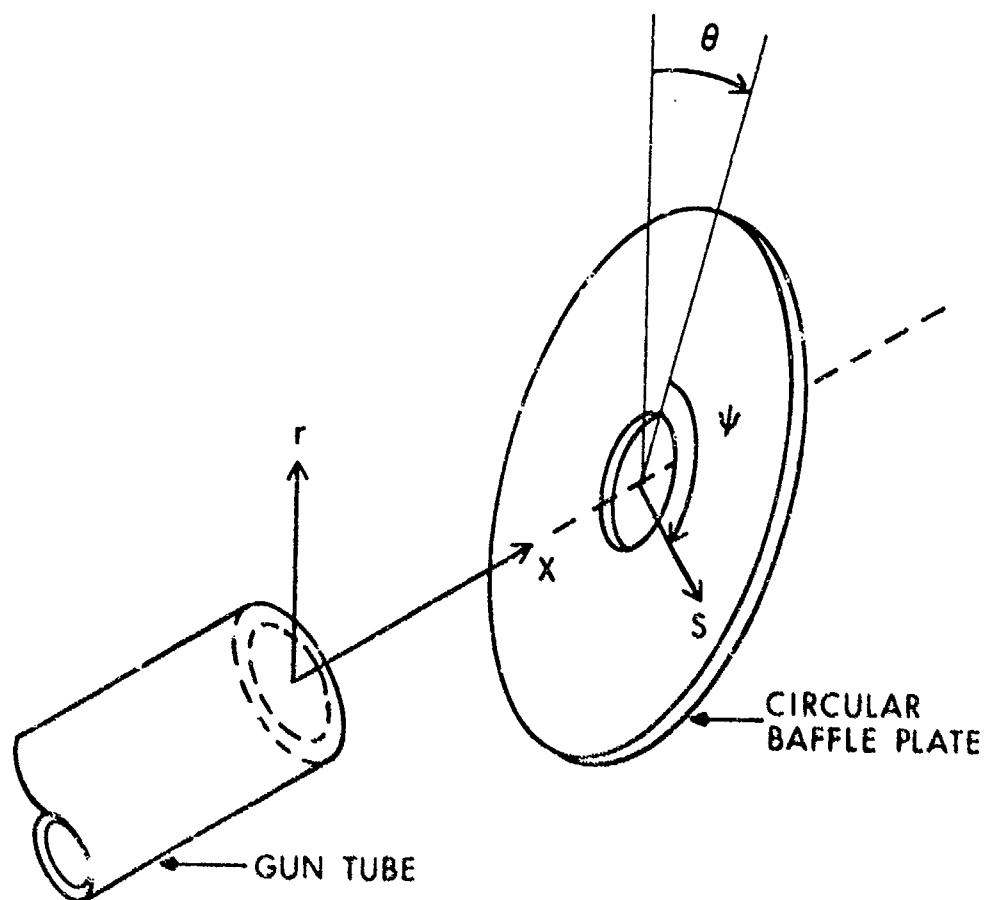
Figure 3. Coordinate System

28

Figure 4. Photograph of Instrumented Plate
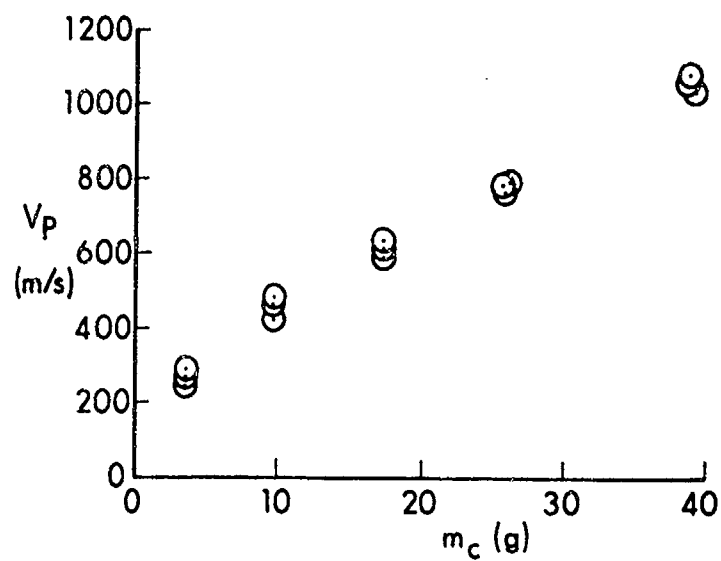
a. Projectile Velocity versus Charge Mass
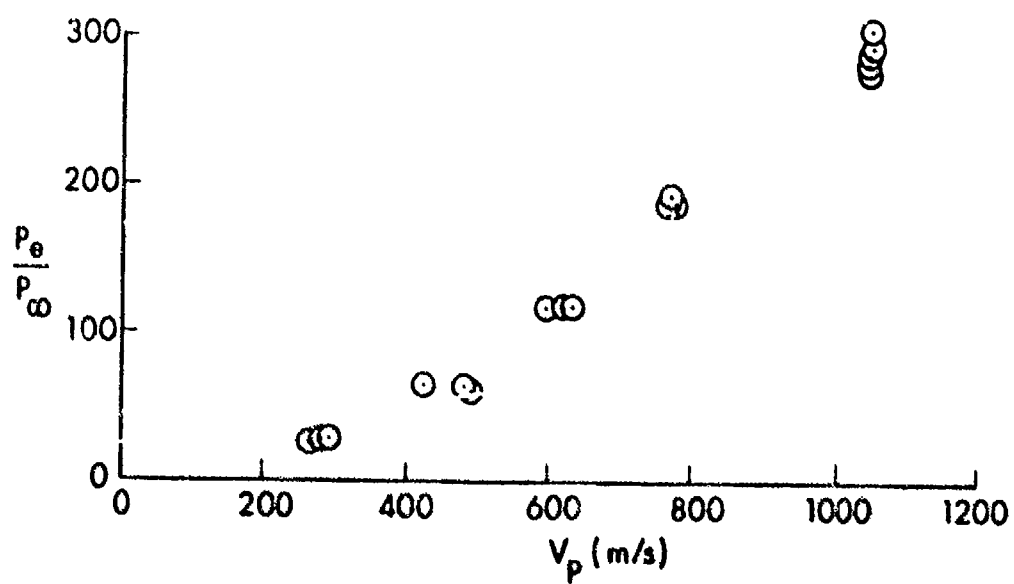
b. Pressure Ratio

Figure 5. Muzzle Exit Conditions

30
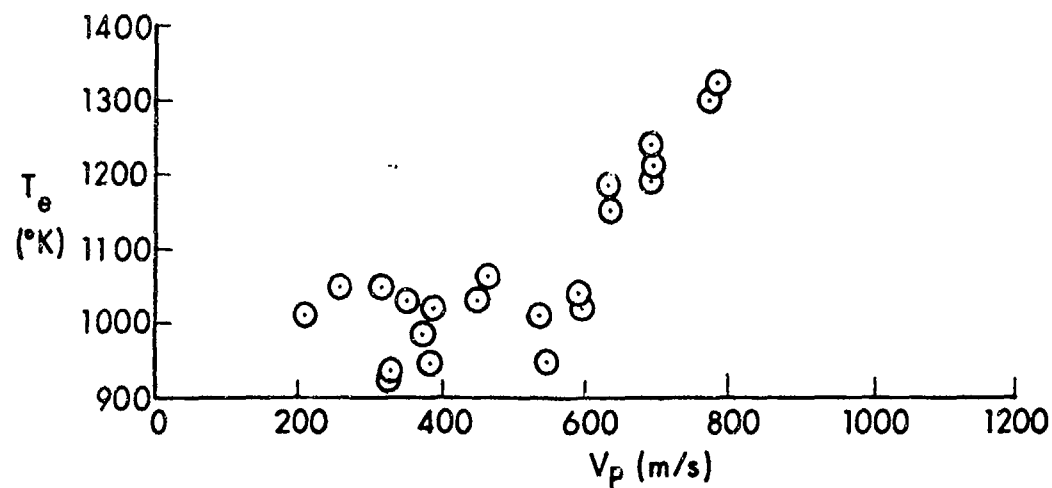
c. Temperature
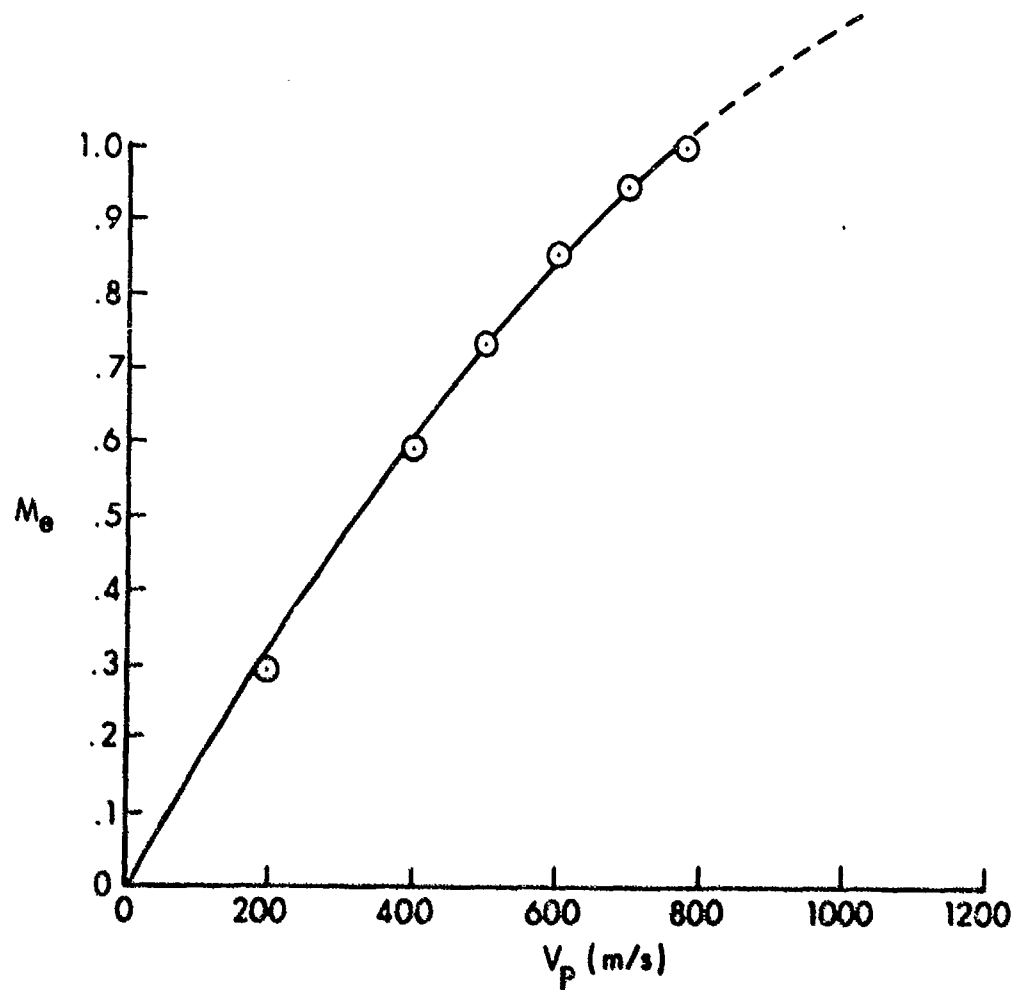
d. Mach Number

Figure 5. Muzzle Exit Conditions
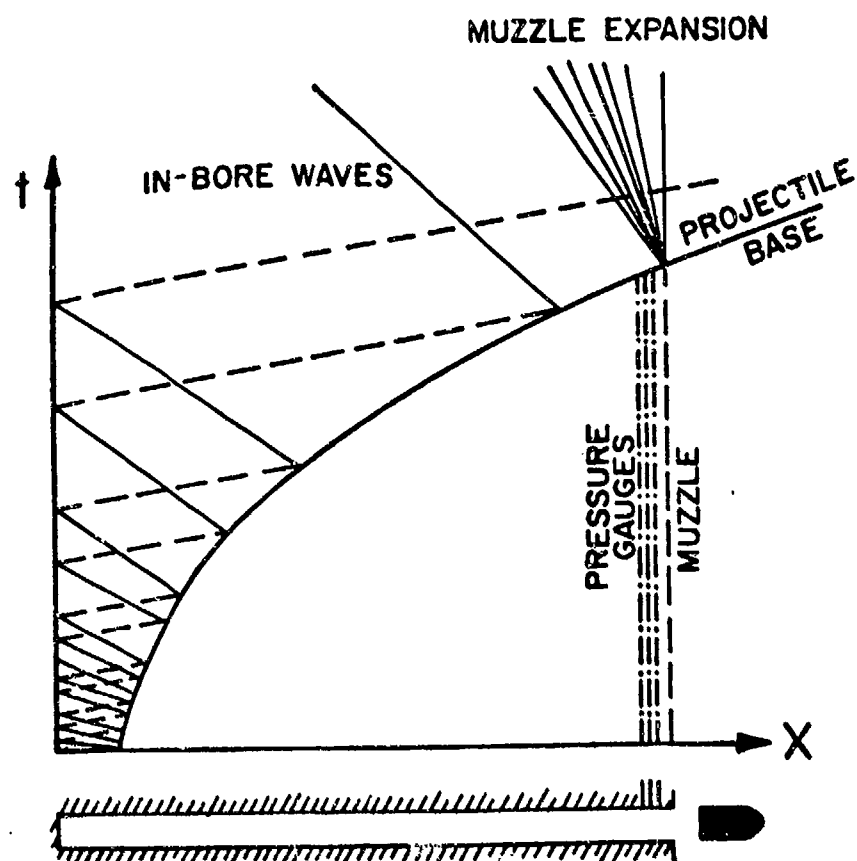
Figure 6. In-bore Wave Diagram

MUZZLE

$$u_e \approx V_p$$
$$a_e$$

IF $u_e < a_e$

AIR BLAST

2-D, UNSTEADY, EXP.

I-D, UNSTEADY, EXP.

$$u_e$$
$$a_e$$

$$c_e$$

SONIC LINE

$$c_e = u_e - a_e$$
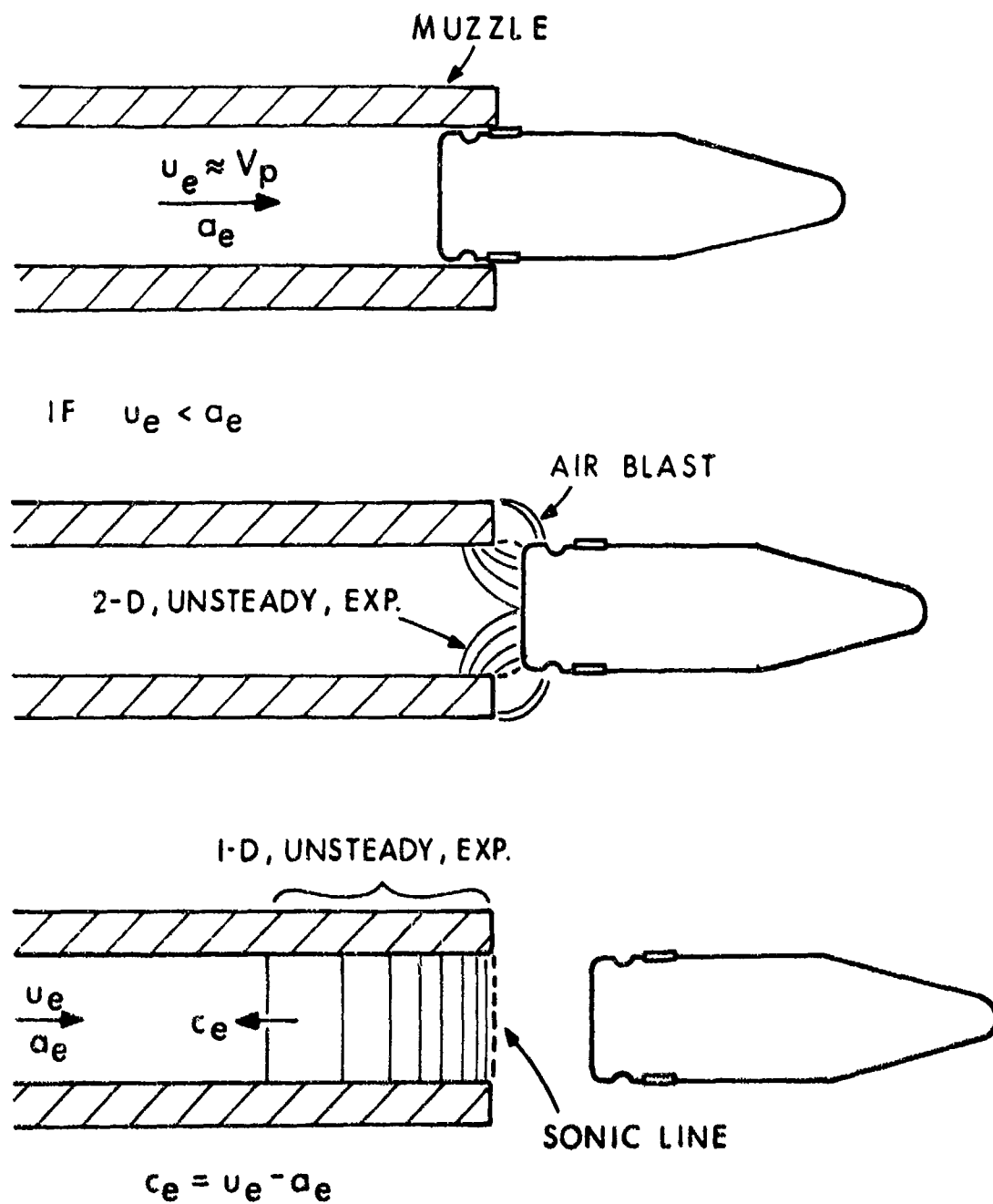
Figure 7. Schematic of Muzzle Expansion

33
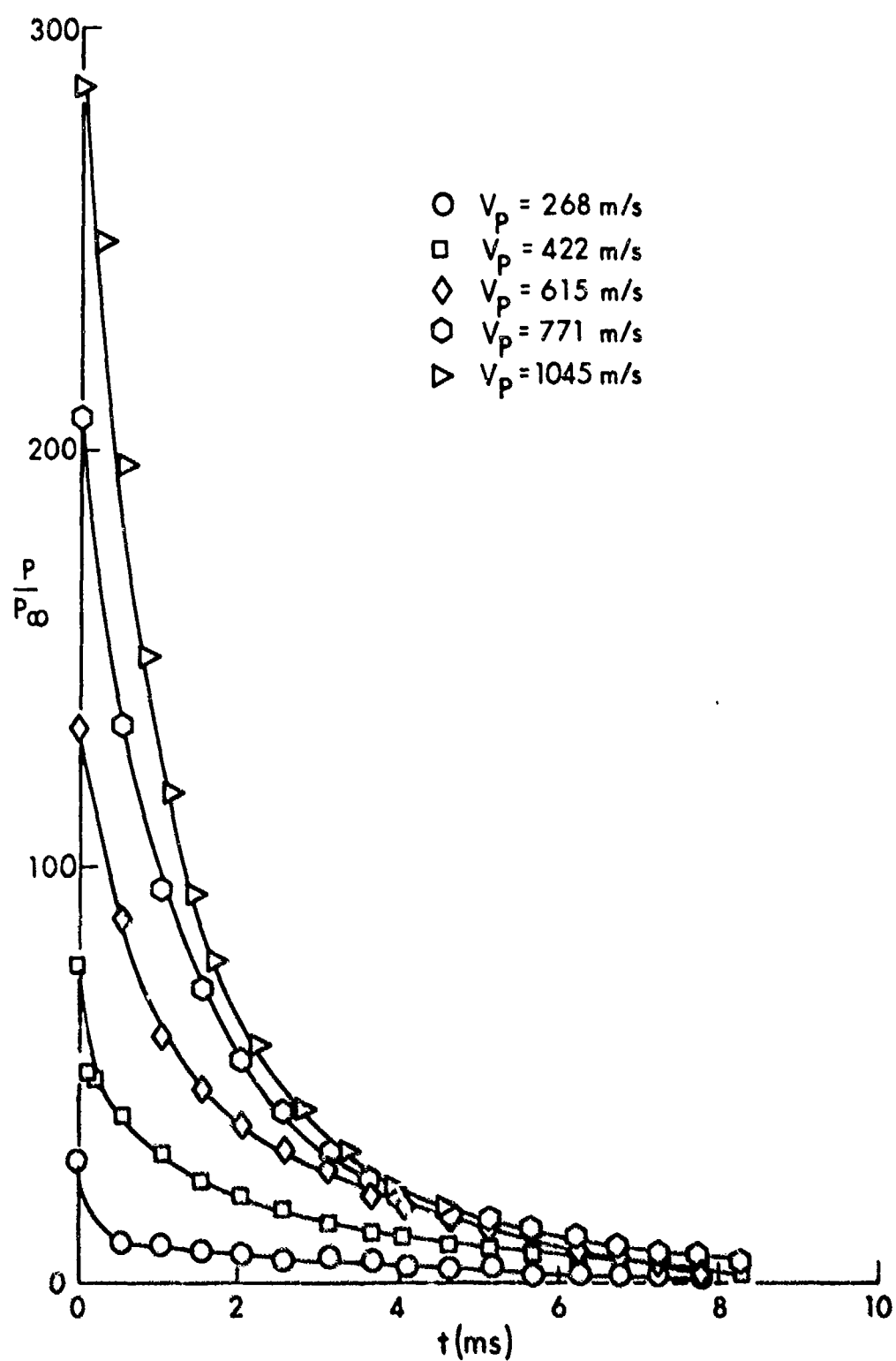
Figure 8. Muzzle Pressure Variation with Time During Gun Tube Emptying
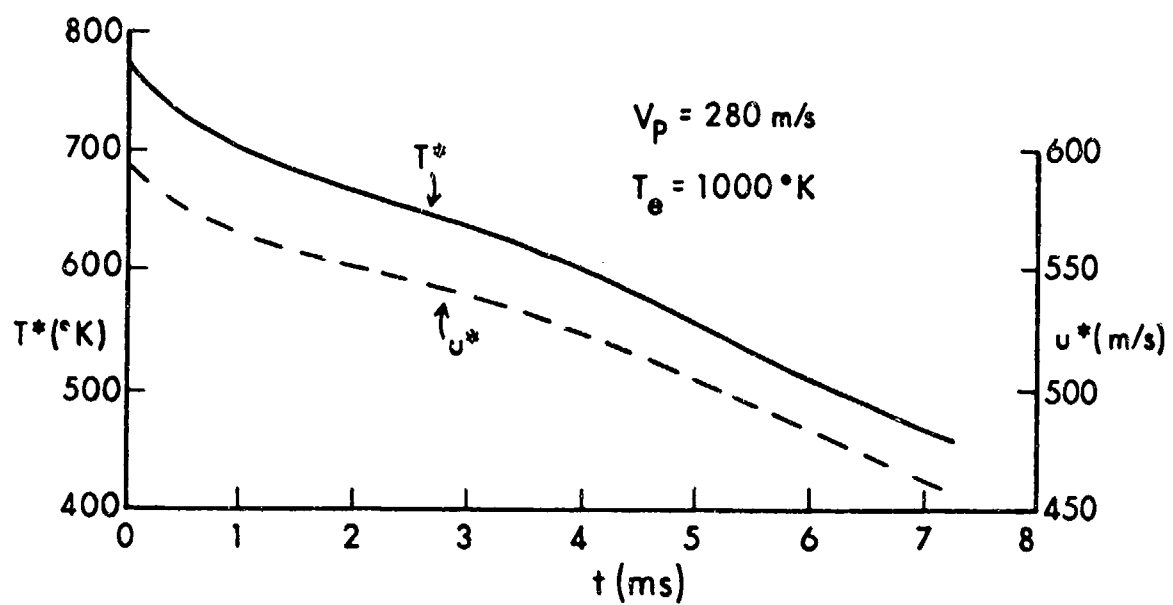
a. V_p = 280 m/s
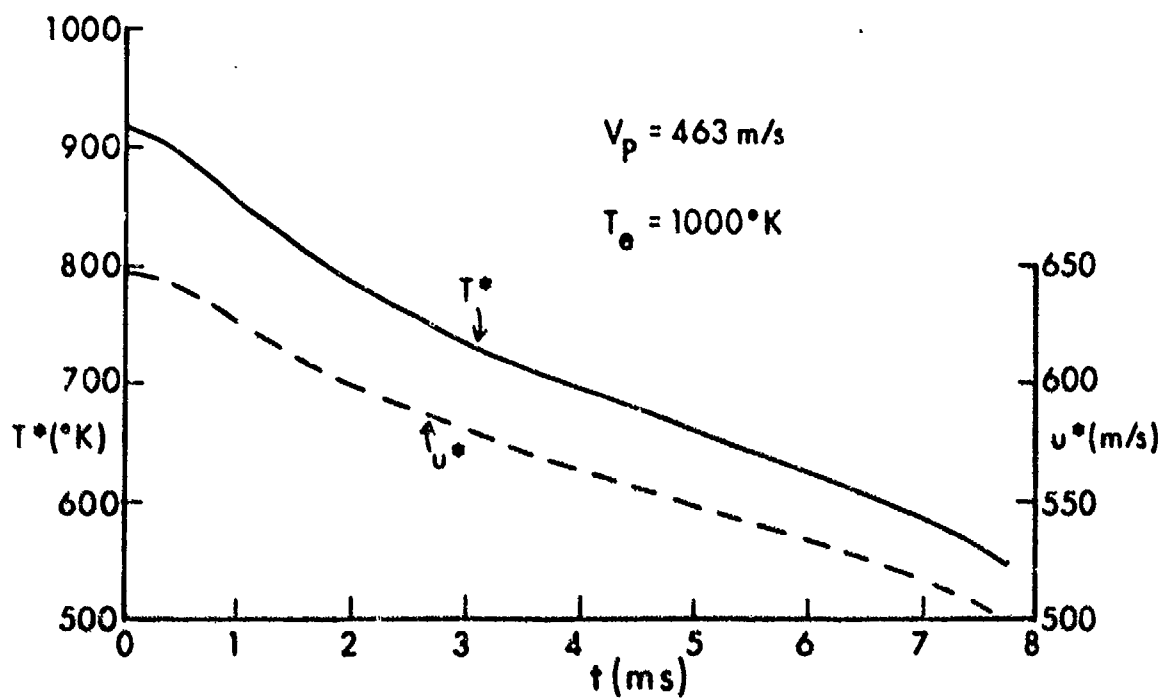
b. V_p = 463 m/s

Figure 9. Muzzle Property Decay

35
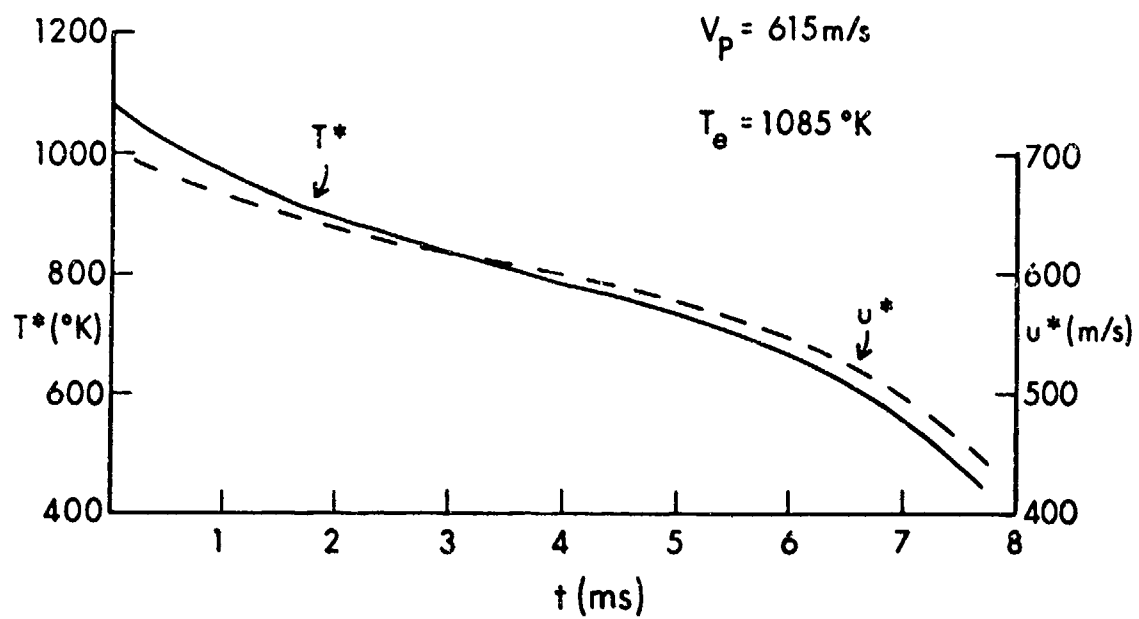
c. V_p = 615 m/s
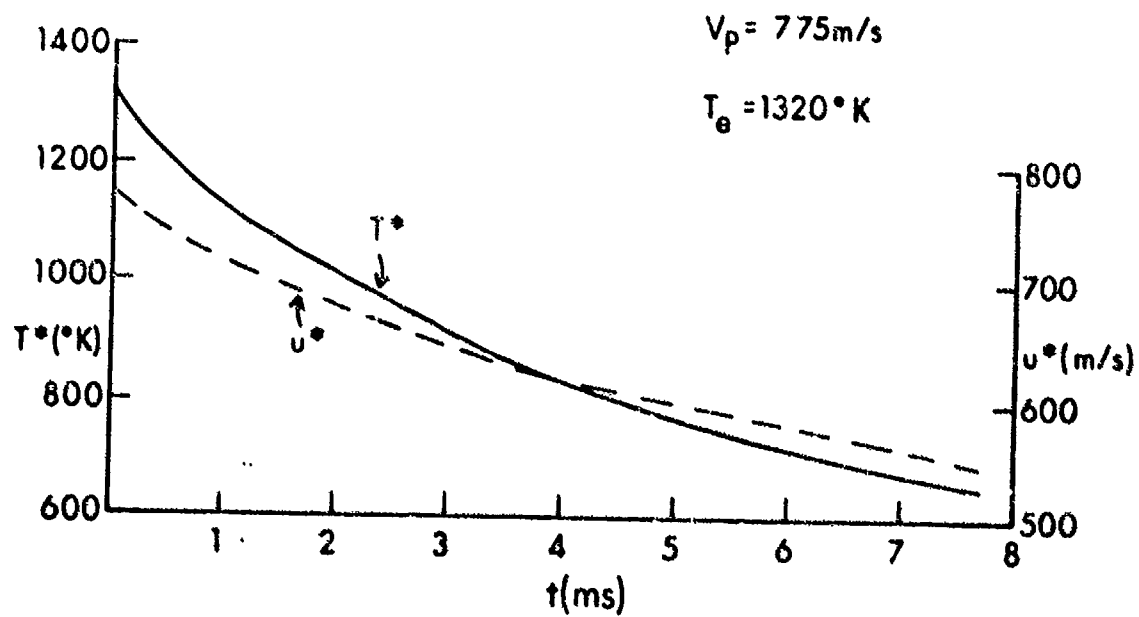
d. V_p = 775 m/s

Figure 9. Muzzle Property Decay

36

$V_p = 1050$ m/s

$T_e = 1705\,°K$
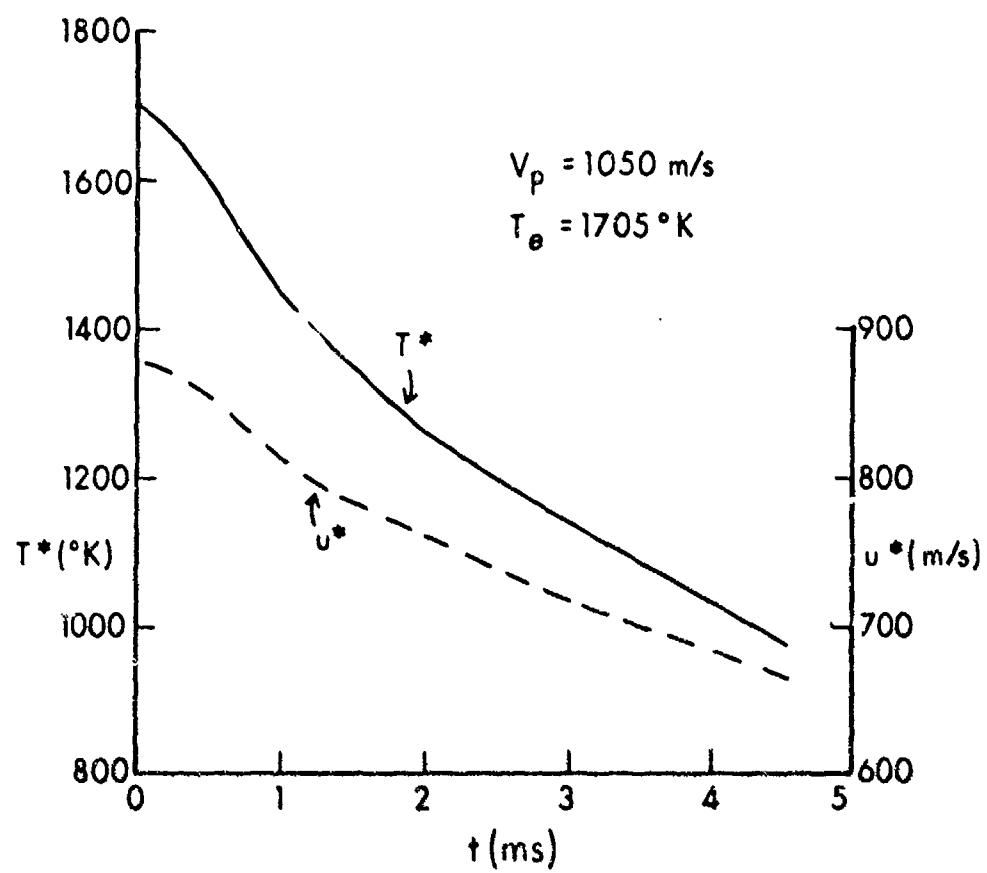
e. $V_p = 1050$ m/s

Figure 9. Muzzle Property Decay

37
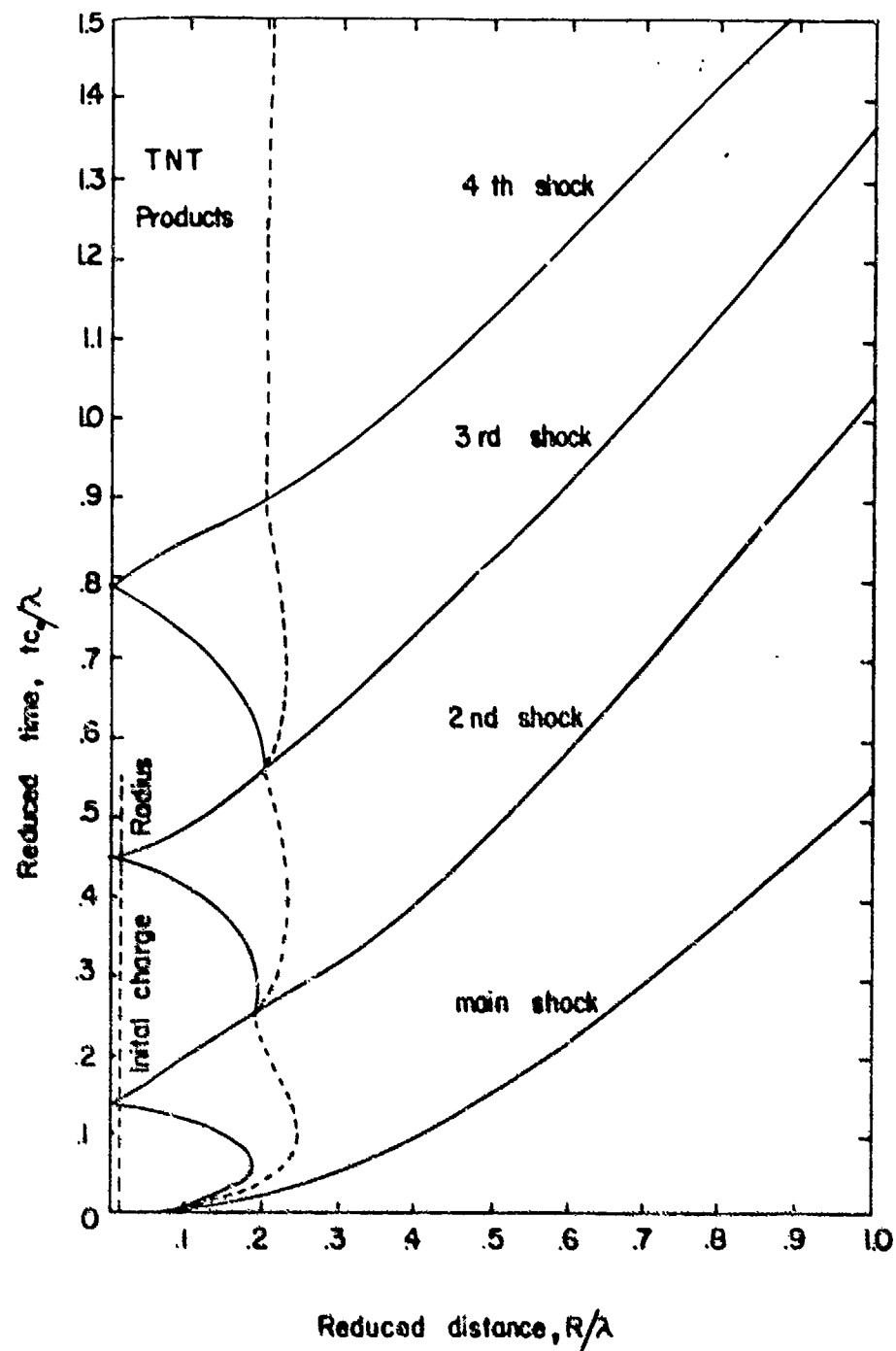
Figure 10. Space-time Diagram for Shocks and Contact Surface for TNT Blast in Air

38
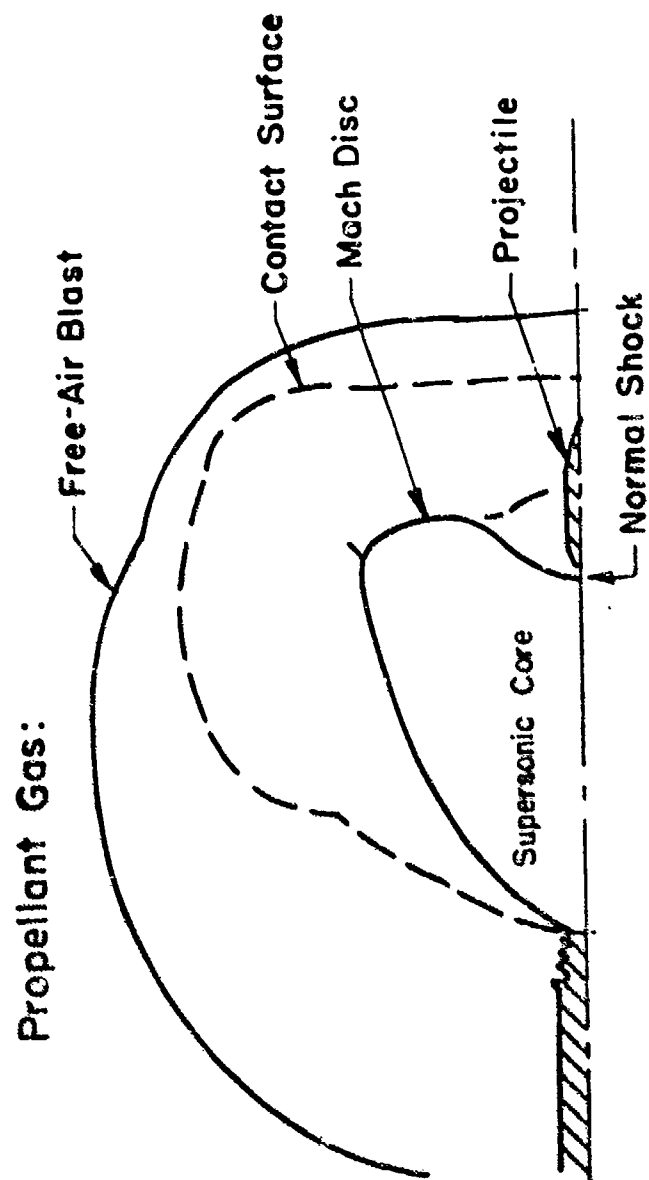
Figure 11. Flow Field Schematic

39
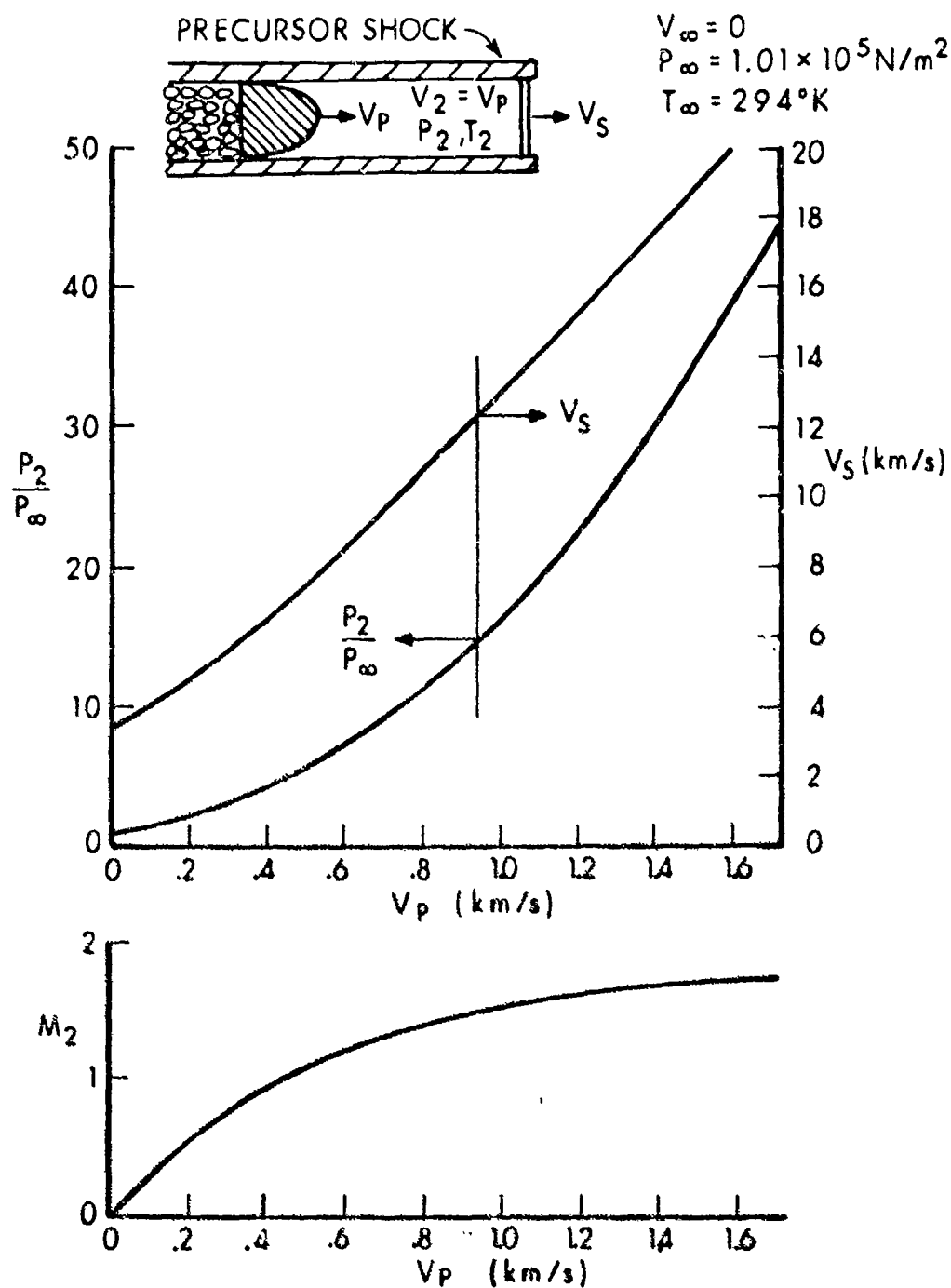
Figure 12.   Precursor Muzzle Flow Properties versus Projectile Launch
            Mach Number

40
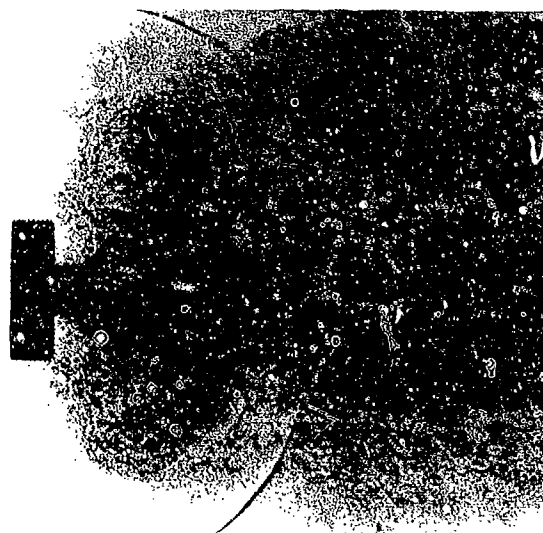
Precursor   Propellant gas

a. $V_p = 280$ m/s
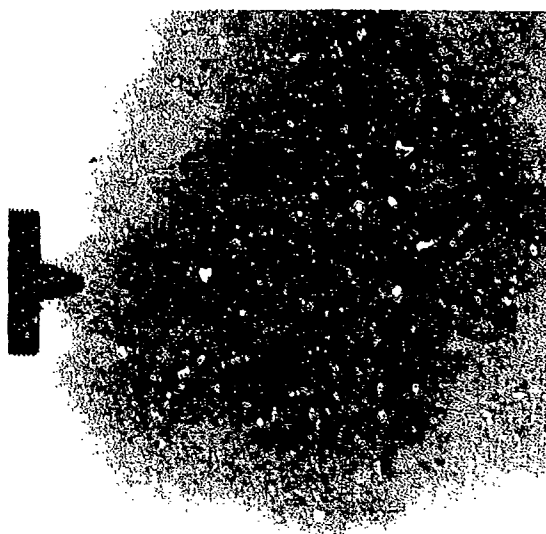
Precursor   Propellant gas

b. $V_p = 463$ m/s

Figure 13.   Spark shadowgraphs of muzzle exit flows illustrating the variation in precursor/propellant gas interaction as muzzle velocity increases

41
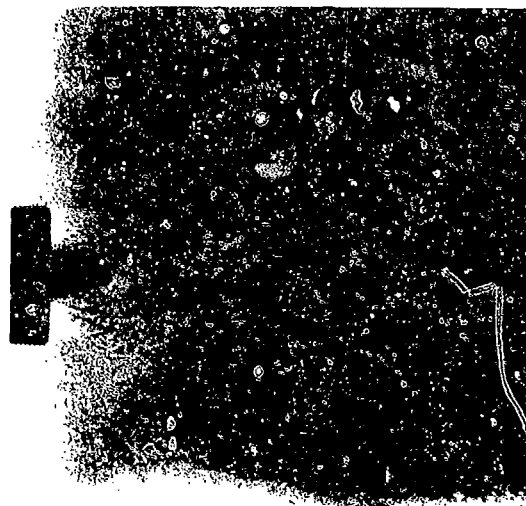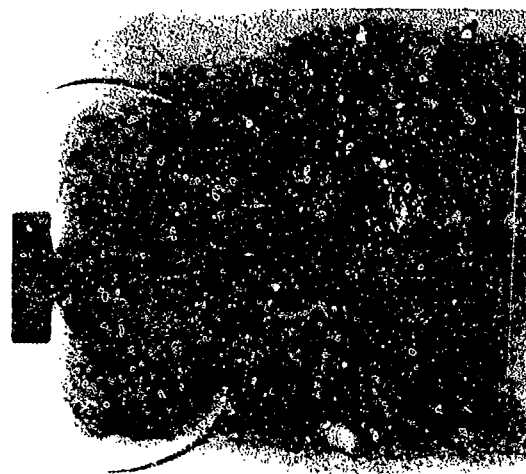
Precursor   Propellant gas

c. $V_p = 615$ m/s
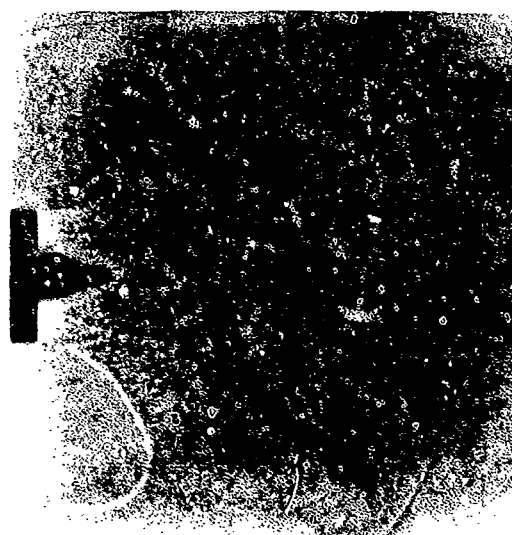
Precursor   Propellant gas

d. $V_p \approx 775$ m/s

Figure 13.   Spark shadowgraphs of muzzle exit flows illustrating the
             variation in precursor/propellant gas interactions as muzzle
             velocity increases

42
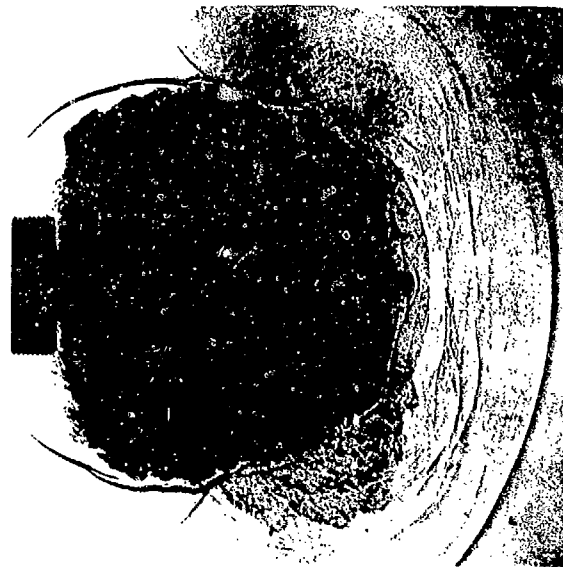
Precursor   Propellant gas

e. V_p = 1050 m/s

Figure 13. Spark shadowgraphs of muzzle exit flows illustrating the
           variation in precursor/propellant gas interactions as muzzle
           velocity increases

Figure 14. Discontinuity Trajectories Along Axis of Symmetry

a. $V_p = 280$ m/s

44
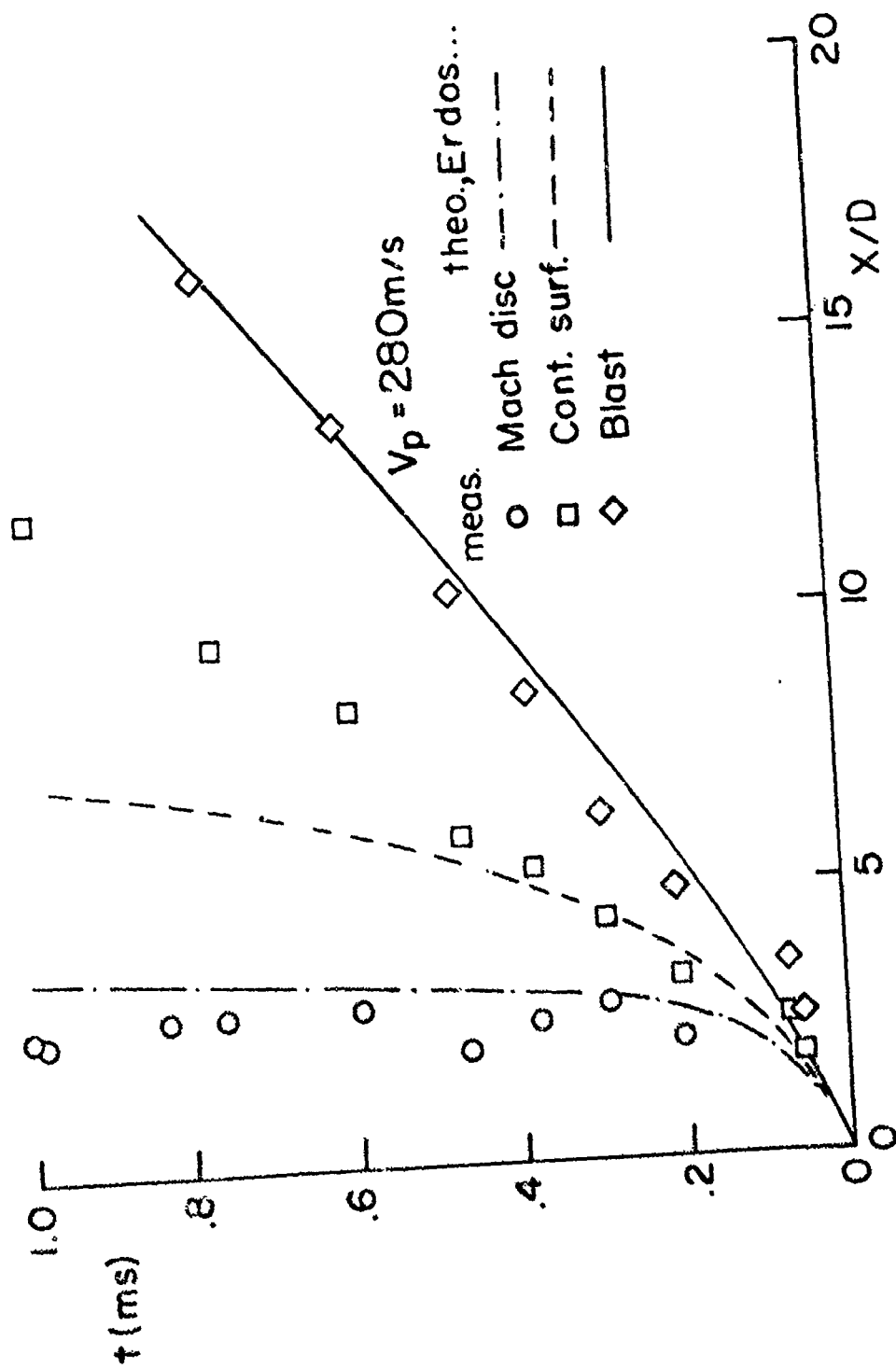
Figure 14. Discontinuity Trajectories Along Axis of Symmetry
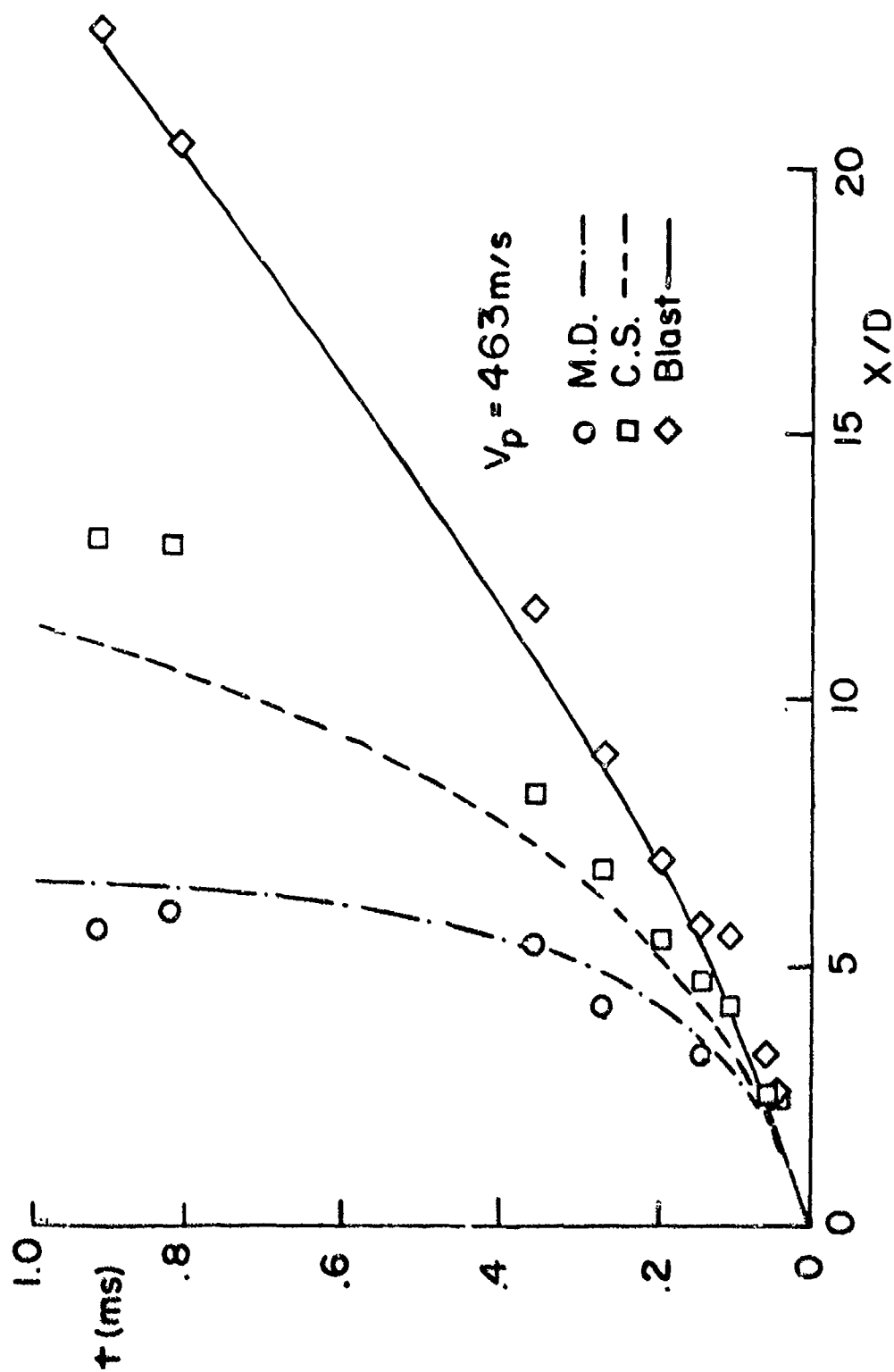
b. V_p = 463 m/s

Figure 14. Discontinuity Trajectories Along Axis of Symmetry
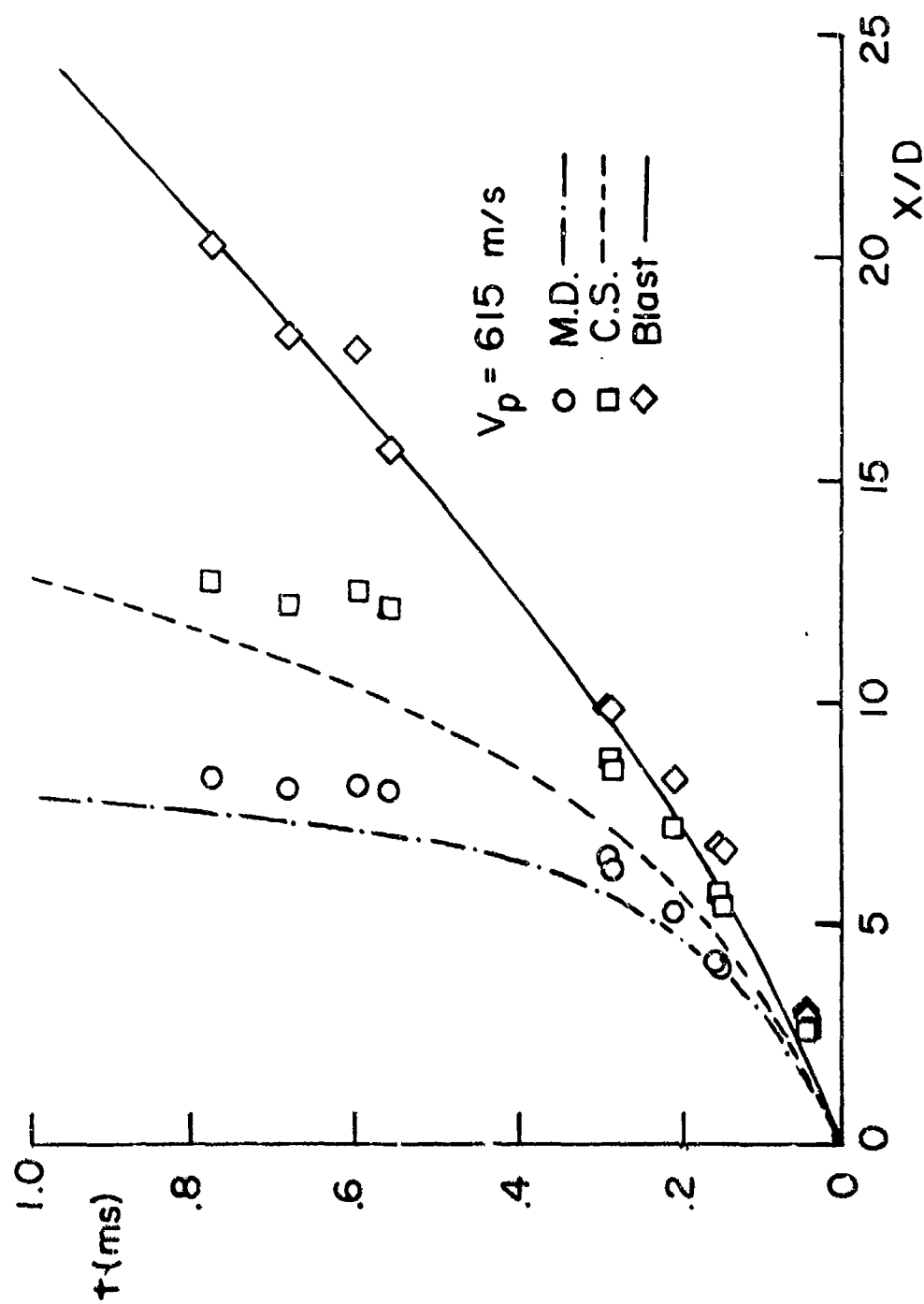
c. $V_p = 615$ m/s

$V_p = 775$ m/s
- o M.D. $-\cdot-$
- □ C.S. $---$
- ◇ Blast $\longrightarrow$
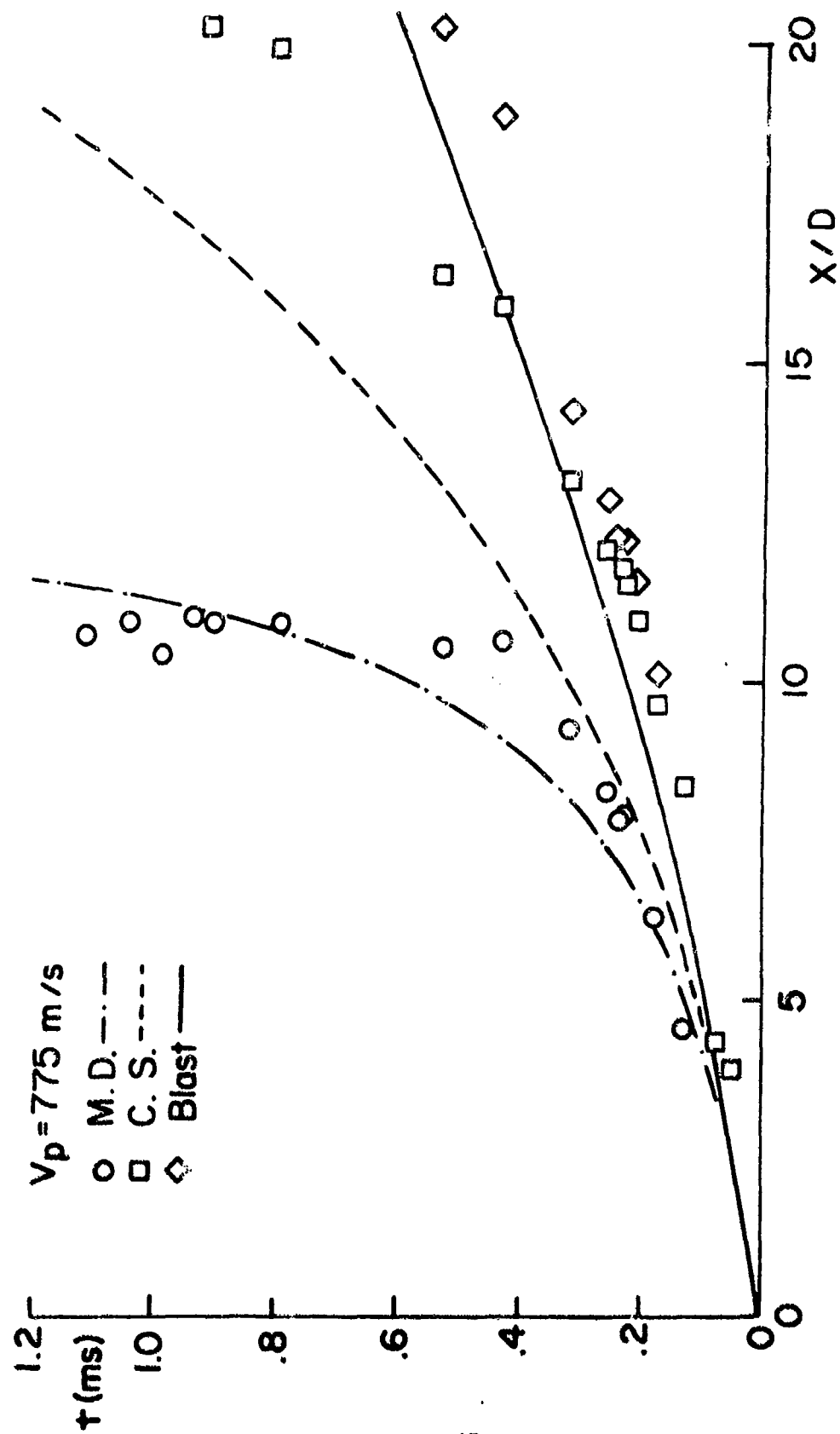
d. $V_p = 775$ m/s

Figure 14. Discontinuity Trajectories Along Axis of Symmetry

47
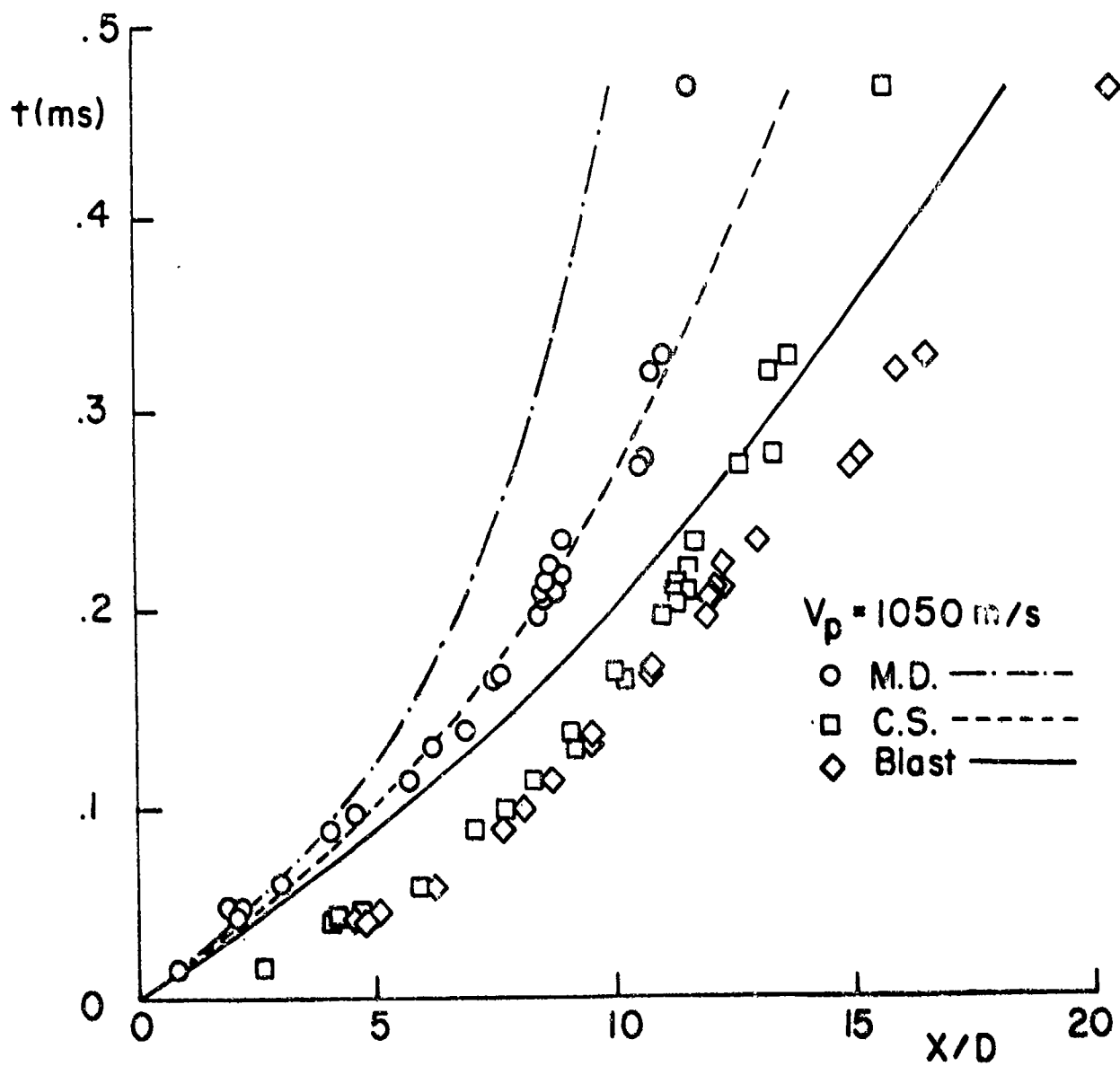
e. $V_p = 1050$ m/s

Figure 14. Discontinuity Trajectories Along Axis of Symmetry

48
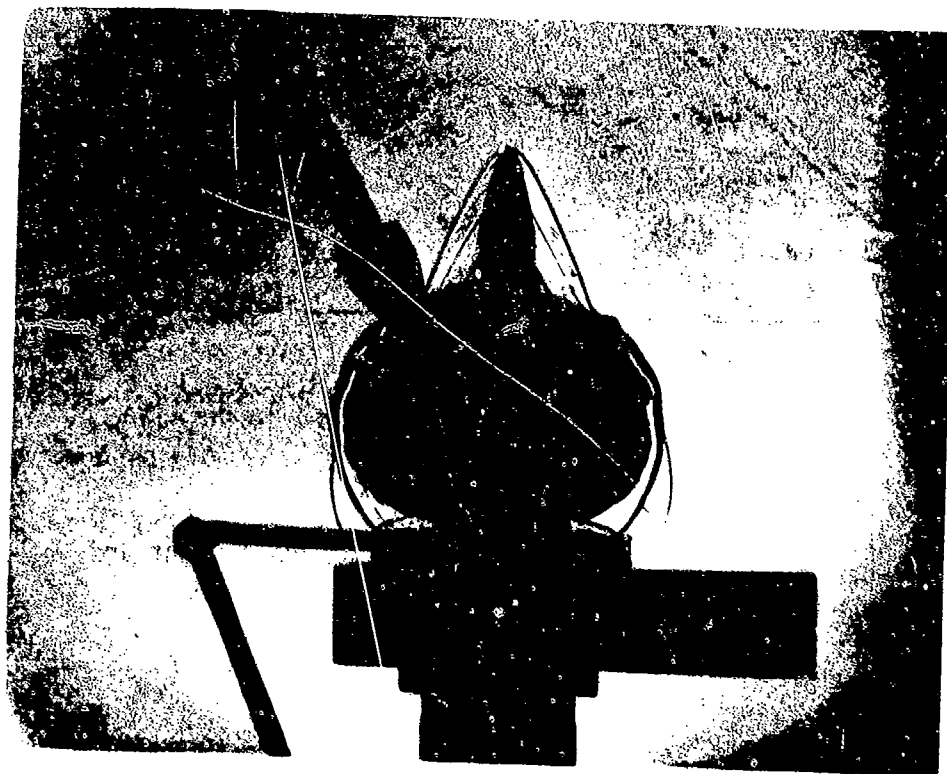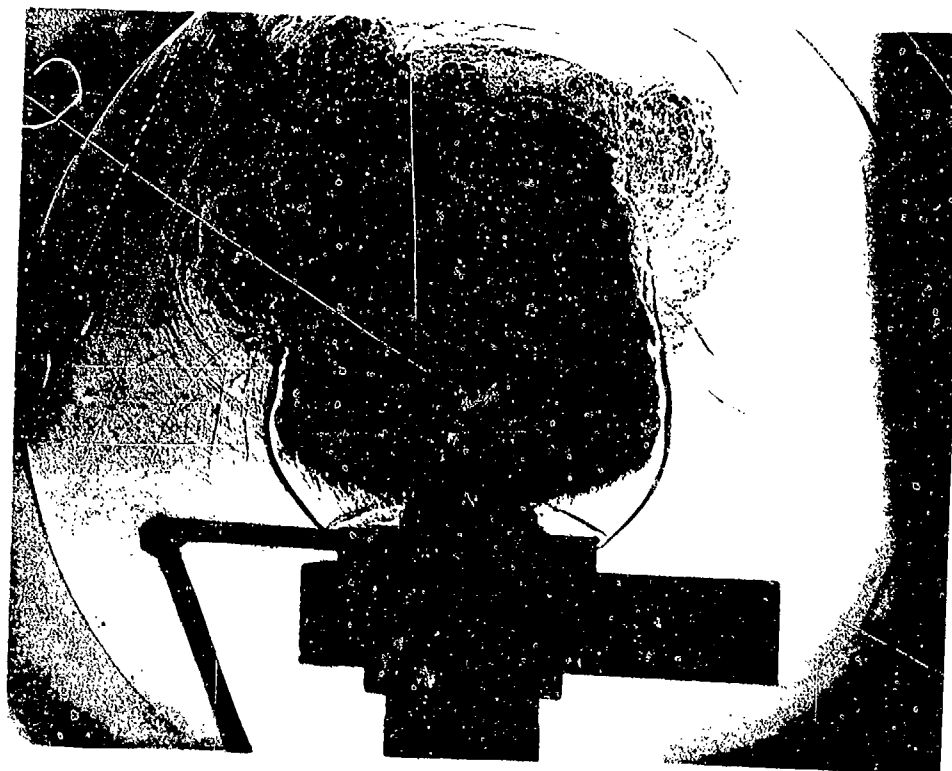
a. Evacuated (30 μm Hg) Gun Tube   b. Ambient Gun Tube

Figure 15. Spark Shadowgraphs Comparing Ambient and Evacuated Gun Tube Precursor/Propellant
            Gas Interactions, V_p = 1050 m/s

49
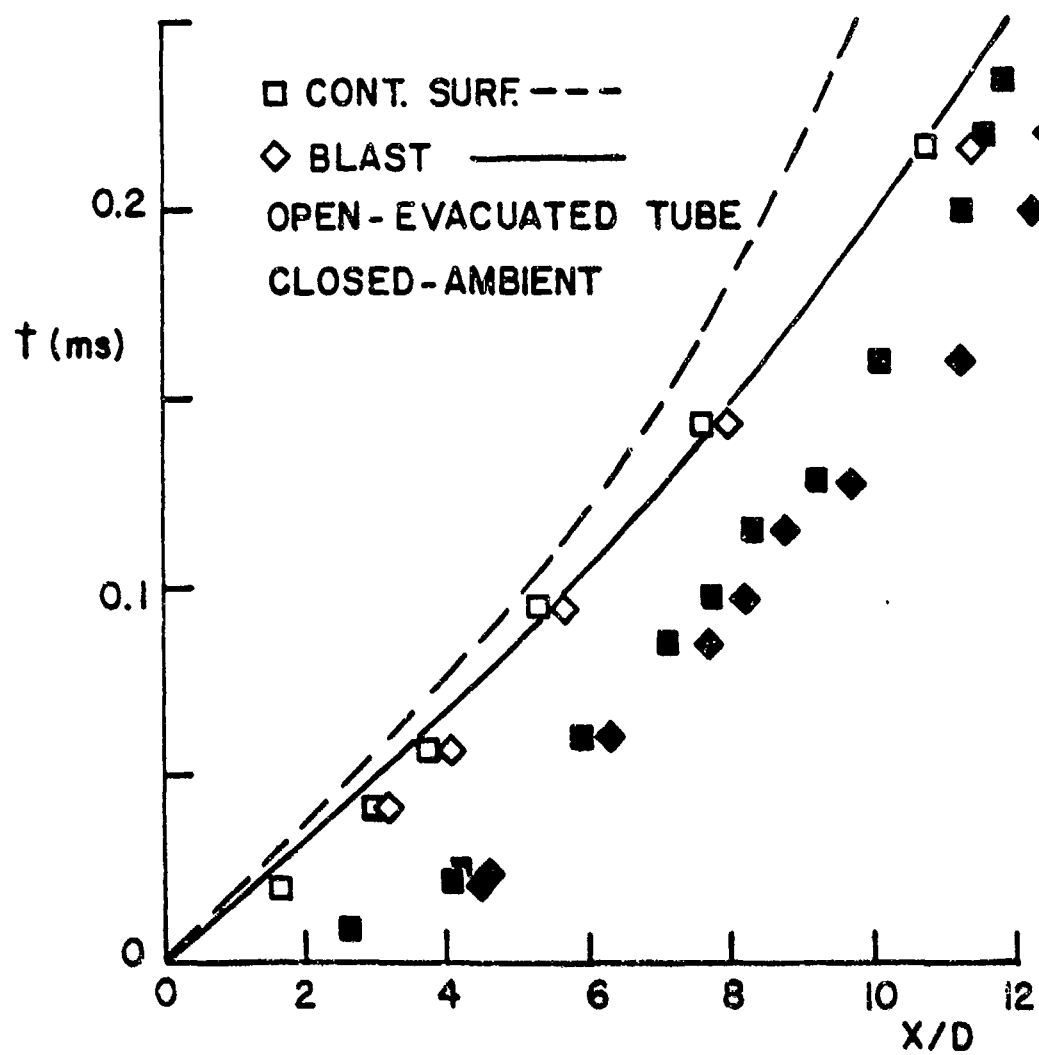
Figure 16. Comparison of Discontinuity Trajectories for Ambient and Evacuated Tube, V_p = 1050 m/s
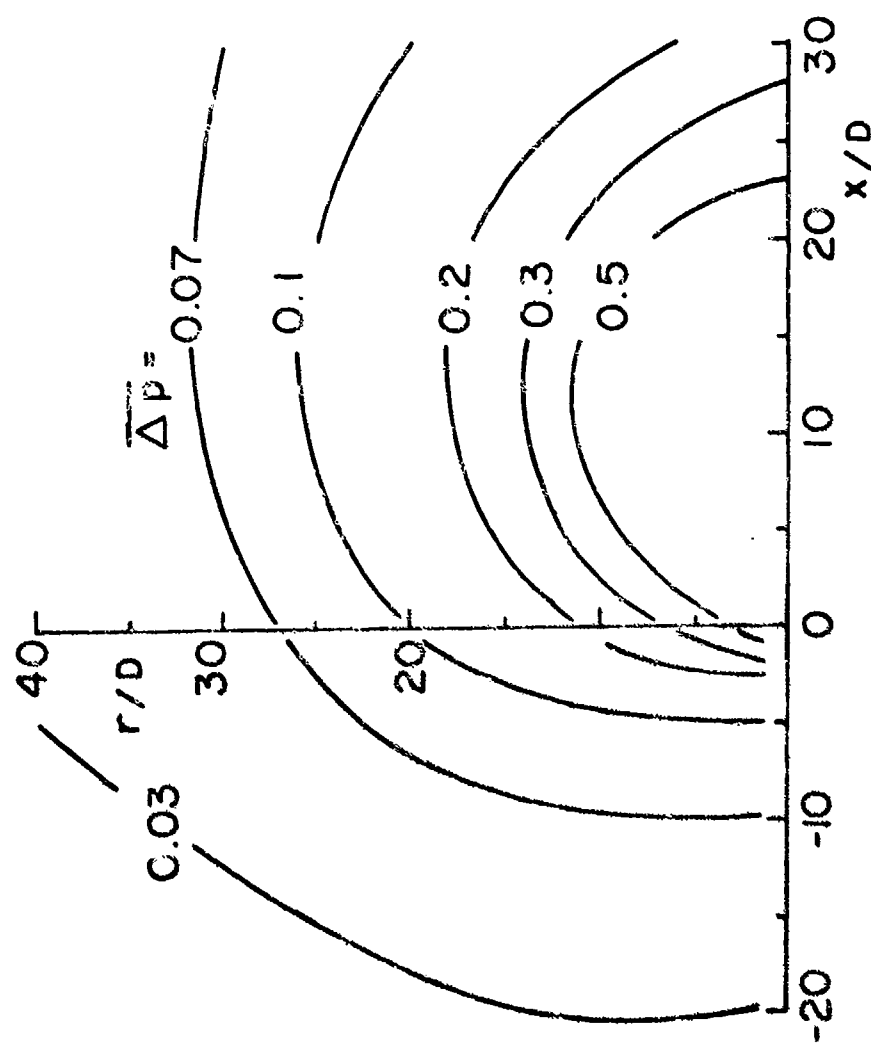
50
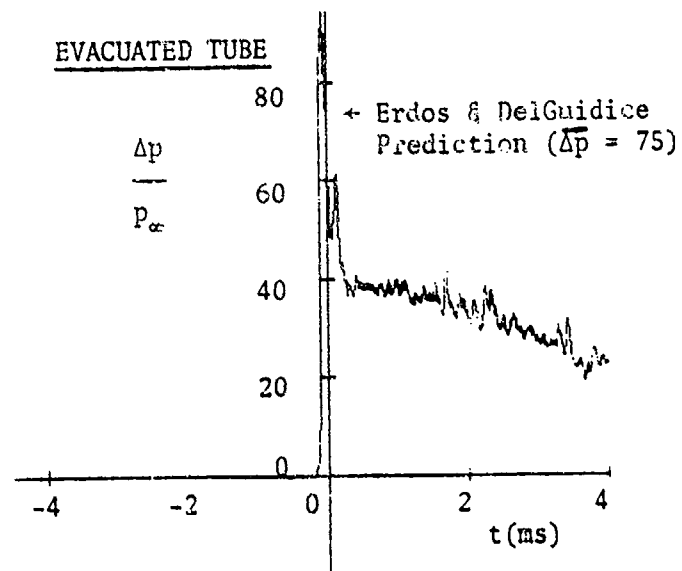
a. Evacuated Gun Tube
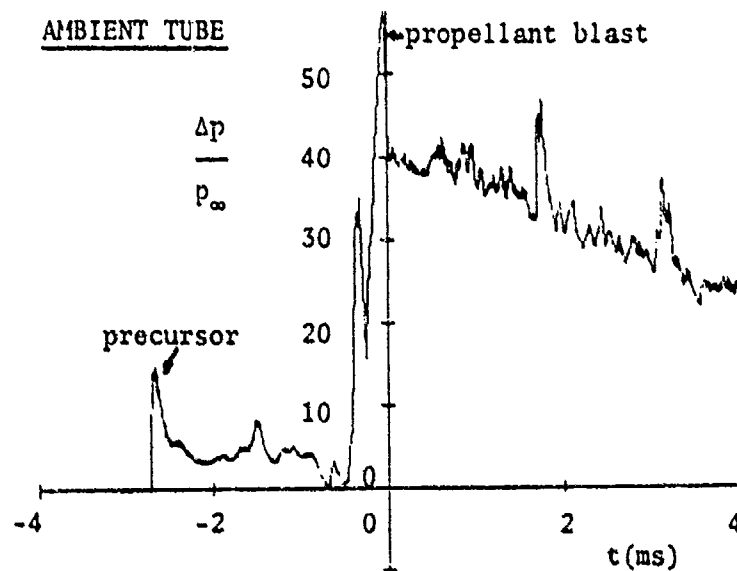
b. Ambient Gun Tube

Figure 17. Pitot Pressures Measured by a Probe 60mm from Muzzle
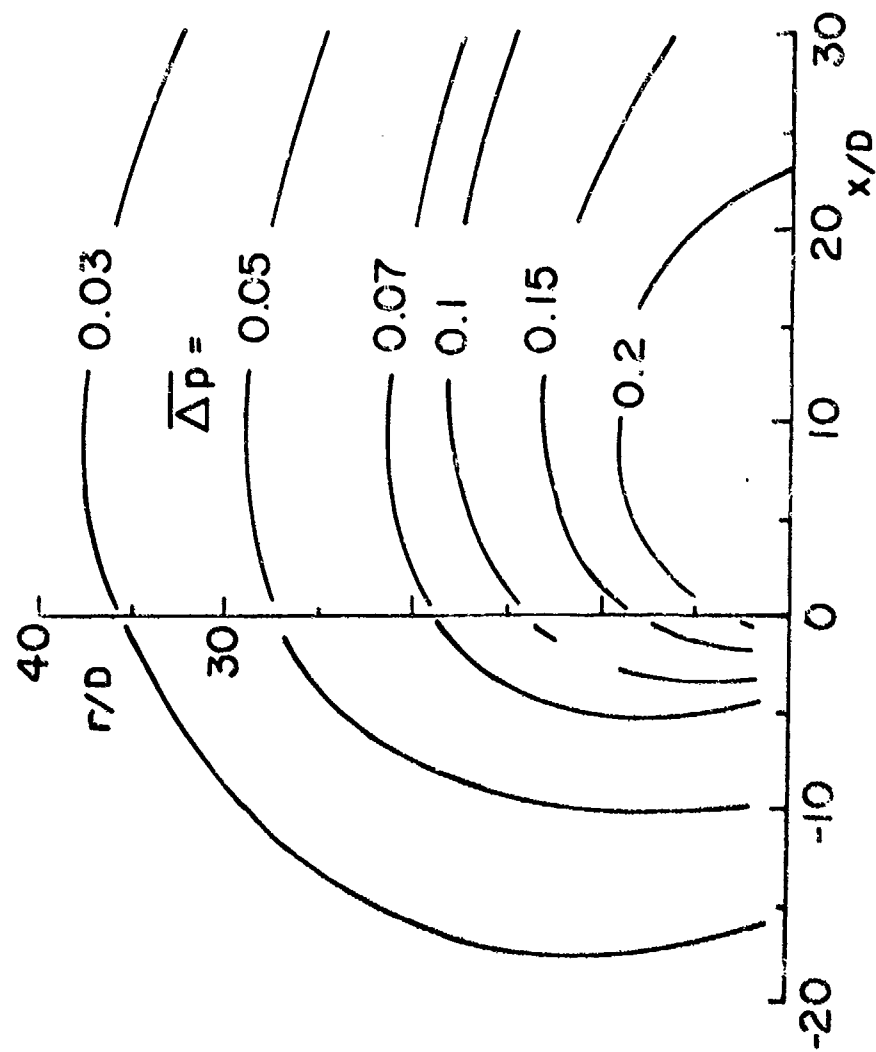
Figure 18. Static (or Side-on) Values of Peak Overpressure Contours around Weapon Muzzle

a. $V_p = 280$ m/s

b. V_p = 463 m/s

Figure 18. Static (or Side-on) Values of Peak Overpressure Contours around Weapon Muzzle

53

c. $V_p = 615$ m/s

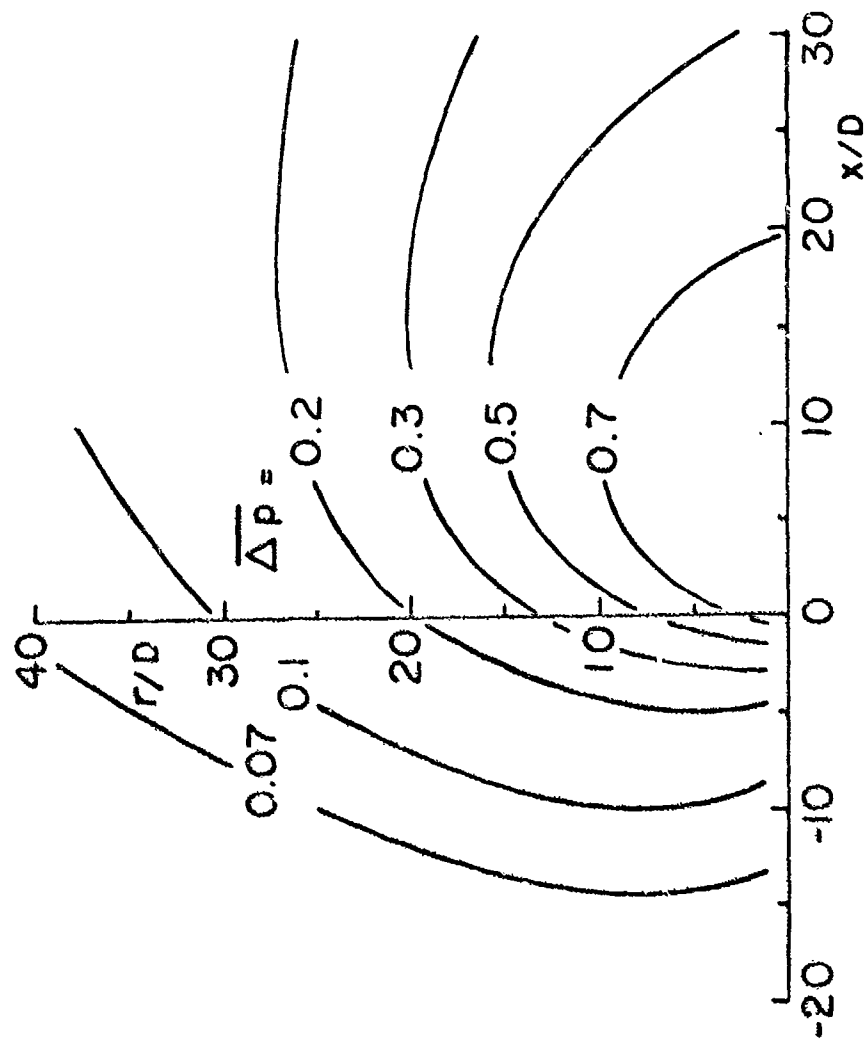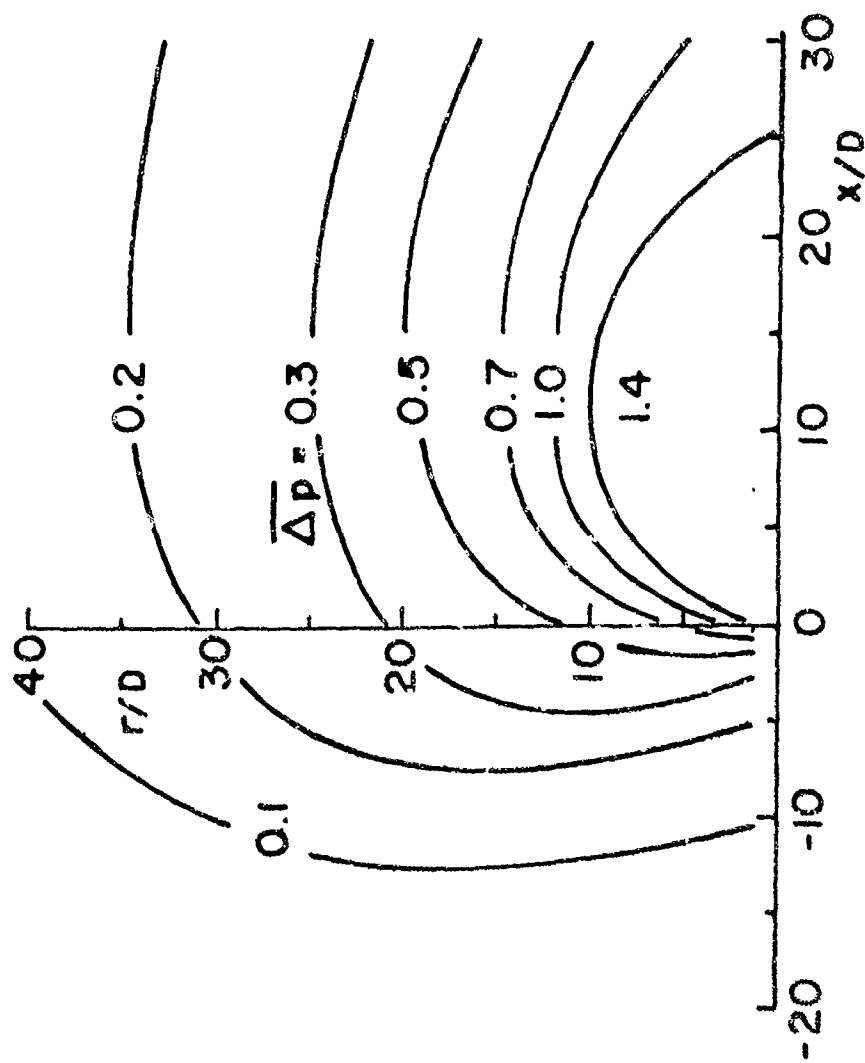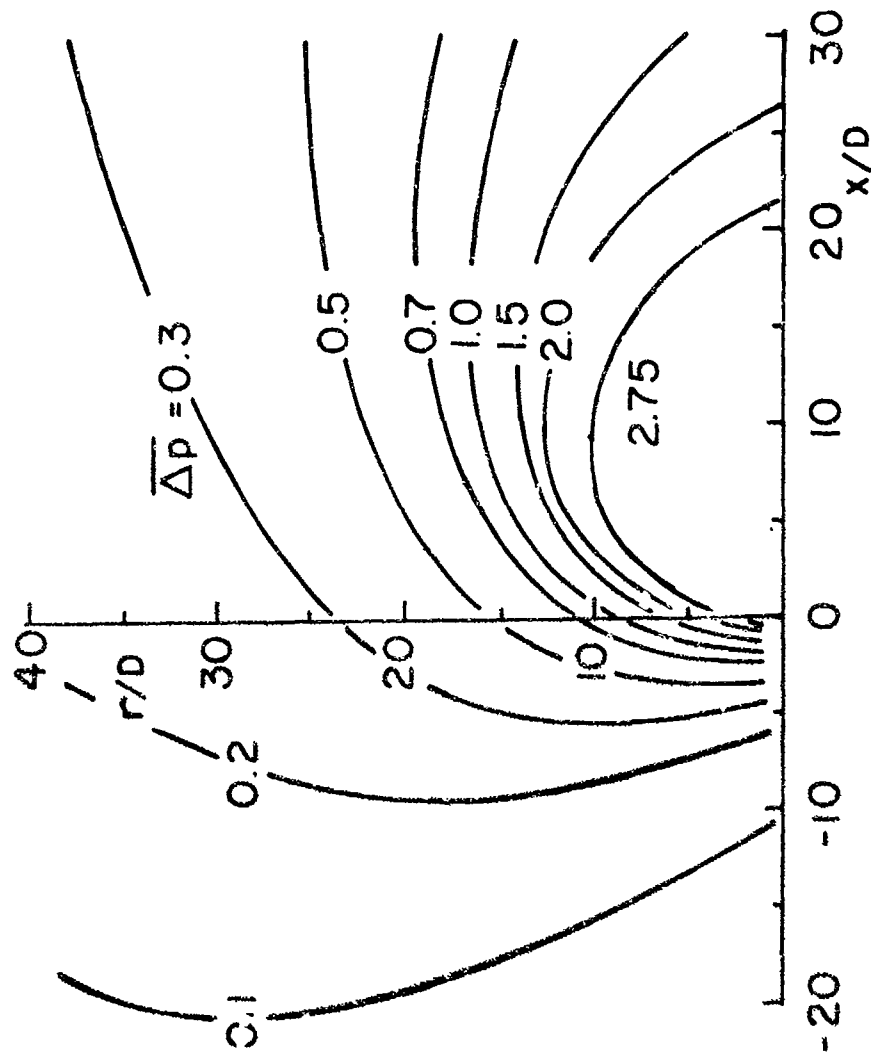Figure 18. Static (or Side-on) Values of Peak Overpressure Contours around Weapon Muzzle

54

Figure 18. Static (or Side-on) Values of Peak Overpressure Contours around Weapon Muzzle

d. $V_p = 775$ m/s

Figure 18. Static (or Side-on) Values of Peak Overpressure Contours around Weapon Muzzle
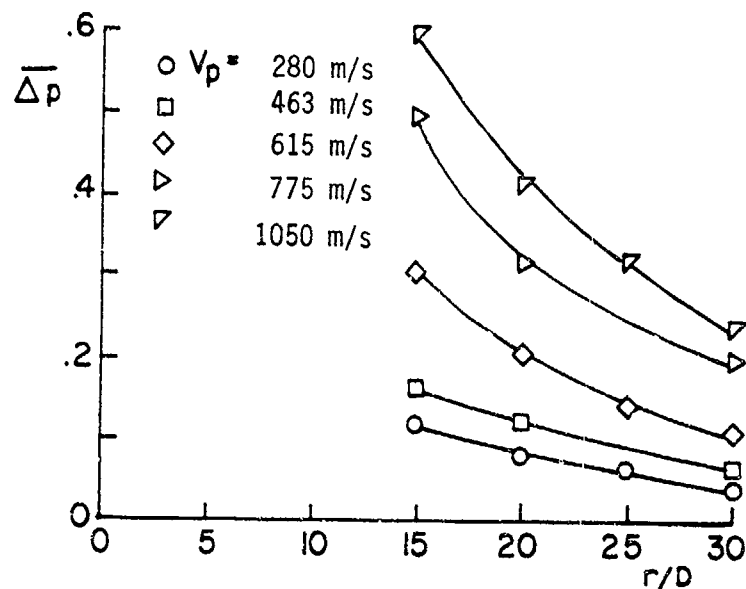
e. V_p = 1050 m/s

56

Figure 19. Blast Overpressure versus Radial Distance along the 90° Radial to Muzzle
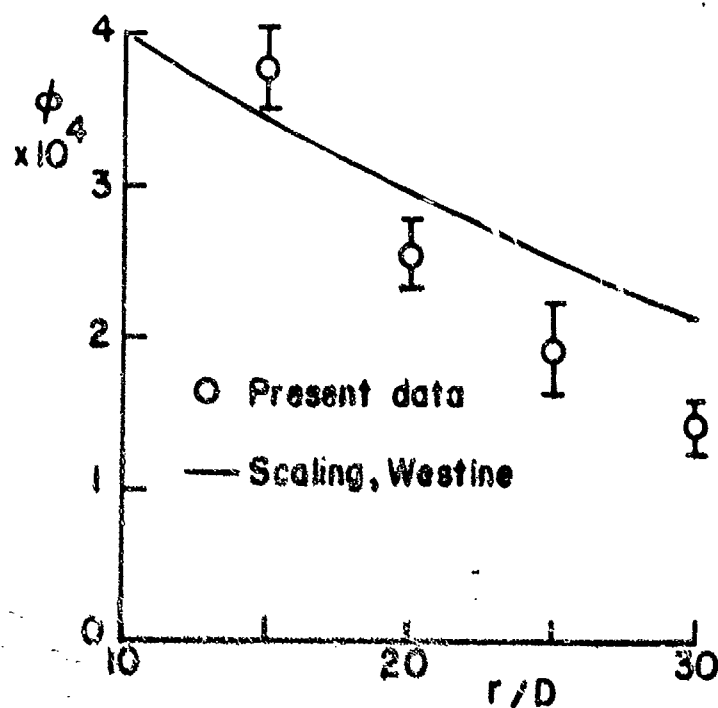

Figure 20. Scaled Blast Overpressure along the 90° Radial to Muzzle
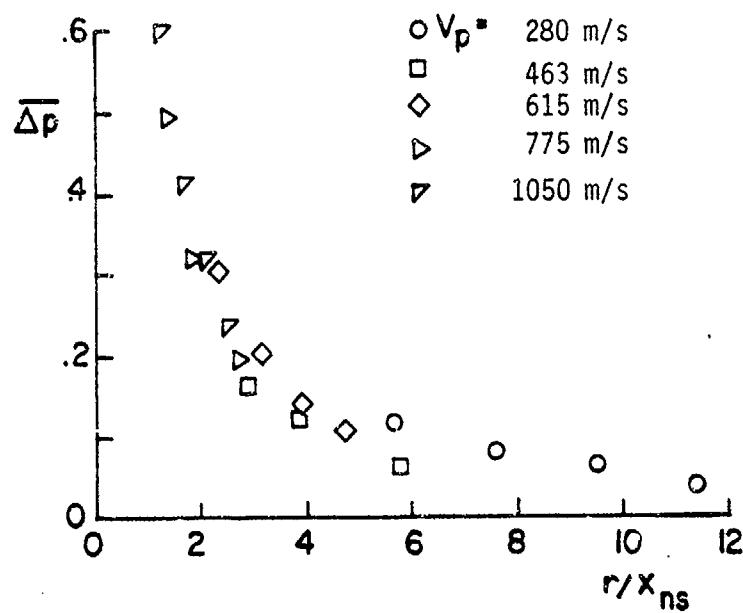
57

Figure 21. Overpressure along 90^0 Radial versus Distance Scaled by X_{ns}
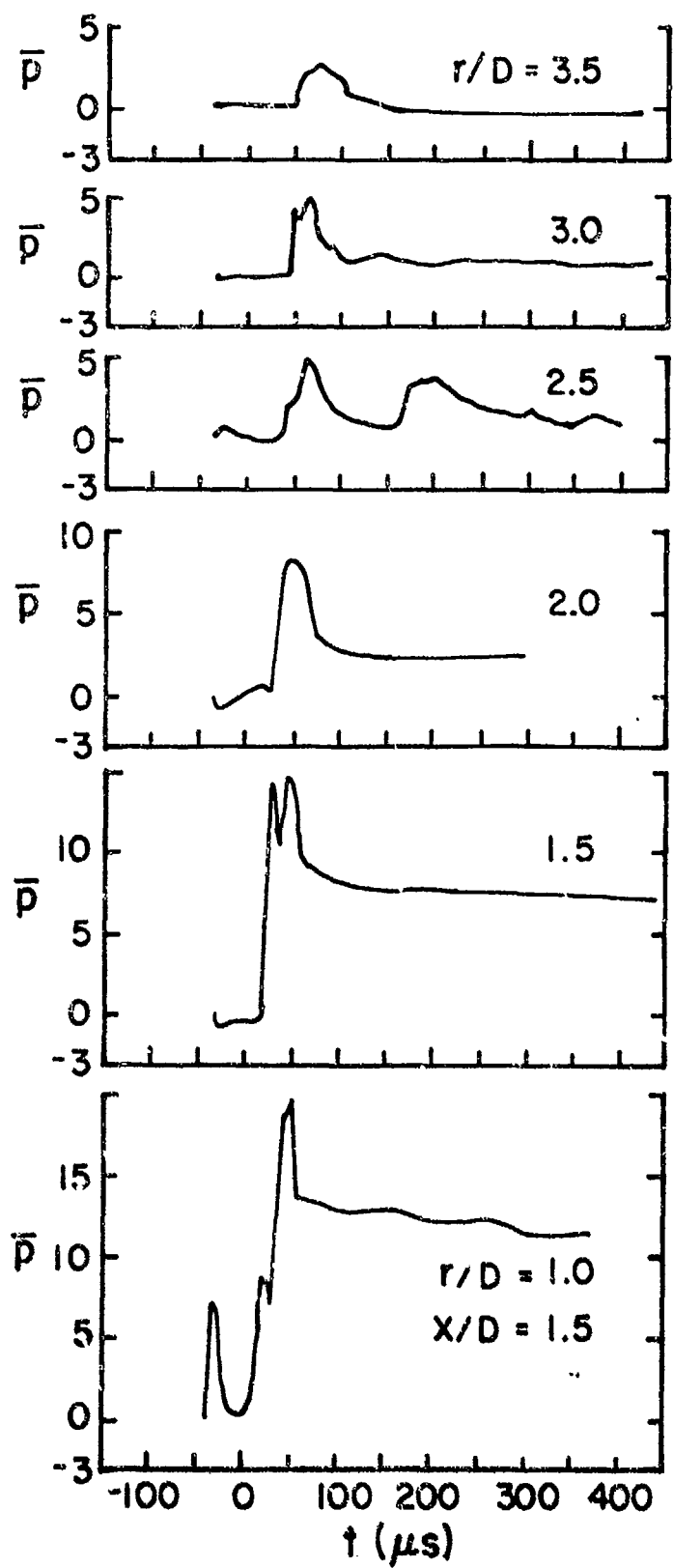
Figure 22. Sample Pressure Pulses Measured on Vertical Plate at
X/D = 1.5

59
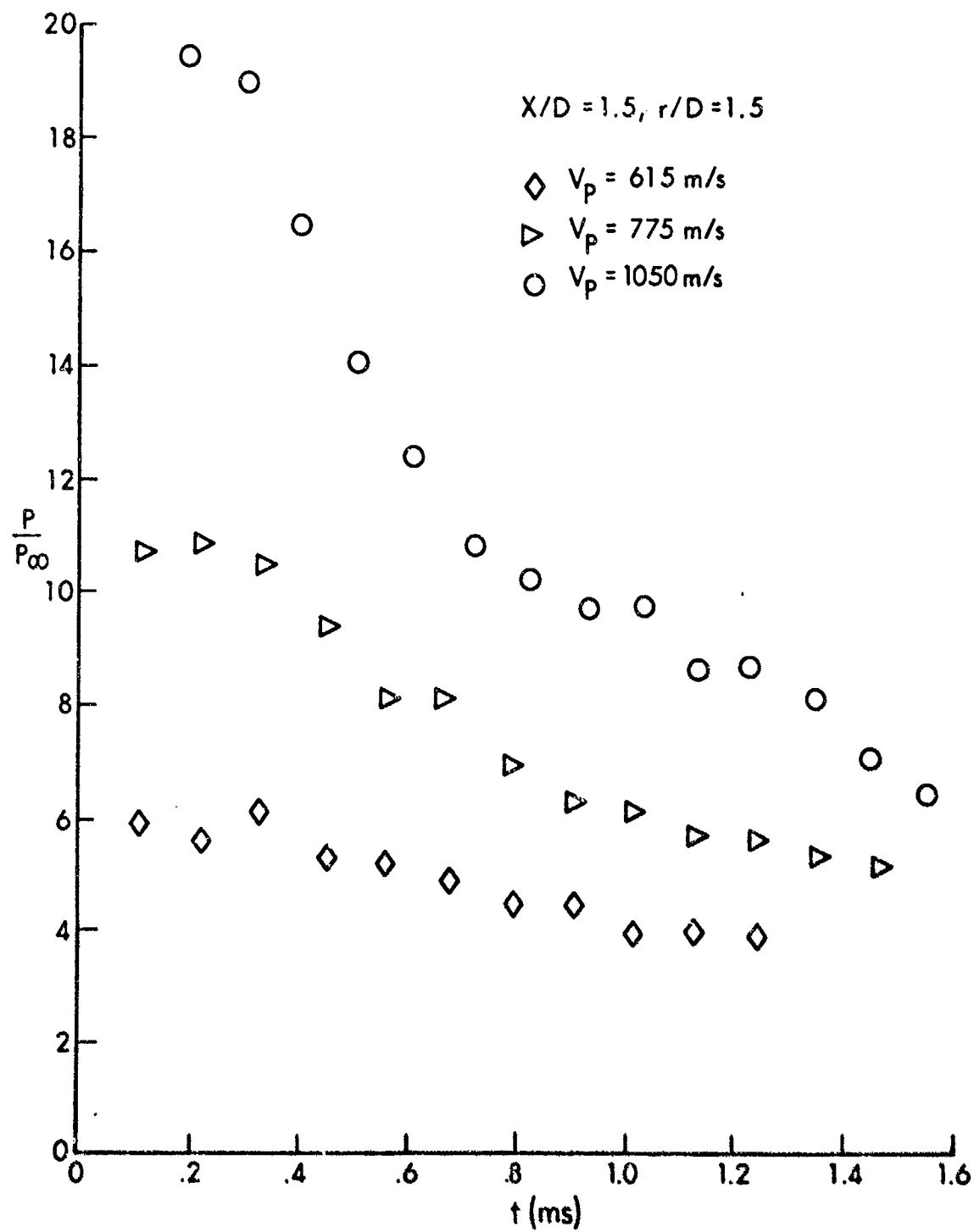
Figure 23. Variation in Plate Surface Pressure with Time

60.
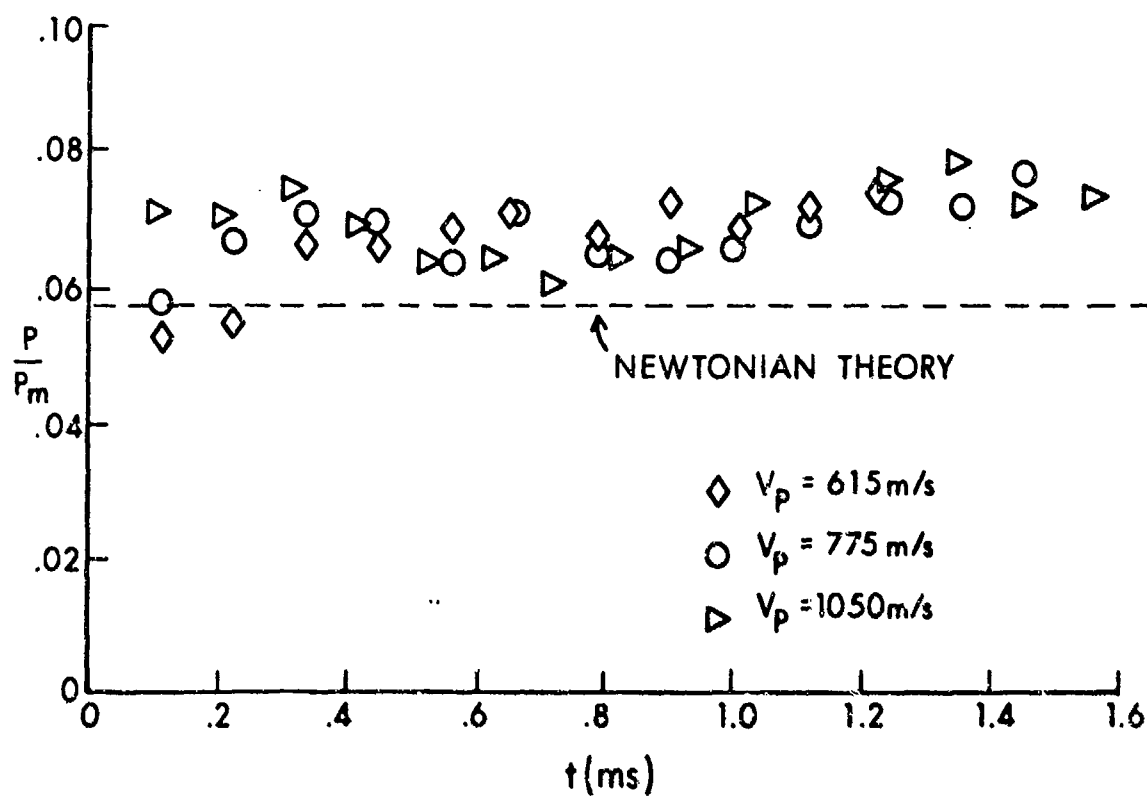
Figure 24.   Variation in Ratio of Plate Surface Pressure to Gun Muzzle
             Pressure with Time, $\lambda/D = 1.5$, $r/D = 1.5$

61
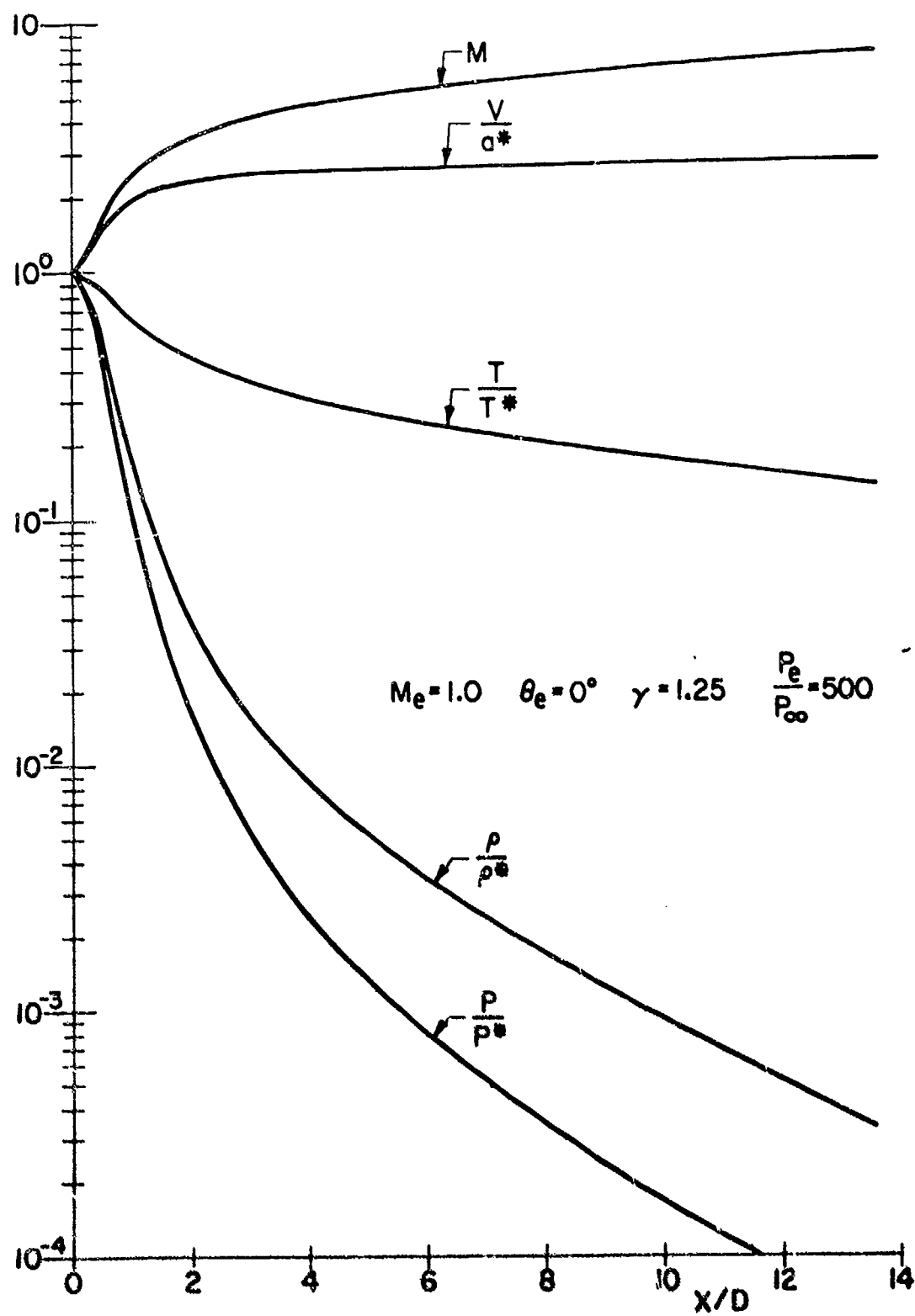
Figure 25. Property Distribution Along Jet Centerline

62
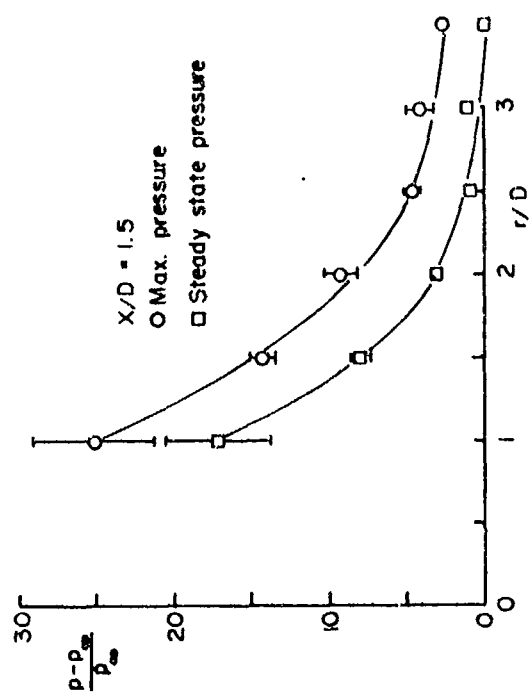
c. X/D = 1.5
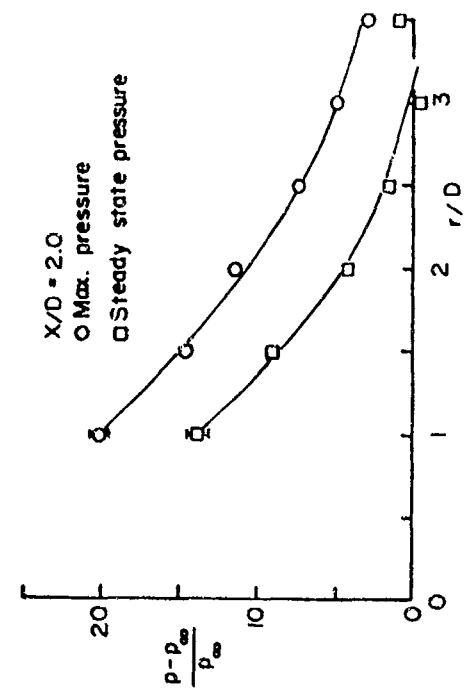
d. X/D = 2.0
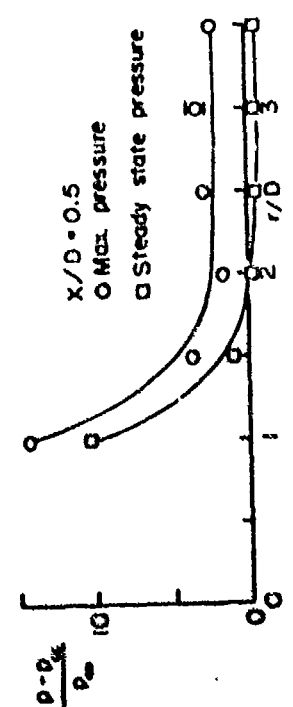
a. X/B = 0.5
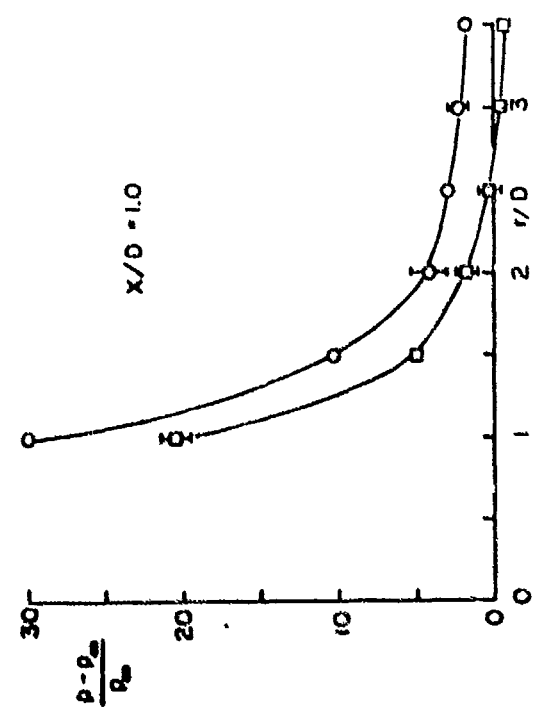
b. X/D = 1.0

Figure 26. Maximum and Steady State Pressures on Vertical Plate at Various Axial Stations
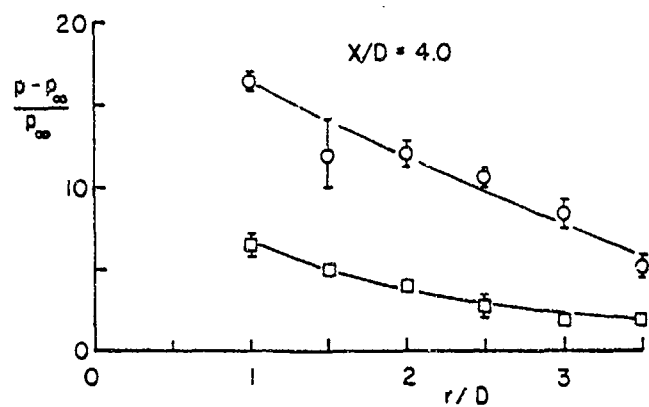
e. X/D = 4.0
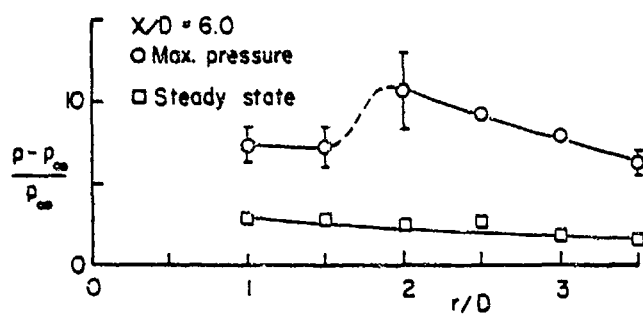
f. X/D = 6.0
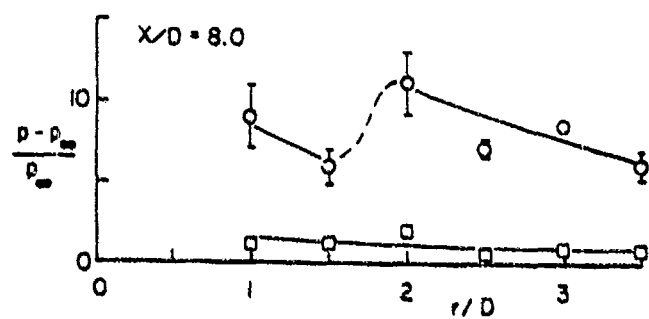
g. X/D = 8.0

Figure 26. Maximum and Steady State Pressures on Vertical Plate at Various Axial Stations

64
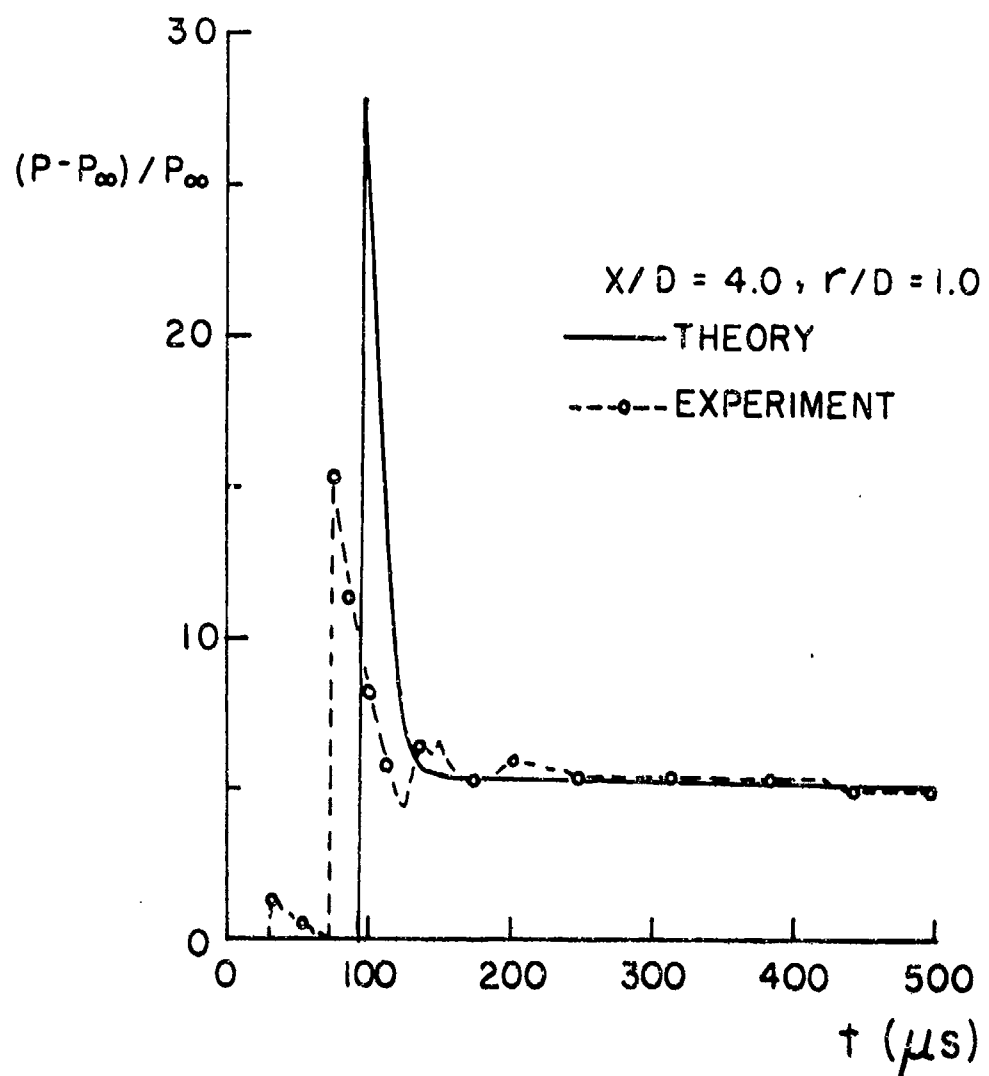
Figure 27. Comparison of Measured Pressure Pulse with Prediction of
            Simple Model

X/D = 4.0

□ EXPERIMENT
— THEORY

b. X/D = 4.0

X/D = 1.5

□ EXPERIMENT
— THEORY
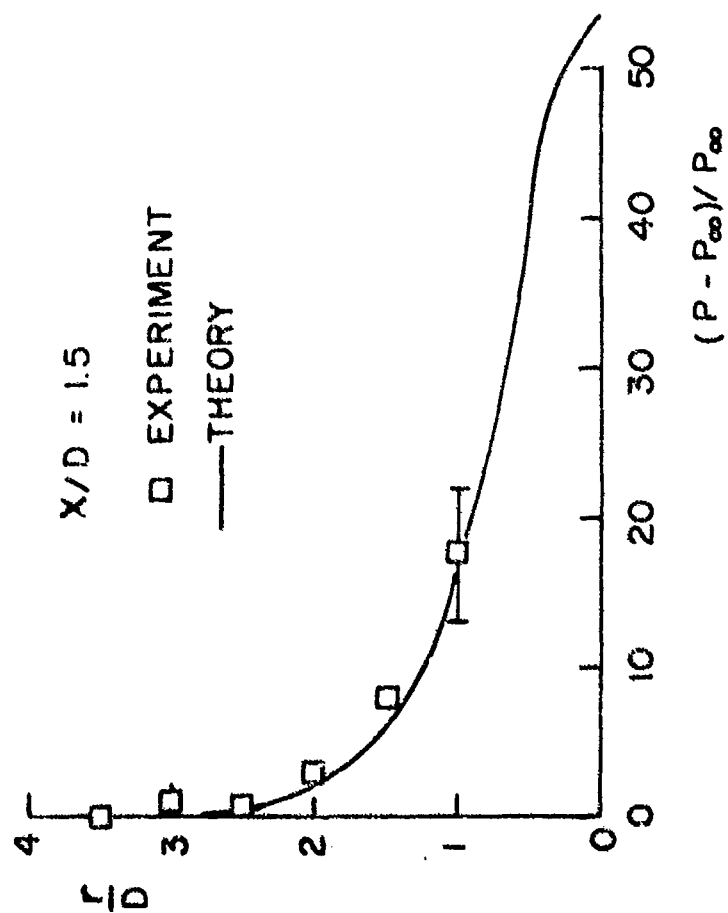
a. X/D = 1.5
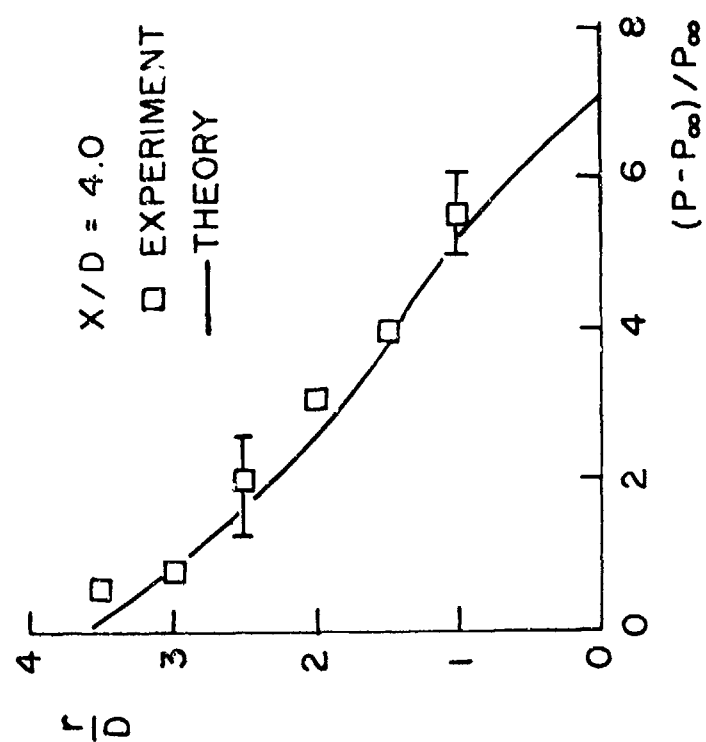
Figure 28. Comparison of Measured Values of Steady State Pressure on Vertical Plate with the Predictions of Newtonian Theory
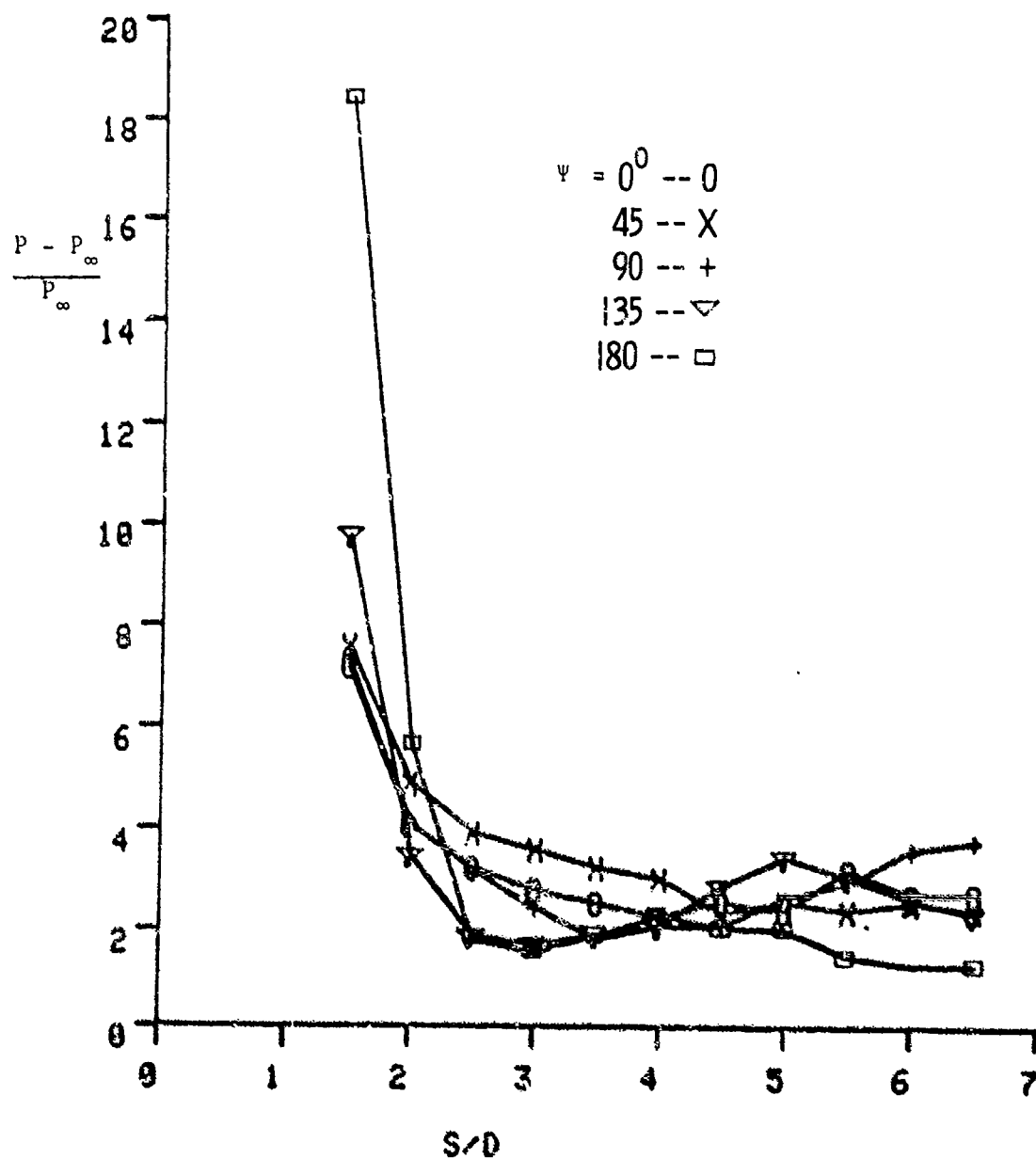
a. Axial Location X/D = 1.27

Figure 29. Maximum Surface Pressures Over Inclined Plate. Plate and Gages Rotated to Various Angles ψ About Plate Normal

67

$$\frac{P - P_\infty}{P_\infty}$$

$$\Psi = 0^0 -- 0$$
$$45 -- X$$
$$90 -- +$$
$$135 -- \triangledown$$
$$180 -- \square$$

S/D
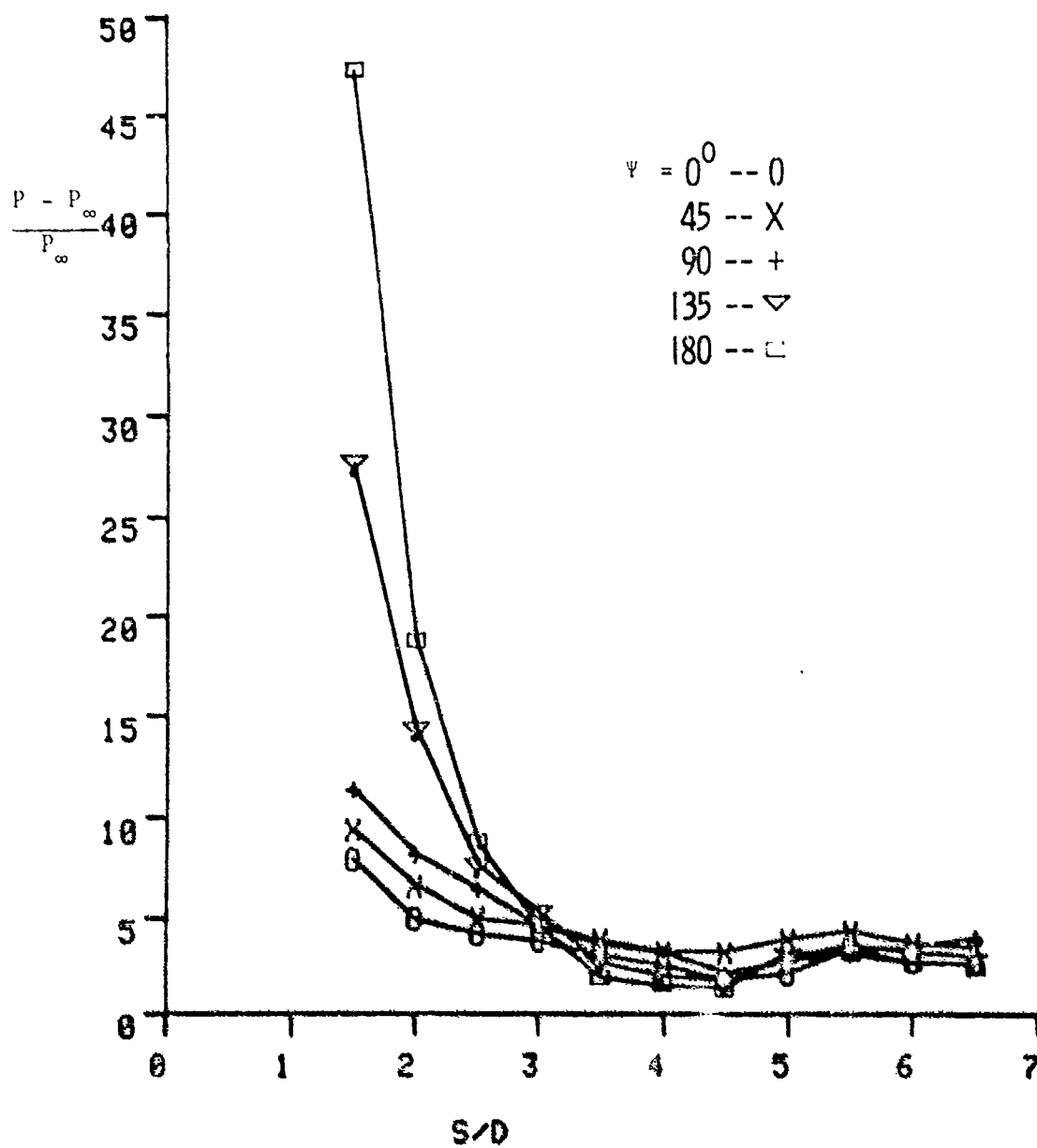
b. Axial Location X/D = 2.50

Figure 29. Maximum Surface Pressures Over Inclined Plate. Plate and
Gages Rotated to Various Angles Ψ About Plate Normal
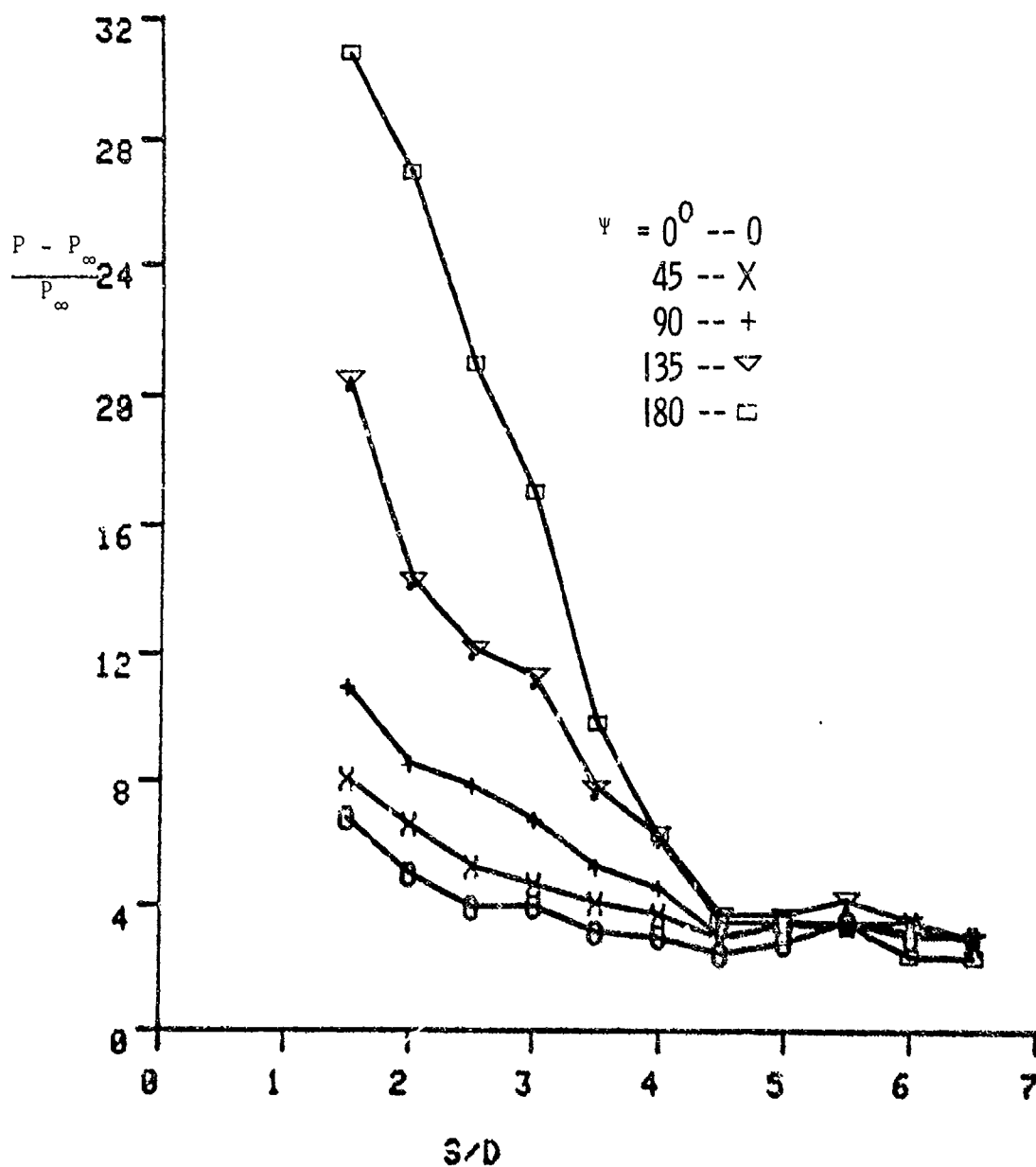
c. Axial Location X/D = 3.75

Figure 29.   Maximum Surface Pressures Over Inclined Plate.   Plate and
Gages Rotated to Various Angles Ψ About Plate Normal

69
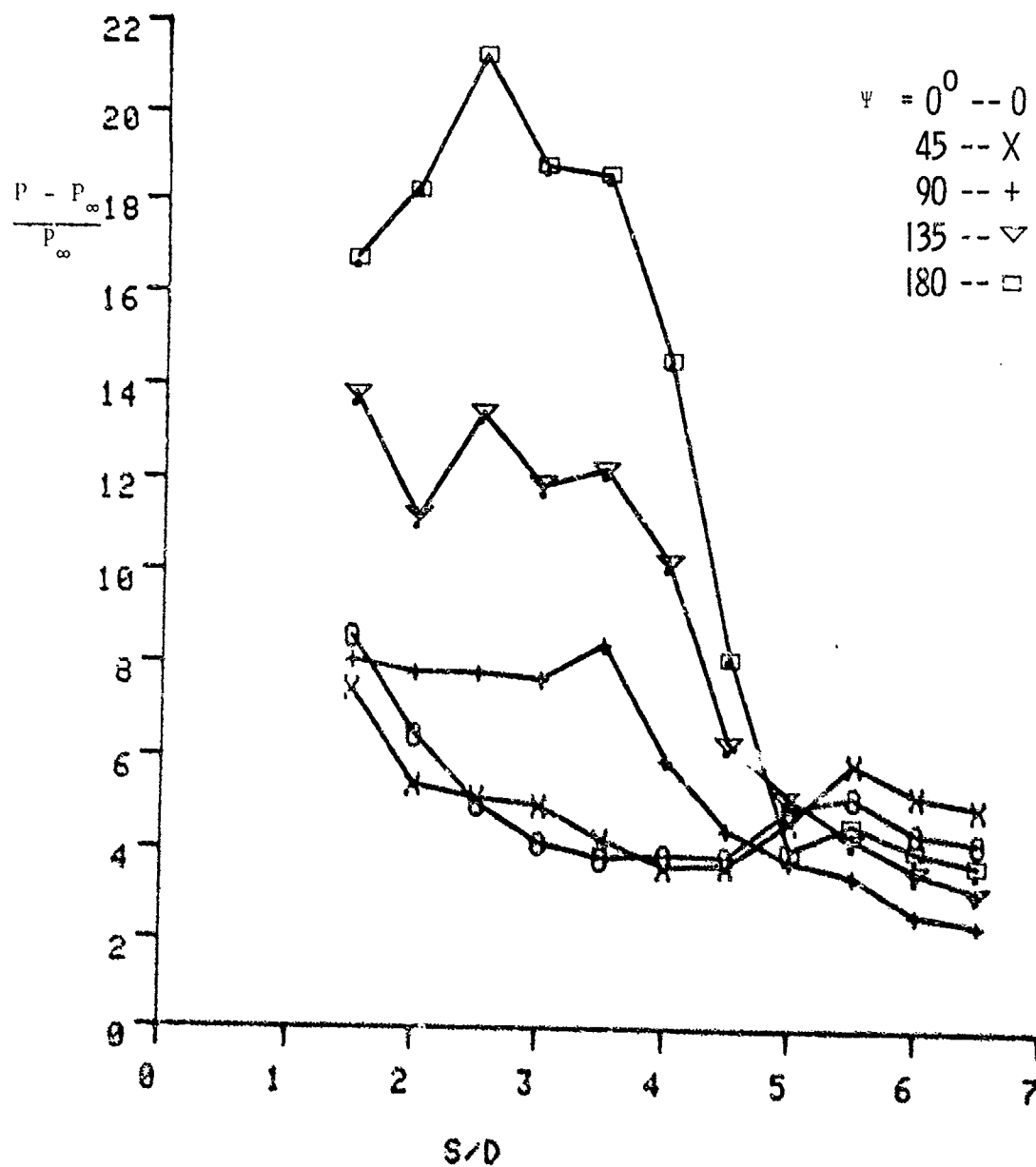
d. Axial Location X/D = 5.00

Figure 29. Maximum Surface Pressures Over Inclined Plate. Plate and
Gages Rotated to Various Angles Ψ About Plate Normal
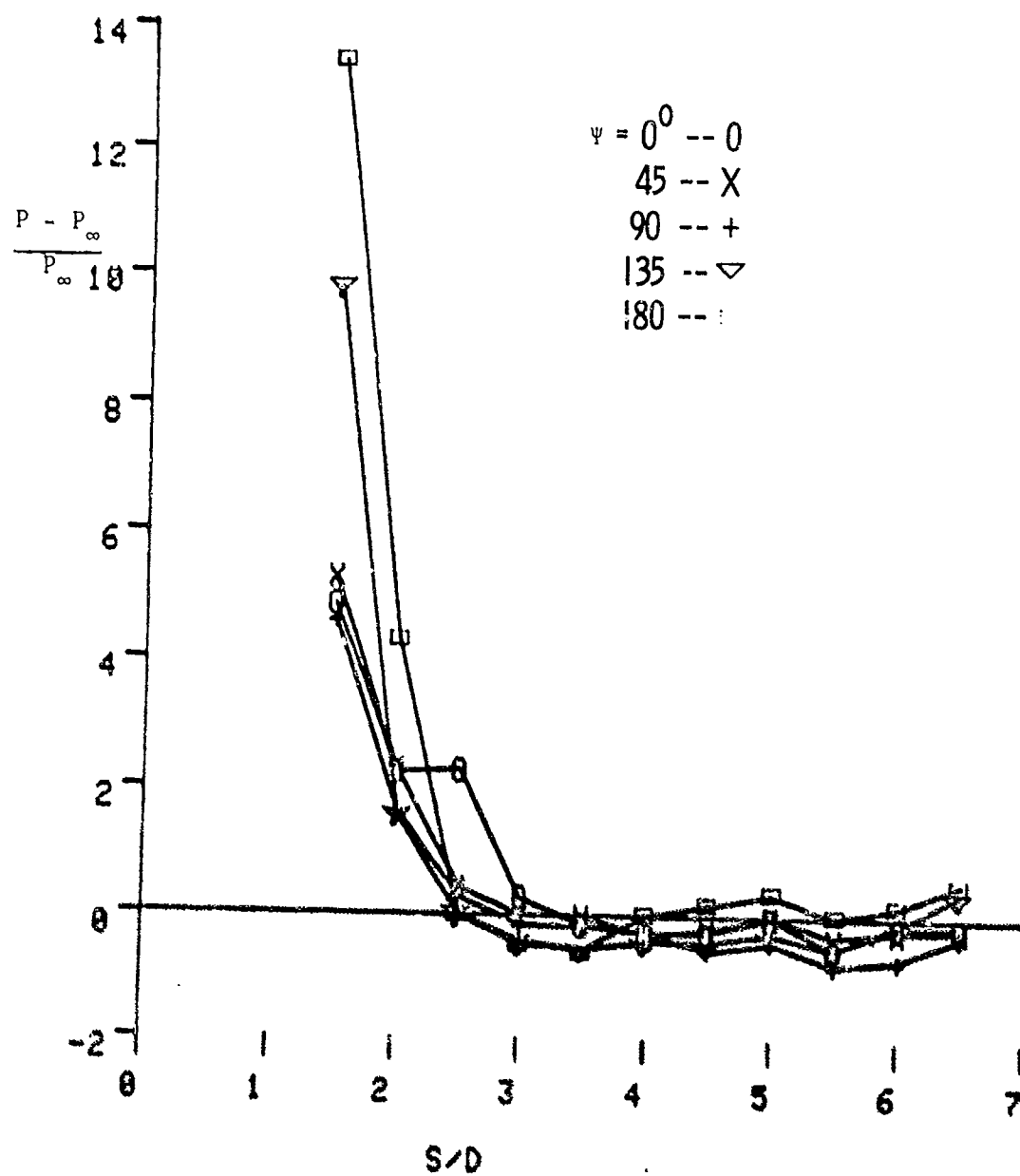
a. Axial Location X/D = 1.27

Figure 30. Steady State Surface Pressures Over Inclined Plate. Plate and Gages Rotated to Various Angles ψ About Plate Normal

71
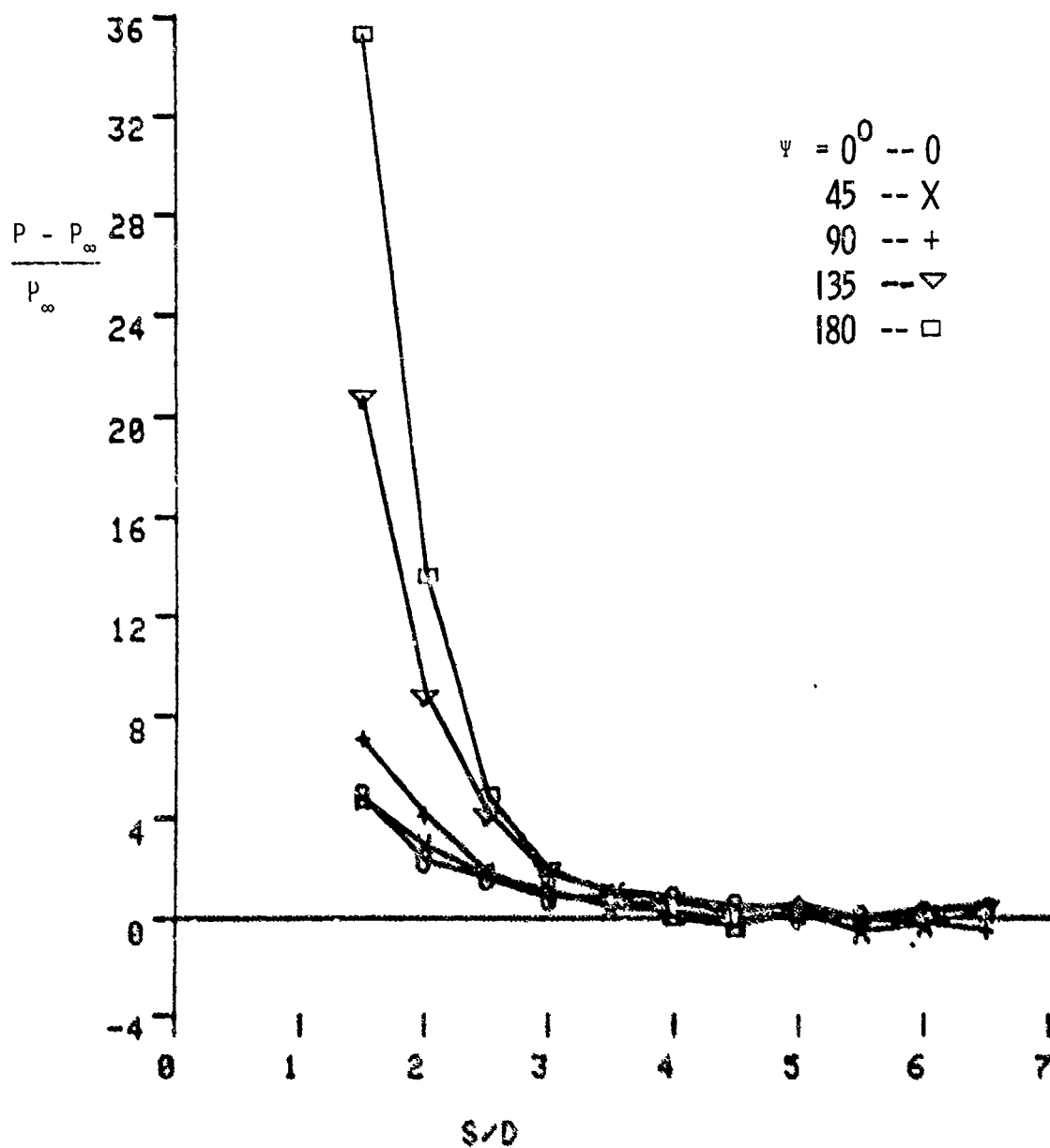
b. Axial Location X/D = 2.50

Figure 30. Steady State Surface Pressures Over Inclined Plate. Plate and Gages Rotated to Various Angles Ψ About Plate Normal

72
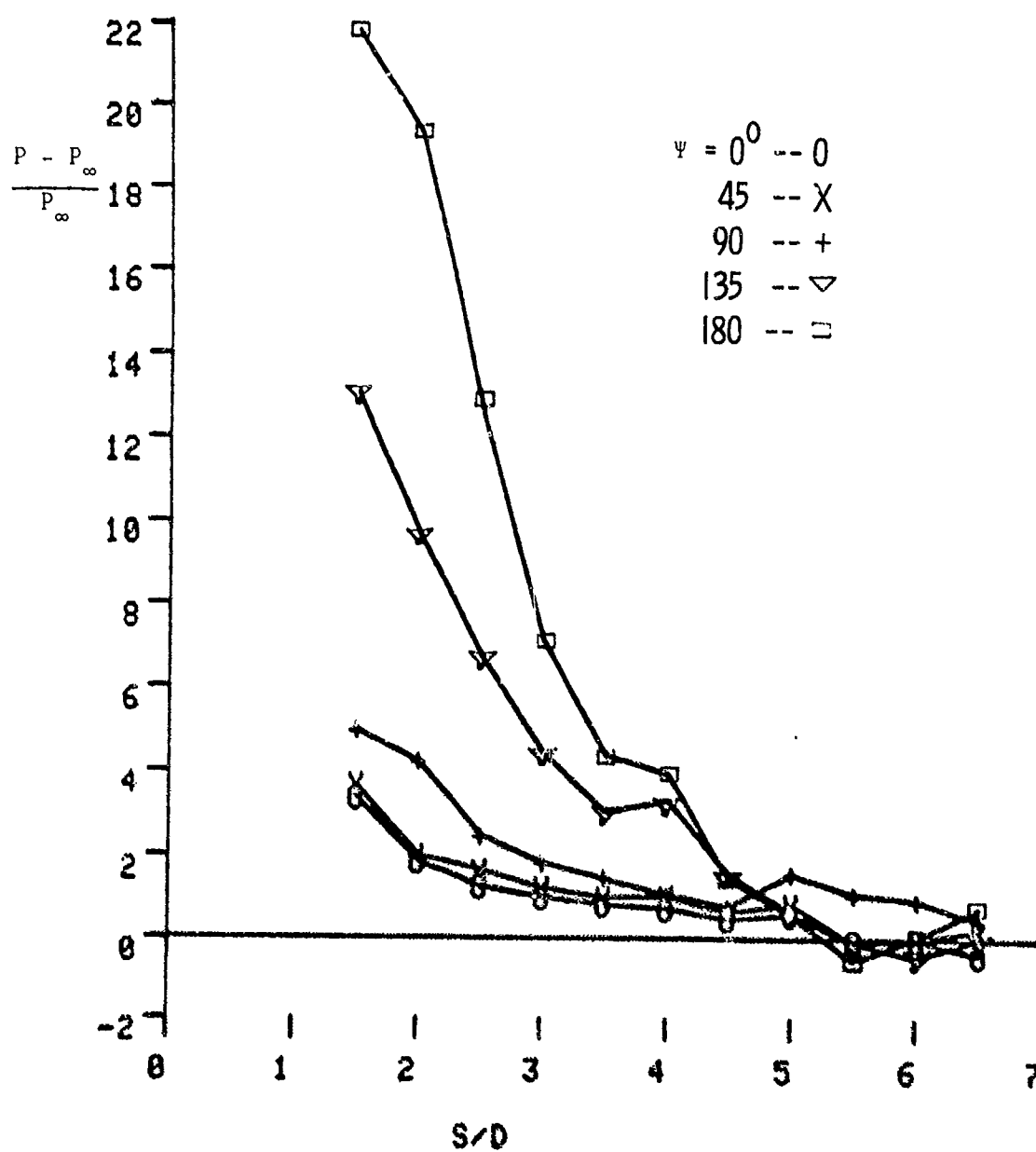
c. Axial Location X/D = 3.75

Figure 30. Steady State Surface Pressures Over Inclined Plate. Plate and Gages Rotated to Various Angles Ψ About Plate Normal

73
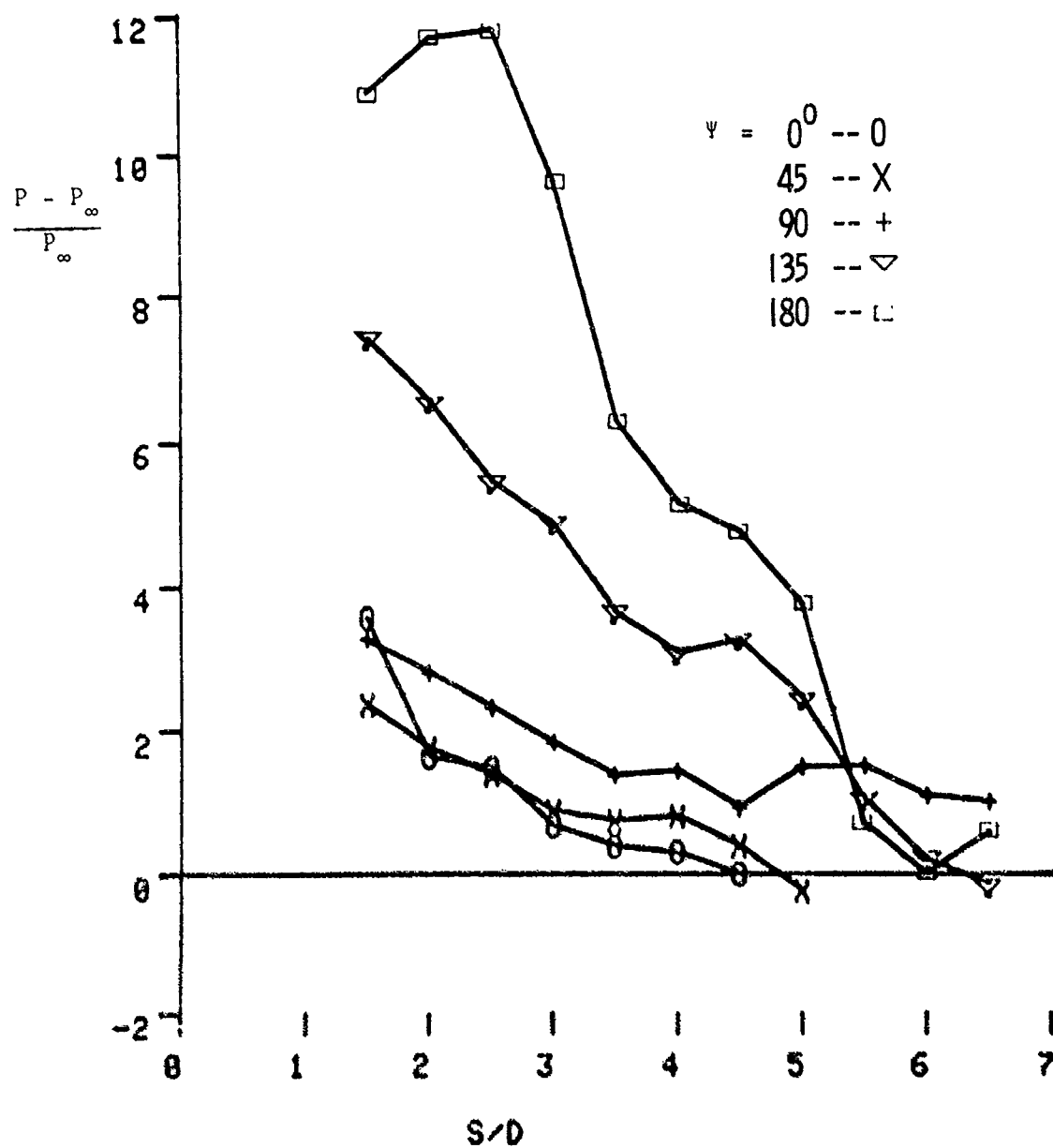
d. Axial Location X/D = 5.00

Figure 30. Steady State Surface Pressures Over Inclined Plate. Plate
and Gages Rotated to Various Angles Ψ About Plate Normal
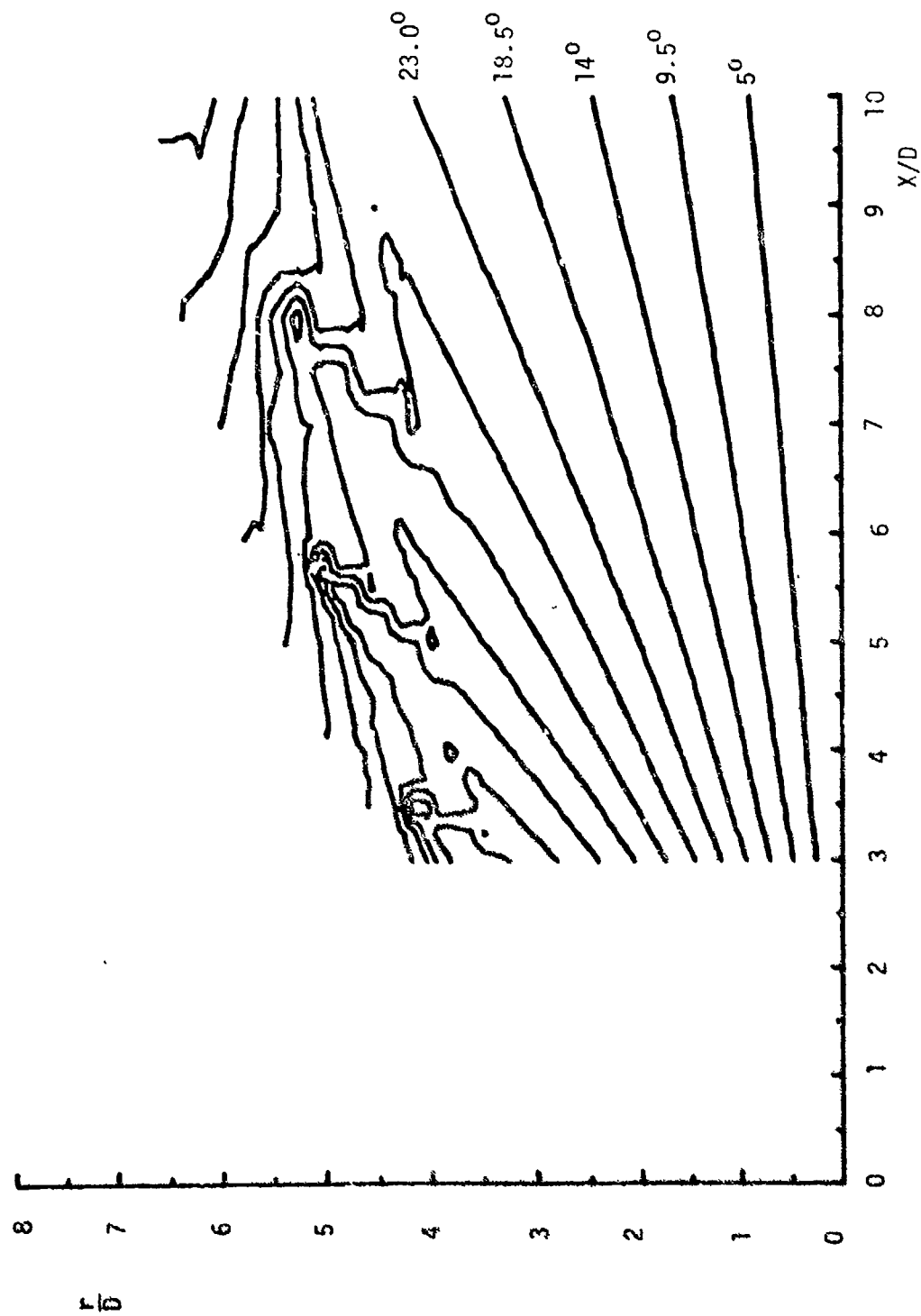
a. Streamline Inclination Angles

Figure 31. Isoproperty Contours from M.O.C. Jet Calculation
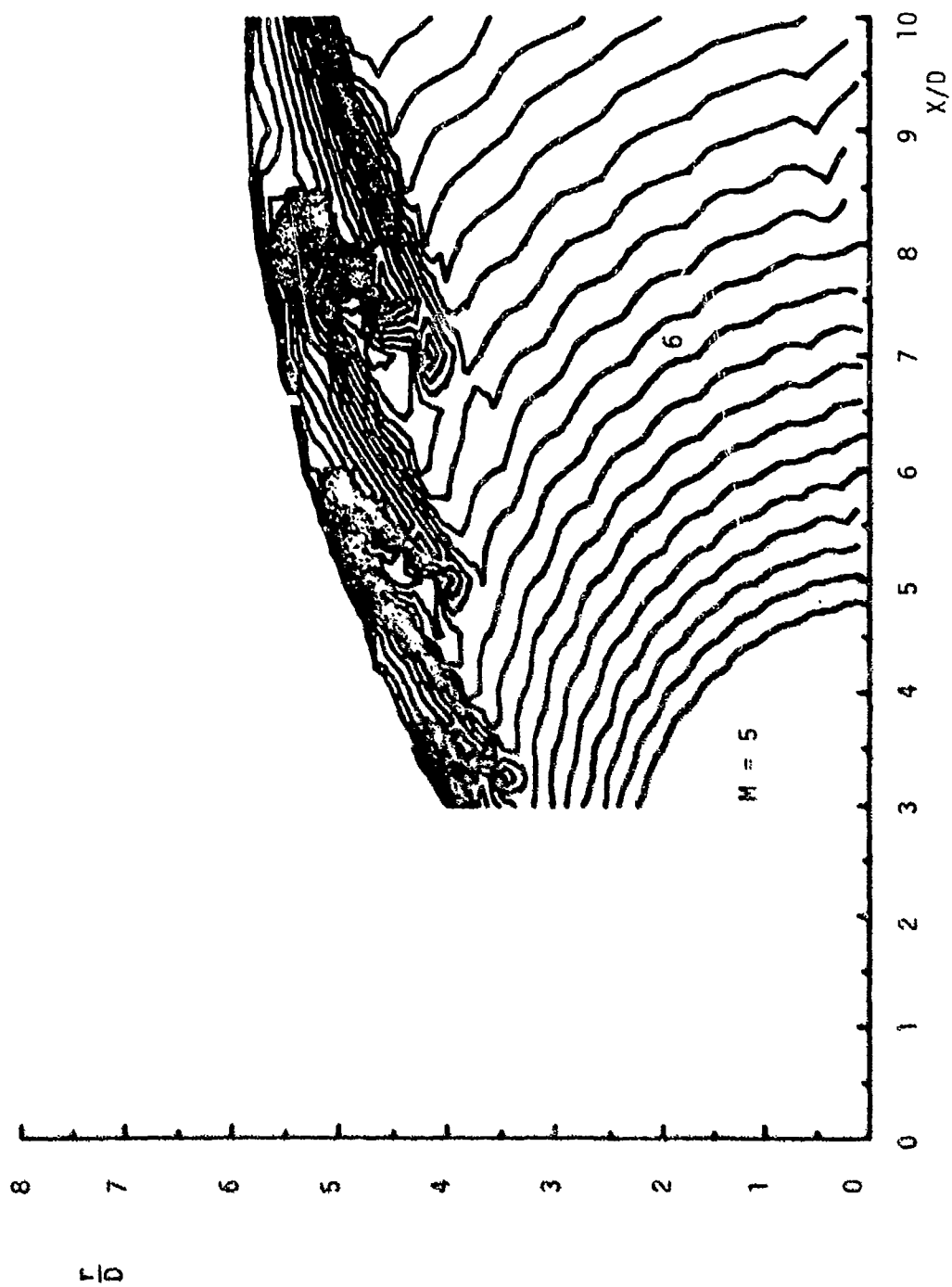
75

b. Mach Number

M = 5

Figure 31. Isoproperty Contours from M.O.C. Jet Calculation

a. $\Psi = 0^0$
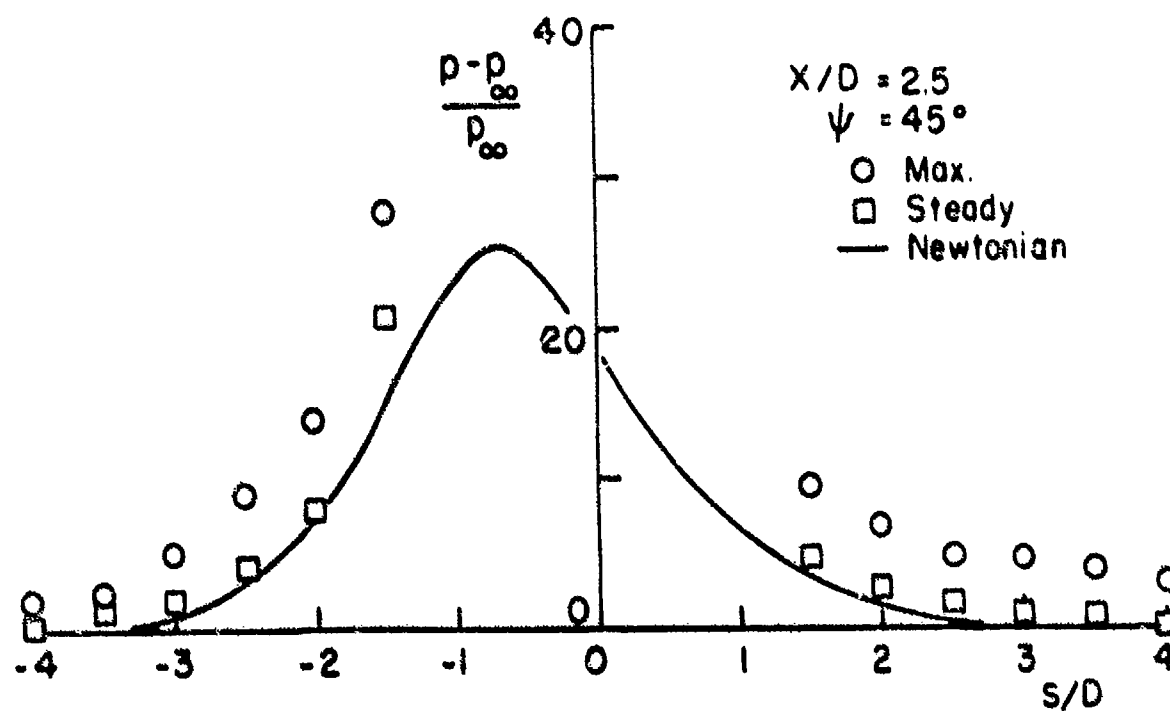
b. $\Psi = 45^0$

Figure 32. Maximum and Steady State Pressures on Plate Inclined with its Surface Normal at an Angle of 40^0 to the Axis of the Gun Tube, X/D = 2.5

$X/D = 2.5$

$\psi = 90°$

$\dfrac{p - p_\infty}{p_\infty}$

O   Max.
□   Steady
—   Newtonian

c. $\psi = 90°$

Figure 32.   Maximum and Steady State Pressures on Plate Inclined
with its Surface Normal at an Angle of $40°$ to the
Axis of the Gun Tube, $X/D = 2.5$

REFERENCES

1. D. G. Mabey and D. S. Capps, "Blast from Moving Guns," *AIAA Journal of Aircraft*, Vol. 14, 1977, pp. 687-692.

2. J. Erdos and P. DelGuidice, "Calculation of Muzzle Blast Flow Fields," *AIAA Journal*, Vol. 13, No. 8, August 1975, pp. 1048-1056.

3. T. D. Taylor and T. C. Lin, "A Numerical Model for Muzzle Blast Flow Fields," AIAA Paper No. 80-0273, January 1980.

4. J. Yagla, "Analysis of Gun Blast Phenomena for Naval Architecture, Equipment, and Propellant Charge Design," 3d International Symposium on Ballistics, Karlsruhe, Germany, March 1977, ADPA, Washington, D.C.

5. C. S. Zoltani, "Numerical Simulation of the Muzzle Flow Field with a Moving Projectile," 1st International Symposium on Ballistics, Orlando, FL, November 1974, ADPA, Washington, D.C.

6. G. Moretti, "Muzzle Blast Flow and Related Problems," AIAA Paper 78-1190, July 1978.

7. G. Klingenberg, "Investigation of Combustion Phenomena Associated with the Flow of Hot Propellant Gases," Combustion and Flame, Vol. 29, 1977, pp. 289-309.

8. F. Smith, "A Theoretical Model of the Blast from Stationary and Moving Guns," 1st International Symposium on Ballistics, Orlando, FL, November 1974, ADPA, Washington, D.C.

9. M. Walther, "Gun Blast from Naval Guns," TR 2733, Naval Weapons Laboratory, Dahlgren, VA, August 1972. AD 902672L

10. E. M. Schmidt and D. D. Shear, "Optical Measurements of Muzzle Blast," *AIAA Journal*, Vol. 13, No. 8, August 1975, pp. 1086-1091.

11. E. M. Schmidt, E. J. Gion, and D. D. Shear, "Acoustic Thermometric Measurements of Propellant Gas Temperatures in Guns," *AIAA Journal*, Vol. 15, No. 2, February 1977, pp. 222-226.

12. P. Westine and F. Hoese, "Blast Gauge for Measuring Shocks with Short Wavelengths," IR-02-2643-01, Southwest Research Institute, San Antonio, TX, May 1970. AD 907402L.

13. W. D. Williams and H. M. Powell, "Laser-Raman Measurements in the Muzzle Blast Region of a 20-mm Cannon," AEDC-TR-79-72, Arnold Engineering Development Center, Tullahoma, TN, August 1980. AD A088729.

REFERENCES (Continued)

14. W. M. Farmer, et. al., "Laser Velocimetry Measurements of the Chronological Velocity at Selected Positions in the Muzzle Blast from 20mm Cannon," University of Tennessee Space Institute, Tullahoma, TN, September 1979.

15. A. H. Shapiro, The Dynamics and Thermodynamics of Compressible Fluid Flow, Ronald Press, New York 1953.

16. Principles of Explosive Behavior, AMCP 706-180, Army Materiel Command, Washington, D. C., 1972.

17. E. M. Schmidt, E. J. Gion, and K. S. Fansler, "Measurement of and in the Muzzle Blast of 20mm Cannon," 4th International Symposium on Ballistics, Monterey, CA, ADPA, Washington, D.C., October 1978.

18. P. Westine, "The Blast Field About the Muzzle of Guns," Shock and Vibration Bulletin, Vol. 39, Part 6, March 1969, pp. 139-149.

19. C. H. Lewis and D. J. Carlson, "Normal Shock Locations in Underexpanded Gas and Gas-Particle Jets," *AIAA Journal*, Vol. 2, No. 4, April 1964, pp. 776-777.

20. P. Owen and C. Thornhill, "The Flow in an Axially Symmetric Supersonic Jet from a Nearly Sonic Orifice into a Vacuum," R 30/48, Royal Armament Research and Development Establishment, Kent, UK, 1948. AD 57 261.

21. A. R. Vick, et. al., "Comparison of Experimental Free-Jet Boundaries with Theoretical Results Obtained with the Method of Characteristics," TN D-2327, NASA, June 1964.

22. C. D. Donaldson and R. S. Snedeker, "A Study of Free Jet Impingement," *Journal of Fluid Mechanics*, Vol. 45, Part 2, 1971, pp. 281-319.

23. J. Carling and B. Hunt, "The Near Wall Jet of a Normally Impinging, Uniform, Axisymmetric, Supersonic Jet," JFM, Vol. 66, 1974, pp. 159-176.

24. S. Glasstone (ed), The Effects of Nuclear Weapons, AEC, Government Printing Office, Washington, D.C., 1976.

25. D. W. Eastman and L. P. Radtke, "Flow Field of an Exhaust Plume Impinging on a Simulated Lunar Surface," *AIAA Journal*, Vol. 1, No. 6, June 1963, pp. 1430-1431.

80

APPENDIX A: CALCULATION OF PLATE SURFACE PRESSURE FROM NEWTON'S FORMULA

The Newtonian formula for the surface pressure coefficient is

$$c_p = 2 \sin^2 \theta_N$$

where θ_N is the angle between the flow streamline and the surface.
The surface pressure (corresponding to the measured steady state
pressure) is then

$$(p - p_\ell)/p_\ell = \gamma M^2_\ell \sin^2 \theta_N$$

where the subscript ℓ denotes local conditions. Rearrangement to
compare with the plotted overpressures results in

$$\frac{\Delta p}{p_\infty} \equiv \frac{p - p_\infty}{p_\infty} = (p/p_\ell)\,(p_\ell/p_\infty) - 1$$

$$= \left[\gamma M^2_\ell \sin^2 \theta_N + 1 \right]\ (p_\ell/p_\infty) - 1 \qquad (A\text{-}1)$$

The quantities entering into Equation (A-1) are obtained from the
free-jet code and the geometry, as described in the following sections.

The jet-code starting parameters are M_j and p_j/p_∞, the jet Mach
number and pressure ratio respectively, i.e., the muzzle exit conditions.
The code outputs among other quantities, the spatial contours of θ_ℓ,
the local flow inclination (with respect to the bore line), and M_ℓ, the
local Mach number. Sample output for $M_j = 1.01$, $p_j/p_\infty = 180$ are shown
in Figure 31.

The quantity p_ℓ/p_∞ is computed as

$$p_\ell/p_\infty = (p_\ell/p_{j0})(p_{j0}/p_j)(p_j/p_\infty) \quad .$$

Using the isentropic relation,

$$\frac{p_0}{p} = \left(1 + \frac{\gamma - 1}{2}\, M^2\right)^{\gamma/(\gamma-1)}$$

yields

$$\frac{p_\ell}{p_\infty} = \left[\frac{2 + (\gamma - 1)M_j^2}{2 + (\gamma - 1)M_\ell^2}\right]^{\gamma/(\gamma-1)} \left[\frac{p_j}{p_\infty}\right]$$

Substituting into Equation A-1 for the surface pressure ratio now gives

$$\frac{\Delta p}{p_\infty} = \left[\gamma M_\ell^2 \sin^2 \theta_N + 1\right] \left[\frac{2 - (\gamma - 1)M_j^2}{2 - (\gamma - 1)M_\ell^2}\right]^{\gamma/(\gamma - 1)} \frac{p_j}{p_\infty} - 1 \quad \cdot \quad (A-2)$$

The quantity θ_N, for the plate oriented normal to the bore line, is given directly as the complement to the local flow angle θ_ℓ, as seen in Figure A1. For the general case with inclined plate, an angle η may be defined:

η = angle between a flow inclination vector $\vec{v}$ and the plate unit normal $\vec{n}$ that is directed in the -x sense, and is depicted in Figure A2. Then it is seen

$$\theta_N = \eta - \pi/2.$$

The angle η is obtained through the relation $\vec{v} \cdot \vec{n} = |\vec{v}| \cos \eta$. Finding η thus requires specifying a flow inclination vector, $\vec{v}$,* the plate unit normal vector, $\vec{n}$, and performing the scalar product.

The plate unit normal for any rotation Ψ about $\vec{n}$ is fixed in direction in the (r,x)-plane after inclining to θ_p about the q-axis. (See Figure A3). Thus $\vec{n} = (0, \sin \theta_p, - \cos \theta_p)$

The coordinates (v_q, v_r, v_x) of $\vec{v}$ may be determined from the geometry, requiring v_q and v_r to be coordinates of a gage location on the inclined, rotated plate which the flow is incident upon, and requiring the distance v_x along the bore line to be consistent with the local flow inclination θ_ℓ and the placement of the plate gages in the flow field. From Figure A2 we may read off the components of $\vec{v}$:

$$\vec{v} = (- s \sin \Psi, s \cos\Psi \cos \theta_p, x' + s \cos\Psi \sin \theta_p)$$

---

*$\vec{v}$ is a vector tangent to the flow velocity vector at the gauge station and connecting the gauge and the axis of symmetry.

where

> s = gage coordinate along the plate surface measured from bore axis, and x' must satisfy

$$\cos \theta_{\ell} = \frac{x' + s \cos\Psi \sin \theta_p}{|\vec{v}|} \qquad (A-3)$$

Then

$$\cos \eta = \frac{\vec{v} \cdot \vec{n}}{|\vec{v}| \, |\vec{n}|} = \frac{- x' \cos \theta_p}{|\vec{v}|} \qquad (A-4)$$

One additional equation completes the system of equations for the three unknowns η, x', and $\vec{v}$:

$$|\vec{v}|^2 = v_q^2 + v_r^2 + v_x^2$$

$$= s^2 \sin^2\Psi + s^2 \cos^2\Psi \cos^2 \theta_p$$

$$+ |\vec{v}|^2 \cos^2 \theta_{\ell} \, ,$$

utilizing the v_x coordinate as expressed in terms of the local flow inclination from the jet code output. Thus in terms of knowns:

$$|\vec{v}| = (s/\sin \theta_{\ell})(\sin^2\Psi + \cos^2\Psi \cos^2 \theta_p)^{\frac{1}{2}} \, .$$

This result is combined with Equations A-3 and A-4 to give

$$\cos \eta = \frac{\sin \theta_{\ell} \sin \theta_p \cos \theta_p \cos \Psi}{(\sin^2\Psi + \cos^2\Psi \cos^2 \theta_p)^{\frac{1}{2}}} - \cos \theta_{\ell}\cos \theta_p \qquad (A-5)$$

There remains yet determining the appropriate θ_{ℓ} and M_{ℓ} for a particular gage station at given plate orientation x, θ_p, and Ψ. The jet code, as mentioned earlier, can be applied to an axially symmetric flow. The procedure here was to place the line of gages in the (inclined rotated) plate onto the contour plots of θ_{ℓ} and M_{ℓ} given by the jet code, at the chosen axial location of the plate, and at a calculated angle Γ with respect to the bore line. From Figure 3, the angle Γ is seen to satisfy

$$\cos \Gamma = \cos\Psi \sin \theta_p$$

83

thus for a given plate orientation x, θ_p, and Ψ, the gage line is located for the contour maps and may be drawn in; then θ_ℓ and M_ℓ may be read off for each gage location. A double interpolation scheme was necessary for some gage positions. Thus, all the quantities are in hand for calculating reflected pressures in the Newtonial formulation, Equation A-2.
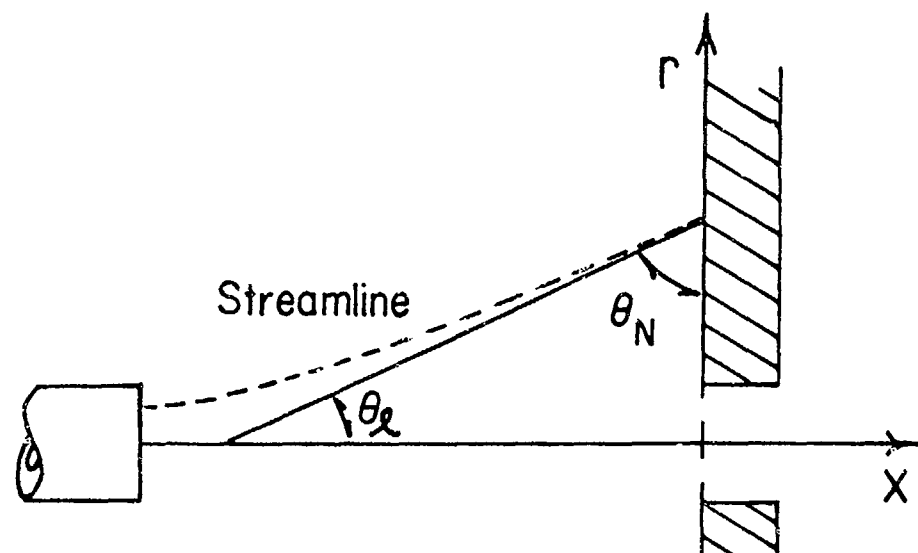
Figure A1. Flow incident on a plate arranged normal to bore axis
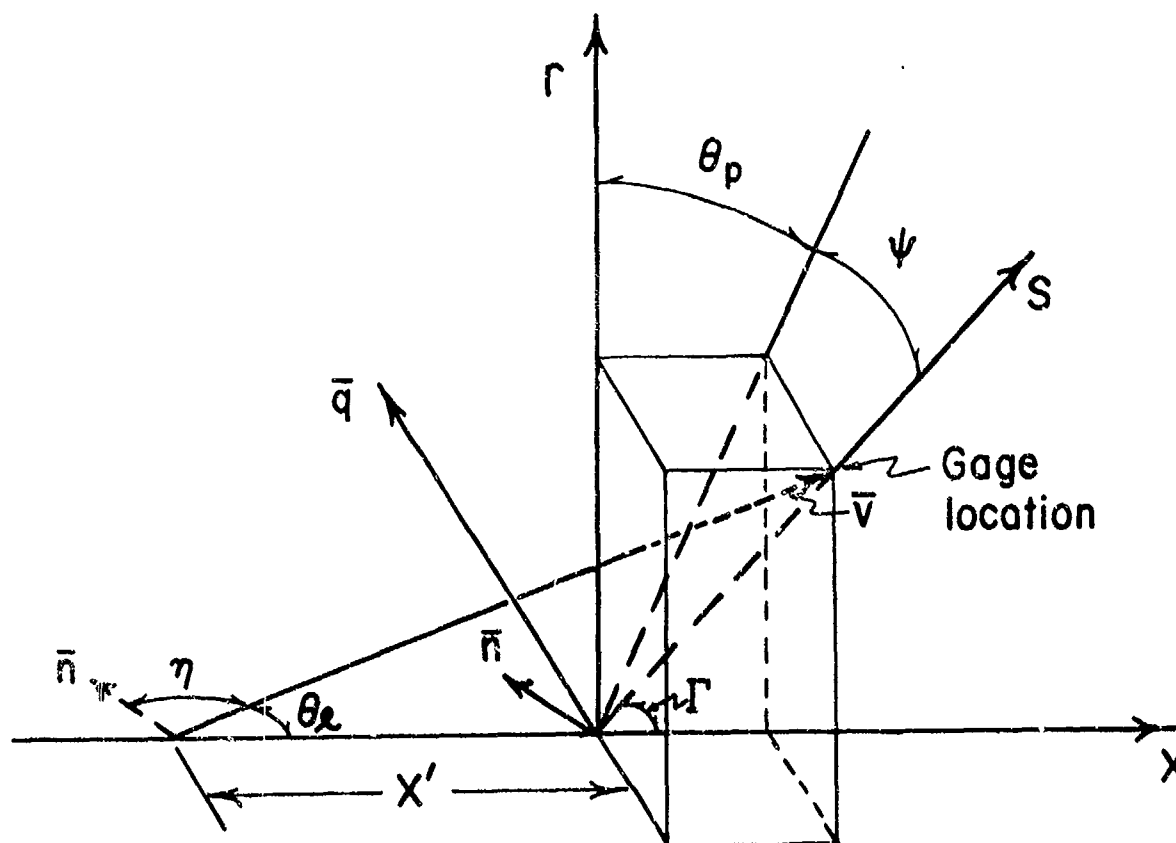
Figure A2. Flow incident on a plate inclined at an angle, θ_p, to bore axis

LIST OF SYMBOLS

a	speed of sound
C_p	pressure coefficient
D	gun tube diameter
e	specific energy
L	gun tube length
m_c	charge mass
M	Mach number
p	pressure
R	gas constant
r	radial distance from bore line
T	temperature
u	gas velocity
V_p	projectile launch velocity
X	axial distance from gun muzzle
γ	ratio of specific heats
θ_N	angle between streamline and plate surface
ψ	azimuthal angle to gauge position on plate

Superscripts

*	sonic conditions

Subscripts

∞	ambient conditions
e	conditions behind projectile immediately prior to shot ejection
s	stagnation conditions

DISTRIBUTION LIST

No. of Copies	Organization	No. of Copies	Organization

12 Commander
Defense Technical Info Center
ATTN: DDC-DDA
Cameron Station
Alexandria, VA 22314

2 HQDA (DAMA-WSA, MAJ Csoka;
DAMA-CSM, LTC Germann)
Washington, DC 20310

1 Commander
US Army Ballistic Missile
Defense Systems Command
Huntsville, AL 35804

1 ODCSI, USAREUR & 7A
ATTN: AEAGB-PDN(S&E)
APO, New York 09403

1 Commander
US Army Materiel Development
and Readiness Command
ATTN: DRCDMD-ST
5001 Eisenhower Avenue
Alexandria, VA 22333

1 Commander
US Army Materiel Development
and Readiness Command
ATTN: DRCDL
DRCDE-R, Mr. Lockert
5001 Eisenhower Avenue
Alexandria, VA 22333

9 Commander
US Army Armament Research
and Development Command
ATTN: DRDAR-TSS (2 cys)
DRDAR-TDS, Mr. Lindner
DRDAR-TDA, Mr. Blick
DRDAR-LC-F, Mr. A. Loeb
DRDAR-SCA, Mr. N. Ford
DRDAR-LCW, Mr. M. Salsbury
DRDAR-LCE, Dr. H. Fair
DRDAR-SEM, W. Bielauskas
Dover, NJ 07801

6 Commander
US Army Armament Research
and Development Command
ATTN: DRDAR-LCV, Mr. Reisman
DRDAR-SCN, Mr. Kahn
DRDAR-LC, Dr. Frasier
DRDAR-SCW, Mr. Townsend
DRDAR-SC, Dr. T. Hung
PM, 30mm Ammo, LTC Logan
Dover, NJ 07801

6 Director
US Army ARRADCOM
Benet Weapons Laboratory
ATTN: DRDAR-LCB-TL
Mr. W. Dock
Dr. G. Carofano
Dr. C. Andrade
DRDAR-LCB, Mr. T. Allen
Mr. R. Billington
Watervliet, NY 12189

2 Commander
US Army Armament Materiel
Readiness Command
ATTN: DRSAR-LEP-L, Tech Lib
Rock Island, IL 61299

3 Commander
US Army Aviation Research
and Development Command
ATTN: DRDAV-E
DRCPM-AAH
Product Manager, AH-1
4300 Goodfellow Boulevard
St. Louis, MO 63120

1 Director
US Army Air Mobility Research
and Development Laboratory
Ames Research Center
Moffett Field, CA 94035

1 Commander
US Army Communications Rsch
and Development Command
ATTN: DRDCO-PPA-SA
Fort Monmouth, NJ 07703

DISTRIBUTION LIST

No. of Copies	Organization		No. of Copies	Organization

1 Commander
US Army Electronics Research
  and Development Command
Technical Support Activity
ATTN: DELSD-L
Fort Monmouth, NJ   07703

1 Commander
US Army Missile Command
ATTN: DRSMI-R
Redstone Arsenal, AL   35809

1 Commander
US Army Missile Command
ATTN: DRSMI-RBL
Redstone Arsenal, AL   35809

1 Commander
US Army Missile Command
ATTN: DRSMI-TLH (Ricks)
Redstone Arsenal, AL   35809

1 Commander
US Army Missile Command
ATTN: DRSMI-RDK
Redstone Arsenal, AL   35809

1 Commander
US Army Missile Command
ATTN: DRSMI-YDL
Redstone Arsenal, AL   35809

1 Commander
US Army Natick Research and
  Development Command
ATTN: DRXRE, Dr. D. Sieling
Natick, MA   01762

1 Commander
US Army Tank Automotive Rsch
  and Development Command
ATTN: DRDTA-UL
Warren, MI   48090

1 Commander
US Army Jefferson Proving Ground
ATTN: STEJP-TD-D
Madison, IN   47250

1 Commander
US Army Materials and
  Mechanics Research Center
ATTN: DRXMR-ATL
Watertown, MA   02172

1 Commander
US Army Research Office
ATTN: CRD-AA-EH
P. O. Box 12211
Research Triangle Park
NC   27709

2 Director
US Army TRADOC Systems
  Analysis Activity
ATTN: ATAA-SL
White Sands Missile Range
NM   88002

1 Commander
US Army ARB
ATTN: SGRD-UAH-AH, Dr. Patterson
P. O. Box 577
Fort Rucker, AL   36362

3 Commander
Naval Air Systems Command
ATTN: AIR-604
Washington, DC   20360

3 Commander
Naval Ordnance Systems Command
ATTN: ORD-9132
Washington, DC   20360

2 Commander and Director
David W. Taylor Naval Ship
  Research & Development Cmd
ATTN: Lib Div, Code 522
Aerodynamic Lab
Bethesda, MD   20084

3 Commander
Naval Surface Weapons Center
ATTN: Code 6X
          Mr. F. H. Maille
          Dr. J. Yagla
          Dr. G. Moore
Dahlgren, VA   22448

DISTRIBUTION LIST

No. of Copies	Organization
1	Commander Naval Surface Weapons Center ATTN: Code 730, Tech Lib Silver Spring, MD 20910
1	Commander Naval Weapons Center ATTN: Code 553, Tech Lib China Lake, CA 93555
1	Commander Naval Research Laboratory ATTN: Tech Info Div Washington, DC 20375
1	Commander Naval Ordnance Station ATTN: Code FS13A, P. Sewell Indian Head, MD 20640
1	AFRPL/LKCC, C. D. Penn Edwards AFB, CA 93523
2	AFATL (DLRA, D. Davis; Tech Lib) Eglin AFB, FL 32542
1	AFWL/DEV Kirtland AFB, NM 87117
1	ASD/XRA (Stinfo) Wright-Patterson AFB, OH 45433
1	Director National Aeronautics and Space Administration George C. Marshall Space Flight Center ATTN: MS-I, Lib Huntsville, AL 38512
1	Director Jet Propulsion Laboratory ATTN: Tech Lib 2800 Oak Grove Drive Pasadena, CA 91103

No. of Copies	Organization
1	Director NASA Scientific & Technical Information Facility ATTN: SAK/DL P. O. Box 8757 Baltimore/Washington International Airport, MD 21240
1	AAI Corporation ATTN: Dr. T. Stastny Cockeysville, MD 21030
1	Advanced Technology Labs ATTN: Mr. J. Erdos Merrick & Steward Avenues Westbury, NY 11590
1	Aerospace Corporation ATTN: Dr. G. Widhopf P. O. Box 92957 Los Angeles, CA 90009
1	ARO, Inc. ATTN: Tech Lib Arnold AFS, TN 37389
2	ARO, Inc. Von Karman Gasdynamics Facility ATTN: Dr. J. Lewis Mr. W. D. Williams Arnold AFS, TN 37389
1	ARTEC Associates, Inc. ATTN: Dr. S. Gill 26046 Eden Landing Road Hayward, CA 94545
1	AVCO Systems Division ATTN: Dr. D. Siegelman 201 Lowell Street Wilmington, MA 01887
1	Battelle Columbus Laboratories ATTN: J. E. Backofen, Jr. 505 King Avenue Columbus, OH 43201

91

DISTRIBUTION LIST

No. of Copies	Organization
1	Technical Director Colt Firearms Corporation 150 Huyshope Avenue Hartford, CT 14061
1	General Electric Corporation Armaments Division ATTN: Mr. R. Whyte Lakeside Avenue Burlington, VT 05401
1	Honeywell, Inc. ATTN: Mail Station MN 112190 (G. Stilley) 600 Second Street, North Hopkins, MN 55343

3	Hughes Helicopter Company
	Bldg. 2, MST22B
	ATTN: Mr. R. Forker
	          Mr. M. Kane
	          Mr. R. Flood
	Centinella and Teel Streets
	Culver City, CA 90230

1	Kaman Tempo ATTN: Mr. J. Hindes 715 Shamrock Road, Suite UL-1 Bel Air, MD 21014
1	Martin Marietta Aerospace ATTN: Mr. A. J. Culotta P. O. Box 5387 Orlando, FL 32805
1	Winchester-Western Division Olin Corporation New Haven, CT 06504
1	Sandia Laboratories ATTN: Aerodynamics Dept Org 5620, R. Maydew Albuquerque, NM 87115
1	Guggenheim Aeronautical Lab California Institute of Tech ATTN: Tech Lib Pasadena, CA 91104

No. of Copies	Organization
1	Franklin Institute ATTN: Tech Lib Race & 20th Streets Philadelphia, PA 19103
1	Director Applied Physics Laboratory The Johns Hopkins University Johns Hopkins Road Laurel, MD 20810

1	Massachusetts Institute of
	   Technology
	Dept of Aeronautics and
	   Astronautics
	ATTN: Tech Lib
	77 Massachusetts Avenue
	Cambridge, MA 02139

1	Ohio State University Dept of Aeronautics and Astronautical Engineering ATTN: Tech Lib Columbus, OH 43210

3	Polytechnic Institute of
	   New York Graduate Center
	ATTN: Tech Lib
	          Prof. S. Lederman
	          Dr. G. Moretti
	Route 110
	Farmingdale, NY 11735

1	Director Forrestal Research Center Princeton University Princeton, NJ 08540
1	Southwest Research Institute ATTN: Mr. Peter S. Westine P. O. Drawer 28510 8500 Culebra Road San Antonio, TX 78228

DISTRIBUTION LIST

Aberdeen Proving Ground

Dir, USAMSAA
  ATTN: DRXSY-D
          DRXSY-MP, H. Cohen

Cdr, USATECOM
  ATTN: DRSTE-TO-F

Dir, USAHEL
  ATTN: Dr. Weisz
          Dr. Cummings

Dir, USAMTD
  ATTN: Mr. S. Walton

Cdr, USACSL, Bldg. E3516, EA
  ATTN: DRDAR-CLB-PA